Studying conduction-electron/interface interactions using transverse electron focusing

V. S. Tsoi

Grenoble High Magnetic Field Laboratory, Max-Planck-Institut für Festkörperforschung and Centre National de la Recherche Scientific, B.P. 166, F-38042 Grenoble Cedex 9, France and Institute of Solid State Physics, Russian Academy of Sciences, Chernogolovka, Moscow Region, 142432 Russia

J. Bass

Grenoble High Magnetic Field Laboratory, Max-Planck-Institut für Festkörperforschung and Centre National de la Recherche Scientific, B.P. 166, F-38042 Grenoble Cedex 9, France and Department of Physics and Astronomy, Michigan State University, East Lansing, Michigan 48824-1116

P. Wyder

Grenoble High Magnetic Field Laboratory, Max-Planck-Institut für Festkörperforschung and Centre National de la Recherche Scientific, B.P. 166, F-38042 Grenoble Cedex 9, France

Understanding the microscopic processes by which the electrons within conductors are scattered at surfaces and interfaces is important for both fundamental physics and technology. The authors review what has been learned so far about scattering of electrons at a variety of surfaces and interfaces using a technique, transverse electron focusing (TEF), that involves two point contacts in a uniform magnetic field. Transverse electron focusing is a sort of β-ray spectrometer in a metal, except that, whereas the β-ray spectrometer requires a narrow beam because the energy and momentum of a free electron can be arbitrary, in TEF the electrons of interest all have the Fermi energy and momentum, so focusing occurs even for electrons injected isotropically in angle. Transverse electron focusing is unique in its ability to probe localized and selectable portions of the interface from inside the conductor, using conduction electrons on only small parts of the Fermi surface. The authors first briefly review the essential features of TEF and of ideal and rough surfaces and describe the three techniques now used for injecting and detecting electrons: needle contacts, lithographically fabricated contacts, and light-induced injection. They then turn to measurements in metals and semimetals of the probability of specular reflection q from a given interface for electrons at the Fermi energy impinging at perpendicular incidence. They examine how q varies over different crystal faces for different electron orbits on the Fermi surfaces of a variety of conductors and how it is affected by changes in the de Broglie wavelength λ_{dB}, by chemical etching, ion etching, or physical damage, by a molecular overlayer condensed from the surrounding atmosphere, and, for semimetals, by surface band bending (surface charge). The authors also explain how to measure the dependence of q upon the angle of incidence $q(\theta)$, which gives information about surface structure. Transverse electron focusing studies of a variety of quasiparticle effects arising because the electrons are in a solid are described. These include (a) scattering of excitations moving on ''holelike'' orbits—q can depend upon the sign of the particle charge; (b) scattering involving a surface reciprocal-lattice vector $\mathbf{G}_\tau$, including surface resonances induced by an artificial grating etched onto a Bi surface; and (c) scattering between different parts of the Fermi surface—intervalley scattering (IVS)—including scattering in which the sign of the quasiparticle charge changes. The authors review studies of scattering of electrons from a normal-metal (or semimetal)/superconductor interface, which involves an unusual phenomenon called Andreev reflection, in which the signs of both the charge and mass change. Also described are TEF studies of scattering of light-excited electrons from an intercrystalline boundary and recent TEF measurements of q for scattering from the boundary of the two-dimensional electron gas. The authors conclude with a list of future TEF studies of conduction-electron/interface interactions that they believe to be interesting and important. [S0034-6861(99)01105-8]

CONTENTS

I. Introduction and Overview 1642
II. Basic Concepts Underlying Transverse Electron Focusing 1644
A. Excitation motion in a uniform magnetic field 1644
B. Focusing and TEF 1645
III. Transverse Electron Focusing Techniques 1646
A. Needle contacts 1646
B. Lithography 1647
C. Light excitation 1647
IV. Conduction-Electron Reflection from a Surface 1647
A. Ideal surface 1647
B. Rough surface 1648
1. Wavelength scale random roughness 1648
2. Terracing and faceting 1649

C. Screening surface roughness—band bending 1649
D. What information is obtained from experiment? 1650
1. Techniques other than TEF 1650
2. TEF 1651
V. Metal Surfaces 1652
A. Specularity of reflection from polished and roughened surfaces 1652
1. Summary of experimental results 1652
2. Testing the random Gaussian roughness model 1655
3. Scanning tunneling microscopy and anisotropy of specular reflection 1655
4. Effects of an adsorbed film 1656
B. Umklapp process 1657
VI. Semimetal Surfaces, Especially Bi 1657
A. Bi crystal lattice, Fermi surface, and sample characteristics 1658
B. Crystallographic and charge anisotropy and effects of surface treatment 1659
1. Electron and hole reflections in Bi for (111) and (1$\bar{1}$0) surfaces 1659
2. Electron and hole reflections in Sb for the (111) surface 1660
3. Electron reflections in Bi for surfaces tilted from the (111) surface 1661
4. Analysis of data on crystallographic anisotropy and charge sign 1661
C. Drift electron focusing and $q(\theta)$ 1662
D. Intervalley scattering 1663
1. Electron-electron intervalley scattering 1664
2. Electron-hole intervalley scattering 1666
E. Surface band bending 1668
1. $q(\theta)$: TEF at multiples of H_0 1668
2. Artificial band bending 1669
VII. Conduction-Electron Surface Resonances 1670
A. Physics underlying conduction-electron surface resonances 1671
B. Samples, data, and analysis 1672
VIII. Intercrystalline Boundary 1672
A. Drift flux 1674
B. Ballistic flux 1675
IX. Normal-Metal/Superconductor Interface 1675
A. Andreev reflection 1676
B. TEF Techniques for studying Andreev reflection 1676
C. Change in sign of charge 1677
D. Change in sign of velocity 1678
E. Probability of Andreev reflection 1679
F. Dependence of Andreev reflection on energy and temperature 1679
G. Screening of surface roughness by the electronic potential 1680
1. Intravalley and intervalley scattering 1680
2. Intervalley scattering alone 1681
X. Electron Reflection from the 2D Electron-Gas Channel Edge 1681
A. Samples and experimental techniques 1682
B. Results and analysis 1683
1. Focusing spectra 1683
a. Short-period oscillations 1684
b. Peak broadening 1685
c. Increasing peak amplitude 1685
2. Electron "pileup" 1686
3. Inferred values of q 1686
a. Mean-free-path studies 1686
b. Hot electrons 1687
4. Miscellaneous 1689
5. Conclusion 1689
XI. Summary, Conclusions, and Opportunities 1689
Acknowledgments 1690
References 1690

I. INTRODUCTION AND OVERVIEW

Understanding how electrons inside conductors scatter from interfaces and boundaries is of both fundamental and practical interest for a wide variety of subfields of modern condensed-matter physics. This scattering is important at the surfaces of bulk metals, metallic foils, films, and wires (Schumacher, 1993); in small conducting particles (Martin, 1996) or mesoscopic conductors (Datta, 1995); at internal boundaries in conglomerates of metals with metals or insulators (Chien, 1990); at ferromagnetic/nonmagnetic metal interfaces in magnetic multilayers (Levy, 1994); at superconductor/normal-metal or superconductor/semiconductor boundaries in bulk systems (van Duzer and Turner, 1981) and mesoscopic (Beenakker, 1991) systems; and at interfaces of semiconductors with metals (McKelvey, 1966) or vacuum (Mönch, 1993), including interfaces at the edges of the two-dimensional electron gas (Beenakker and van Houten, 1991).

In this review we describe what has been learned about scattering of electrons at several of these interfaces using a technique, transverse electron focusing (TEF; V. Tsoi, 1974), that is unique in its ability to probe the scattering of electrons on only small parts of the Fermi surface from localized (and selectable) portions of the interface. Because of space limitations, other techniques used to learn about scattering of electrons at surfaces and interfaces are only briefly mentioned. Over the past decade, TEF studies have been extended to a new medium, the 2D electron gas. Recent improvements in lithographic techniques, combined with the discovery that TEF excitations can be induced by laser light and then probed in two dimensions, promise to make TEF both easier to apply and more widely applicable. This review is intended to give the reader a clear picture of what has already been done with TEF and of the wide range of opportunities that exist for new applications.

Earlier reviews covered the theory underlying TEF (Kolesnichenko, 1992) and the use of TEF to probe surface structure (V. Tsoi *et al.*, 1992). The latter article describes the history of TEF and how to study it with needle contacts. In the present review, we reexamine only those parts of previously covered topics that are crucial for understanding the new information we present. We focus upon the experimental information to be gleaned from TEF, adopting a phenomenological approach involving propagation of free quasiparticles—electrons and holes. For a more complete discussion of the theory see Kolesnichenko (1992).

In Sec. I we briefly describe what TEF is and summarize the main topics to be covered in this review. Together Secs. I and XI should give the reader with a casual interest a picture of what TEF has told us about scattering of conduction electrons from interfaces and of

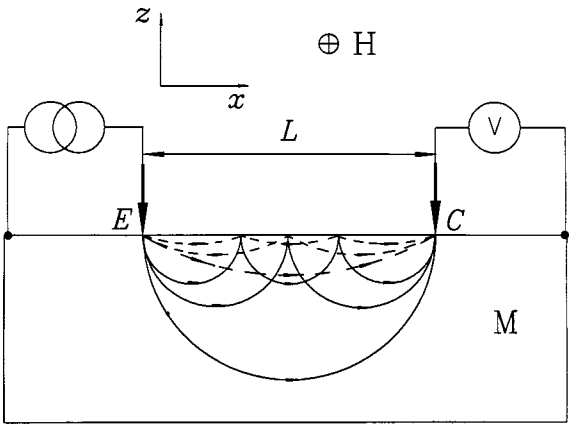

FIG. 1. Standard TEF scheme. *M* is a single crystal, nonequilibrium electrons are injected at emitter *E*, and the potential difference between collector *C* and an outer point of the sample is measured as a function of magnetic-field strength *H*. *E* and *C* are separated by *L*, $\mathbf{H}\perp\mathbf{L}\perp\mathbf{N}$, and **N** is the surface normal. The solid curves denote electrons emitted from *E* and incident on *C* perpendicular to the surface after zero, one, and two specular reflections. The dashed curves denote electrons emitted and incident at smaller angles.

its potential for future studies. Sections II–IV provide background to more detailed analysis, reviewing the concepts underlying TEF, describing experimental techniques, and briefly surveying electron-surface and interface interactions. In the remaining sections we treat metal surfaces (Sec. V), semimetal surfaces (Sec. VI), conduction-electron surface resonances (Sec. VII), the intercrystalline boundary (Sec. VIII), the normal-metal/superconductor interface (Sec. IX), and electron reflection from the channel edge of the 2D electron gas (Sec. X).

The standard geometry of TEF and its essential features are illustrated in Fig. 1. Two microcontacts, called Sharvin probes (Sharvin, 1965) when they are much smaller than the electron mean free path (mfp) *l*, are applied to the surface of a single-crystal conductor at a separation *L* smaller than *l*. One microcontact (emitter—*E*) injects excitations, and a spatially and temporally constant external magnetic field **H** focuses the ballistically traveling excitations onto the other microcontact (collector—*C*), after zero or one or more reflections from the surface of the conductor between the two contacts. This process of transverse (conduction) electron (magnetic) focusing (TEF) allows determination of the probability of specular reflection *q* from the surface. Most published data have been taken with needle point contacts. Recently, however, point contacts have begun to be made by lithography (studies of the 2D electron gas at GaAs/AlGaAs semiconductor heterojunctions will be described in Sec. X) and a small scanned laser spot has been used to give a two-dimensional TEF pattern (Sec. VIII). These techniques are briefly described in Sec. III.

Because of the Pauli exclusion principle and rapid decay of excitations off the Fermi surface, the excitations reaching the collector in a focusing experiment are generally only those within k_BT of the Fermi surface, where k_B is Boltzmann's constant; i.e., the detected excitations are only those with essentially the Fermi energy ε_F and moving with the Fermi velocity v_F. Studies of the dependence of TEF on excitation energy are mostly outside the purview of this review, but will be commented upon briefly in Secs. IX and X.

The field **H** in TEF is usually applied perpendicular ($\perp$) to **L**, the vector connecting the contacts. The excitations can be visualized as electrons (or holes) traveling ballistically through the conductor, except when they are reflected specularly at boundaries. This visualization is known as the geometrical model (V. Tsoi *et al.*, 1992). For a free-electron Fermi surface, the electrons move in **k** space on circular arcs perpendicular to **H**. In real (**r**) space, the projection of their motion onto the plane perpendicular to **H** corresponds to equivalent circular arcs, but scaled and rotated by 90° relative to the **k** space arcs. The Fermi surfaces of real conductors usually differ from a perfect sphere. The electron orbits in **k** space then correspond to portions of orbits on that Fermi surface, and the projections in **r** space are again simply rescaled and rotated by 90°. As the field *H* is increased from zero, the cyclotron radius $R_c=p_Fc/(eH)$ (where *e* is the electron charge, p_F the Fermi momentum, and *c* the speed of light) in **r** space decreases until the orbit diameter (twice R_c) reaches *L*, where the electrons are focused onto the collector, giving a voltage spike or peak *U*. If reflection at the sample surface is at least partly specular, as *H* is increased further, additional peaks appear at fields $H=nH_0$, where $H_0=2p_Fc/eL$ and $(n-1)$ is the number of reflections. If reflection is perfectly specular, the height of every peak is the same as that of the first, since both the electrons involved and the total distances they travel from *E* to *C* are the same. If the reflection is not perfectly specular, the peak height decreases by a constant fraction upon each reflection. The ratio of adjacent peak heights measures the probability of specular reflection *q*. Figure 2 illustrates TEF data for the metal W.

Strictly speaking, such a sharp peak is the result only of electrons incident perpendicular to the surface—90° incidence. Other angles of incidence are treated in Sec. VI.C. As shown in Fig. 1, collected reflections occur at well-defined fractions of *L*. The inferred probability of specular reflection at 90° thus represents particular locations on the sample surface. Collection for a given *n* also means collection for all multiples of *n*.

Transverse electron focusing has been seen in Bi (V. Tsoi, 1974), Sb (Tsoi and Razgonov, 1976), W and Cu (Tsoi and Razgonov, 1977), Ag (V. Tsoi *et al.*, 1979), Al (Benistant, van Kempen, and Wyder, 1985), Zn (Sato and Kimura, 1984), and K, Na, In, Mo, and Sn (Bozhko *et al.*, 1988), and in the 2D electron gas (van Houten *et al.*, 1988). Observations of TEF in metals, semimetals, and semiconductors with such different and often complex Fermi surfaces means that TEF is intrinsic to high-purity, nonsuperconducting conductors. In metals, which have de Broglie wavelengths λ_{dB} comparable to their lattice parameters a_0 random Gaussian roughness

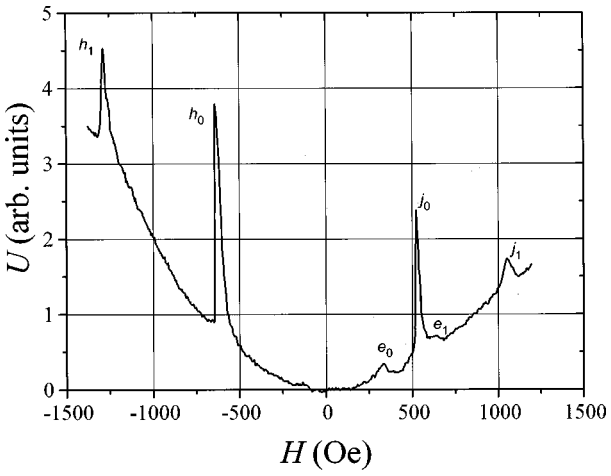

FIG. 2. Electron ($H>0$) and hole ($H<0$) focusing lines for a W sample with surface normal $\mathbf{N}\|[211]$, $\mathbf{H}\|[110]$, and $\mathbf{L}\perp\mathbf{H}$. Different letters denote TEF lines associated with current carriers from different valleys of the W Fermi surface. From Bozhko, Sveklo, and Tsoi (1988).

of even a single monolayer should reduce q to $\ll 1$. In Sec. V, we shall see that q in metals is often >0.5, and that artificially induced roughness sometimes reduces q only modestly. This behavior is attributed to terraced-surface structures. In semimetals and semiconductors, where $\lambda_{dB} \gg a_0$, surface roughness of atomic scale would normally be expected to have only a minor effect. Surprisingly, we shall see in Sec. VI that artificially induced atomic-scale roughness can affect q as much as in metals. This behavior is attributed to a combination of band bending and intervalley scattering.

Figure 2 shows that TEF is not limited to studying the reflection of excitations moving on electronlike orbits in $\mathbf{k}$ space—i.e., rotating in the sense of negatively charged particles. Reversing the field direction allows the study of reflection of excitations on holelike orbits—i.e., rotating in the sense of positive charges. As "holes" and electrons with any λ_{dB} reflect from the same places on the sample surface, TEF allows comparison of how q varies with λ_{dB} for electrons and holes (Secs. V and VI).

For $\mathbf{H}\perp\mathbf{L}$, the electrons focused at C are on extremal orbits with zero velocity component perpendicular to $\mathbf{L}$ (strictly, zero average velocity within the uncertainty due to the finite widths of E and C perpendicular to $\mathbf{L}$). Tilting $\mathbf{H}$ away from the normal to $\mathbf{L}$ lets one study reflection of electrons with finite components of velocity perpendicular to $\mathbf{L}$. Interesting experiments can also be made with $\mathbf{H}$ nearly along $\mathbf{L}$ (Sec. VI.C).

Three different conservation conditions for tangential momentum can be observed in TEF: (1) in specular reflection, tangential momentum is conserved; (2) in diffraction, tangential momentum changes by a surface reciprocal-lattice vector $\mathbf{G}_\tau$; (3) for a faceted or terraced surface, tangential momentum is conserved, but the local surface normal is not the normal to the median plane (see V. Tsoi *et al.*, 1992). Sections V.B and VII describe reflections involving bulk $\mathbf{G}$ or surface $\mathbf{G}_\tau$ reciprocal-lattice vectors.

In some cases, electrons cannot go from E to C on a single portion of the Fermi surface. A TEF signal can then only be obtained, if at all, after intervalley scattering in which the electrons are scattered to another valley of the Fermi surface, from which they can reach C. Section VI.D describes studies of intervalley scattering in the semimetal Bi. Intervalley scattering depends strongly on surface roughness.

By depositing material onto the surface of a crystal between E and C, or onto the opposite face of a thin enough crystal, one can study the reflection of electrons from the interface between the crystal and this overlayer. In Sec. V.A.4, we examine effects of a gaseous overlayer, and in Sec. IX reflection from a normal-metal/superconductor (N/S) interface. N/S reflection involves an unusual phenomenon, Andreev reflection (Andreev, 1964), about which TEF provides unique information.

In this review we focus upon the unique information that has been obtained from TEF about the scattering of conduction electrons from interfaces. We discuss scattering from six different interfaces: (1) the metal/vacuum interface; (2) the semimetal/vacuum interface; (3) an interface with a grating (conduction-electron surface resonances); (4) an intercrystalline boundary; (5) an N/S interface; and (6) the channel edge in the 2D electron gas.

II. BASIC CONCEPTS UNDERLYING TRANSVERSE ELECTRON FOCUSING

A. Excitation motion in a uniform magnetic field

The motion of a particle of charge e and mass m in a spatially and temporally uniform field $\mathbf{H}$ is determined by Newton's law, $\mathbf{F}=d\mathbf{p}/dt$, and the Lorenz force, $\mathbf{F}=(e/m)(\mathbf{v}\times\mathbf{H})$. Since $\mathbf{H}$ does no work on the particle, the particle's energy is conserved. For free particles, when the component of $\mathbf{v}$ parallel to $\mathbf{H}$, $\mathbf{v}_\|$, is zero, both the particle and its momentum rotate in circles perpendicular to $\mathbf{H}$. If $\mathbf{v}_\|\neq 0$, the momentum still rotates in a circle, but the particle executes a spiral. Whether the rotation is clockwise or counterclockwise is determined by the sign of the ratio e/m. Transport analysis usually focuses on the kinetics of the excitation's wave vector, $\mathbf{k}=2\pi\mathbf{p}/h$, where h is Planck's constant.

As noted in Sec. I, the excitations of interest for TEF are only those essentially on the Fermi surface. For free electrons, the Fermi surface is spherical, whereas in a real metal its shape is more complex, and so are the motions of $\mathbf{k}$ and the excitations. But $\mathbf{k}$ generally still rotates around a closed orbit in the plane perpendicular to $\mathbf{H}$, and the projection of the real-space orbit on that same plane still has the same shape as the orbit of $\mathbf{k}$, rescaled and rotated by 90°. For the usual TEF geometry, with $\mathbf{H}$ perpendicular to the line from E to C, the excitation displacement along $\mathbf{H}$ should be zero, so that the detected excitations move on extremal orbits of the Fermi surface, to within the band of values of $\mathbf{v}_\|$ allowed by the finite widths of E and C.

In metals, the current carriers are always electrons. But for motion on some orbits, these electrons may have "negative effective mass" (see, Ashcroft and Mermin, 1976). The motion of such a quasiparticle is often described as if it were a "hole" with positive mass. Figure 2 shows that the TEF peaks for such "holes" have the same polarity as those for electrons, only they are observed in a reversed magnetic field. For use in Sec. IX, we note that reversing the signs of both the charge and the mass of a particle simultaneously leaves the Lorenz force, and thus the particle's motion, unchanged. But in this case, relevant to the phenomenon of Andreev reflection (Andreev, 1964), the TEF peak polarity is reversed (because of the reversal of the charge sign), while the peak occurs for the same field sign as for a particle with the usual negative charge and positive mass.

As we shall see in our analysis of TEF data on Bi in Sec. VI, the Bi Fermi surface contains three nonparallel electron ellipsoids that are so highly elongated that, for most purposes, they can be approximated as cylinders. An electron on a cylindrical Fermi surface moves in **r** space in a plane perpendicular to the cylinder axis, because its velocity lies along the normal to the Fermi surface and thus always in this plane. Excitations are detected at C only if C and E both lie in this plane. Electrons on different cylinders rotate in different planes in **r** space. Certain orientations of **L** relative to the crystal axes allow detection of intravalley scattering on a single cylinder, or both intravalley and intervalley scattering, while others, where C is out of the planes of motion of the electrons emitted from E, can only give focusing after intervalley scattering between cylinders, where electrons change their plane of motion upon reflection. To clarify this situation, Fig. 3 depicts the behavior of electrons moving on a cylindrical Fermi surface of radius $\mathbf{k_F}$, with angle φ between **H** and the cylinder axis. If $\varphi=0$ [Fig. 3(a)], the electron rotates around a circle of radius $\mathbf{k}_F$ in **k** space and one in **r** space of radius R_c. If $\varphi\neq 0$ [Figs. 3(b) and (c)], the orbit in **k** space becomes an ellipse, still perpendicular to **H**, with half its long axis given by $k=k_F/\cos\varphi$. Since **v** is always perpendicular to the cylinder axis, the orbit in **r** space returns to the surface from which it was emitted, but displaced along that surface by a distance $L=2R_c(\varphi)=2R_c(\varphi=0)/\cos\varphi$, directed perpendicular to the cylinder axis. The displacement is perpendicular to **H** only when $\varphi=0$. The location of the first peak, and the separation between peaks, both vary as $H_0=H_0(\varphi=0)/\cos\varphi$. Figure 3 shows that tilting the cylinder, but not **H**, changes the orbit plane in **r** space but not in **k** space, and tilting **H**, but not the cylinder, changes the plane in **k** space but not in **r** space.

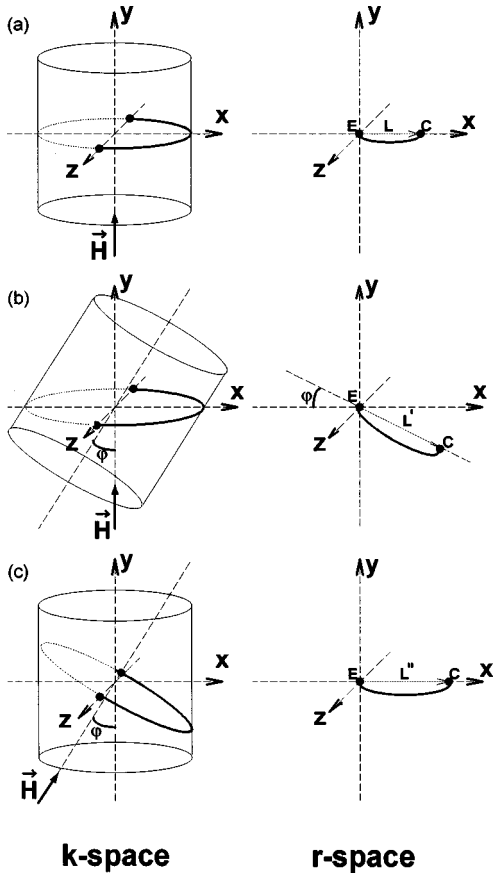

FIG. 3. Electron orbits in **k** space (left side) and real (**r**) space (right side) for motion on a cylindrical Fermi surface: (a) **H** and cylinder axis along the y axis; (b) **H** along the y axis and cylinder axis tilted by angle φ to **H**; (c) cylinder axis along the y axis and **H** tilted at an angle φ to it.

B. Focusing and TEF

It has long been known that a uniform magnetic field focuses a beam of free charged particles. Consider an electron source at the origin, emitting electrons of constant speed isotropically, with the field along the z axis. The density of electrons $\rho(\mathbf{r})$ falling at a point with radius vector **r** is singular on the z axis and on some surfaces called caustics. That is, $\rho(\mathbf{r}_{ct})\rightarrow\infty$ when $\mathbf{r}\rightarrow\mathbf{r}_{ct}$, where $\mathbf{r}_{ct}$ is on a caustic. Focusing—a singularity in detected current—occurs when a caustic crosses a collector or vice versa. Figure 4(a) shows two of the caustic surfaces for free space. In the (xy) plane, they are circles of radius $2R_c$, and they cross the z axis at points $\pm n2\pi R_c$, where n is an integer. Figure 4(a) shows $n=1,2$.

The first studies of magnetic-field focusing of conduction electrons were made by Sharvin and Fisher (1965) and Sharvin and Bogatina (1969), who placed needle point contacts on a line parallel to **H** on opposite sides of a single crystal of Sn. We call this geometry "longitudinal focusing." Figure 4(b) shows the free-electron caustic intersections with the sample surface (which set the locations of focusing peaks). Focusing singularities are present at many points on the collector surface, not just at the intersection with the z axis. At $\pm n2\pi R_c$, higher-order singularities in $\rho(\mathbf{r}_{ct})$ determine when longitudinal focusing occurs.

Magnetic focusing studies were extended by V. Tsoi (1974) to the geometry of Fig. 1, with E and C on the same side of the sample. We call this geometry, and any geometry with the contact line not parallel to **H**, trans-

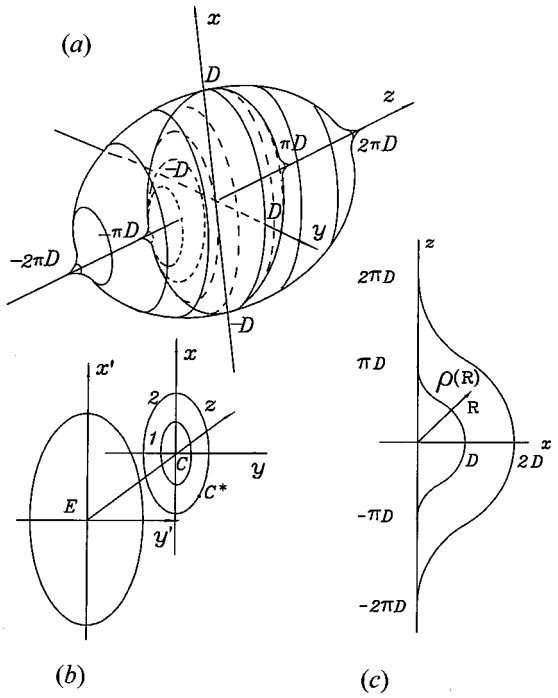

FIG. 4. Caustics for electrons emitted uniformly from the origin, with **H** along the z axis: (a) The first two caustic surfaces in free space. The inner surface goes from $-\pi D$ through the circle of radius $D=2R_c$ to $+\pi D$. The circle is for electrons focused after executing a semicircle. Near points $z=\pm\pi D$, electrons are focused after executing a complete circle. The outer surface goes from $-2\pi D$ through the same circle to $+2\pi D$. Near points $z=\pm 2\pi D$, electrons are focused after executing two circles. (b) Slices by planes $z=0$ and $z=C$ through the caustic surfaces of (a). The slice through $z=C$ ($EC<\pi D$) shows the caustic lines for electrons focused at the surface $z=C$. A collector at C detects longitudinal focusing. As the z axis is a caustic line, longitudinal focusing is observed when $EC=n\,\pi D$. (c) Slice through the plane $y=0$ showing the caustic surfaces of (a) for electrons emitted into half of the space and returning to the $y=0$ plane. Specular reflection results in a series of concentric caustics involving one (shown in the figure), two, three, etc., reflections from the plane. The caustics in (c) apply to TEF.

verse focusing. Because of its greater flexibility, this latter geometry has proved a more bountiful source of physics and is the focus of this review. The caustics for free electrons in the usual TEF geometry (Fig. 1) with a slab thickness larger then $2R_c$ (for an important exception see Sec. IX.B) are shown in Fig. 4(c) (Grishin, 1983). For free electrons, there is now only one curve, the one closest to the origin. The TEF caustics of interest appear when electron reflection from the sample surface is added. Simple specular reflection from this surface gives a series of concentric curves (only the one for a single reflection is shown). In TEF experiments, the collector is usually held fixed and the magnitude of **H** varied, causing the caustics to sequentially cross the collector location. The amplitude ratio of neighboring singularities along a given radius vector remains independent of the electron mean free path l and is just the probability of specular reflection from the surface. This feature of the caustics allows the use of TEF to study conduction-electron/interface interactions.

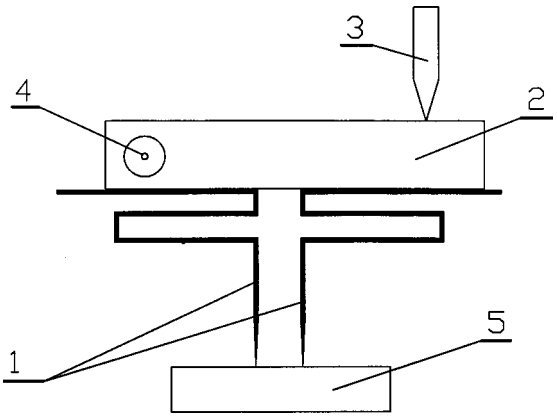

FIG. 5. Standard needle point contact system, consisting of two needles (1), attached to a bar (2) that is caused by an externally controlled screw (3) to rotate about a pivot (4) to bring the needles into contact with the sample (5).

Above, we focused on caustic intersections with the sample surface, where a detector can be placed. For specular reflection, the presence of the surface induces additional caustics within the sample, which can become important when the wave phase of the electrons is treated (see Beenakker *et al.*, 1988).

Finally, "focusing" can also occur in zero magnetic field when injected particles (electrons, phonons, etc.) move along straight lines. The physical basis for such focusing is the presence of saddle points on the constant energy surface of interest—for electrons, the Fermi surface (Kosevich, 1985; Andrievskii and Ass, 1986). Saddle points cause the angular distribution of injected particles to have singularities for some spread directions, leading to focusing. Such focusing has been seen with phonons (Eisenmenger and Kaplyanski, 1986) and low-energy free electrons (Stampfl *et al.*, 1995). The nearly cylindrical electron valleys in Bi allow direct visualization of two-dimensional zero-field focusing patterns of conduction electrons excited by a laser (Heil *et al.*, 1995; Primke, 1997; see Sec. VIII). An unusual zero-field focusing involving Andreev reflection is described in Sec. IX.B.

III. TRANSVERSE ELECTRON FOCUSING TECHNIQUES

Cryogenic techniques used to reach 4.2 K or below for TEF studies and lock-in amplifier techniques for measuring TEF voltages are so routine that we only describe different ways to make point contacts.

A. Needle contacts

Figure 5 shows a simple needle contact system (V. Tsoi and N. Tsoi, 1977) consisting of two sharpened needles (1) attached to a bar (2) the vertical position of which is set by the position of a screw (3). Rotating the screw moves the needles up and down. The needles may be made of a soft metal (e.g., annealed Cu or Ag wire of

diameter ~ 100 μm—softness can be important to minimize damage to the sample area near the contact), or a rigid one (W or Mo of lesser diameter), which after welding provides very stable contacts. A gear provides an appropriate displacement step. The bar is fixed at point supports (4) to exclude accidental displacement. The contact line is placed along a chosen direction by rotating the sample (5) around a vertical axis. During cooldown, the needles can shift by tens of μm, and it is usual to warm up the system once or twice to rebend the needles to a desired separation, after which the system can be stable for many runs. A transparent dewar is convenient for such alignment.

It is sometimes important to be able to translate the sample (Sveklo and Tsoi, 1989a; V. Tsoi *et al.*, 1989). In experiments such as the observation of a surface electron-hole transition in Bi described in Sec. VI.D.2, three contacts are needed. For systems allowing independent displacements of both needles and sample see V. Tsoi *et al.* (1989); Hoevers, Hermson, and van Kempen (1989); and Sveklo and Tsoi (1993).

Usually, a battery is connected across the needle, the sample, and a series ballast resistor, to check when the needle touches the surface. Such contact installation damages the area near the contact over a size that depends on the applied voltage and ballast resistance. Normally a high resistance and small voltage are used to keep the damaged area much smaller than L. If either the emitter or the collector is reinstalled at the same point, the TEF peak amplitude decreases, because more defects are created.

The systems just described can be used for contact separations down to tens of μm. For electron mean free paths less than 10 μm, a modified needle procedure is described by M. Tsoi and V. Tsoi (1996a, 1996b). For examples of its use, see Sec. VI.C and M. Tsoi *et al.* (1996).

B. Lithography

Micron or submicron contact separations can be made with electron-beam (*e*-beam) lithography. Lithography was first used for TEF studies in the 2D electron gas by van Houten *et al.* (1988, 1989), and more recently to make a series of micron-sized contacts along a crystal axis in a Bi single crystal (Jaeger *et al.*, 1996; V. Tsoi, Jaeger, *et al.*, 1996). Lithographic contacts offer advantages over needle probes in electrical integrity, thermal robustness, reduction in contact-site damage, and ability to align multiple contacts along a crystal axis, simplifying the task of adding interface material in between.

C. Light excitation

A promising new technique for observing TEF involves producing excitations by scanning a small laser-beam spot over the crystal and detecting the resulting two-dimensional magnetic-field focusing pattern by means of a fixed-point contact collector (Heil *et al.*, 1995, 1996). For a homogeneous sample, the information obtained is the same as that for fixed emitter and scanned collector. This technique also eliminates needle-induced damage but the excitation distribution differs from that in the usual TEF measurements, as it is produced by a temperature rather than a voltage difference.

IV. CONDUCTION-ELECTRON REFLECTION FROM A SURFACE

A. Ideal surface

Many aspects of conduction-electron/sample-surface interactions have been studied.[1] We consider here only general conditions for conduction-electron/interface scattering. We start with an *ideal surface*—the one that a semi-infinite crystal would have if the positions of its atoms coincided with those in the same, but infinite, crystal. The surface's translation symmetry coincides with that of a similar plane in bulk.

When an electron is reflected from a surface, its energy ε must be conserved (elastic reflection) if no other excitations are produced. The probability of such production can be made as small as desired by reducing the sample temperature. We consider only elastic reflection, where conduction electrons at the Fermi surface are reflected to states also at the Fermi surface.

For an ideal surface, identification of the translation symmetry of the confined crystal with that of the infinite crystal in the same plane requires conservation of the tangential component of the electron's crystal momentum $\mathbf{p}_\tau$ upon reflection (Pippard, 1965; Green, 1969; Andreev, 1971). In the reduced zone scheme (Fig. 6), where $\mathbf{p}$ is limited to the first Brillouin zone, conservation of energy and momentum give

$$\mathbf{p}_\tau^- = \mathbf{p}_\tau^+ + \mathbf{G}_\tau, \tag{1}$$

allowing for reflection processes involving $\mathbf{G}_\tau = \alpha_1 \mathbf{g}_{1\tau} + \alpha_2 \mathbf{g}_{2\tau} + \alpha_3 \mathbf{g}_{3\tau}$, the surface projection of a reciprocal lattice vector $\mathbf{G}$. Here $\mathbf{g}_{1\tau}$, $\mathbf{g}_{2\tau}$, and $\mathbf{g}_{3\tau}$ are the projections of the primitive reciprocal-lattice vectors onto the surface, α_1, α_2, and α_3 are integers, and the signs + and − denote incoming and reflected electrons. In the alternative extended-zone scheme, where $\mathbf{p}$ extends to infinity, $\mathbf{G}_\tau = 0$ in Eq. (1), and tangential momentum is conserved. In the reduced-zone scheme, the tangential momentum is determined only within $\mathbf{G}_\tau$; after reflection, electron A in Fig. 6 can also go into state C. $\mathbf{G}_\tau$ can also be the reciprocal-lattice vector of an artificially imposed surface grating (see Sec. VII).

Electrons in a metal are in a potential "box," with a two-dimensional surface barrier that prevents their escape. This "reflecting surface" is a set of classical turning points called the corrugation surface. If the corrugation surface were perfectly flat, surface scattering would

[1]See, for example, Ziman (1960), Pippard (1965), Green (1969), Andreev (1971), Okulov and Ustinov (1979), V. Tsoi (1980), Fal'kovskii (1983), Kaganov and Edelman (1985), Gantmakher and Levinson (1987), and V. Tsoi *et al.* (1992).

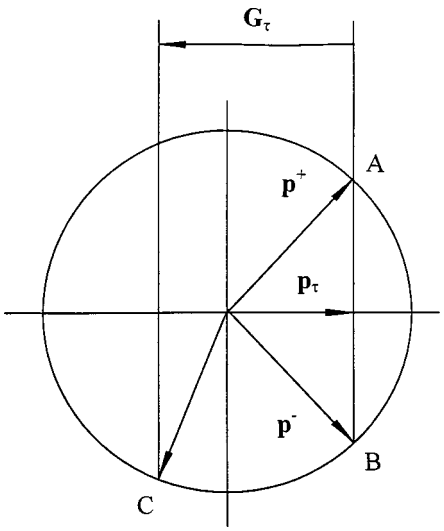

FIG. 6. Specular reflection ($\mathbf{p}_\tau^- = \mathbf{p}_\tau^+ = \mathbf{p}_\tau$) and diffraction ($\mathbf{p}_\tau^- = \mathbf{p}_\tau^+ + \mathbf{G}_\tau$) in the reduced-zone scheme in $\mathbf{p}$ space. $\mathbf{p}_\tau^+$ and $\mathbf{p}_\tau^-$ are the tangential momentum components (i.e., parallel to the horizontal reflecting surface) before and after reflection, and $\mathbf{G}_\tau$ is a tangential component of a reciprocal-lattice vector $\mathbf{G}$. When $\mathbf{G}_\tau$ is itself a reciprocal-lattice vector of the 3D lattice, it takes the electron to an equivalent state in another Brillouin zone resulting in only specular reflection: $\mathbf{p}_\tau^- = \mathbf{p}_\tau^+ = \mathbf{p}_\tau$.

be fully specular, giving, in the reduced-zone scheme, $\mathbf{p}_\tau^- = \mathbf{p}_\tau^+$. But even an ideal surface is not flat; rather, it varies periodically in space. This periodically varying structure causes diffraction into the momentum states $\mathbf{p}_\tau^+ + \mathbf{G}_\tau$. For $\mathbf{G}_\tau \neq \mathbf{G}$, the intensity of such scattering is determined to a first approximation by the ratio of the amplitude A of the corrugation surface to the de Bioglie wavelength λ_{dB}. In a metal, λ_{dB} is usually comparable to the atomic spacing a_0. For semimetals and semiconductors, in contrast, λ_{dB} can be much larger than a_0. To estimate the amount of nonspecular scattering for even an ideal surface, one must know A.

In principle, different probes—conduction electrons, molecular beams (Heinz *et al.*, 1982; Benedek and Valbusa, 1987), scanning tunneling microscopy (STM; Binnig and Rohrer, 1986), etc.—should all yield A. In practice, different probes measure different corrugation surfaces, and it is hard to correct them for comparison. For example, scattering helium from metals such as Ag and Cu (Mattera *et al.*, 1985) yielded corrugation amplitudes ranging from 0.022 Å for Ag(111) to 1.7 Å for Ag(110). Scattering hydrogen from the same surfaces yielded a value four times larger for Ag(111), but 2.5 times smaller for Ag(110). Directly measured STM corrugation amplitudes depend on the tip-sample separation, tip-sample voltage and polarity, method of tip preparation, sample material, and state of the surface. For instance, along the normal to a carbon surface, where helium scattering gave an amplitude of ~0.2 Å (Boata *et al.*, 1978), the STM displacement amplitude was more than the interatomic spacing (Mamin *et al.*, 1986; Soler *et al.*, 1986). Such large STM amplitudes are probably due to a combination of surface deformation and impurities from an absorbed film, as an atomically clean surface, under UHV, gave only 0.9 Å (Mamin *et al.*, 1986). Scanning tunneling microscopy corrugation amplitudes measured on Au(111) (Hallmark *et al.*, 1987), Ag(111) and (100) (Obretenov *et al.*, 1992), Ga (Zuger and Durig, 1992), Pb (Troyanovskii and Edel'man, 1993), Al (Wintterlin *et al.*, 1989), and the semimetal Bi (Troyanovskii and Edel'man, 1994), ranged from 0.2 to 0.7 Å for Au, Ag, Ga, and Bi, from 0.6 to 1.4 Å for Pb, and up to 1 Å for Al.

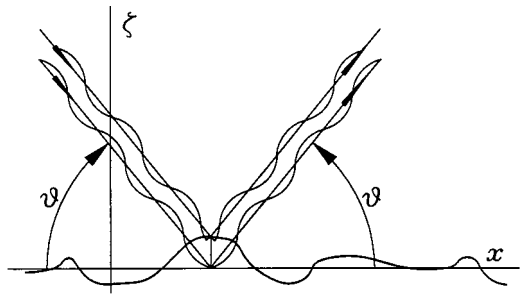

FIG. 7. Plane-wave reflection from a rough surface: $\zeta(x)$ is the surface profile; $\zeta(x) \equiv 0$ is the median plane of the surface; and ϑ is the angle of incidence.

If A is known, the probability of specular reflection for a given λ_{dB} can be estimated from free-electron hard-wall model calculations (Heinz *et al.*, 1982; Benedek and Valbusa, 1987). In metals, $A < 0.2$ Å (i.e., $< \lambda_{dB}/10$) should give specular reflection, whereas $A \sim 1$ Å should not. In Bi, the much larger λ_{dB} (~1000 Å) should give specular reflection for $A \sim 100$ Å $\gg a_0$.

B. Rough surface

1. Wavelength scale random roughness

Unlike an ideal surface, a real surface is usually rough on an atomic scale. We consider first irregular roughness, a random distribution of surface defects, the nature and form of which depend on the method of crystal growth, surface treatment, absorbed films, etc. The dominant parameter for scattering is then the ratio of the characteristic amplitude of roughness to λ_{dB}, which determines whether geometrical or wave optics must be used—i.e., if the problem is classical or quantum. Conduction-electron scattering requires quantum mechanics. In a metal, with $\lambda_{dB} \sim a_0$, random atomic-scale roughness should give diffuse scattering. For a semimetal, in contrast, specular reflection would be expected.

If at a point x the roughness height is $\zeta(x)$ (Fig. 7) relative to the median flat surface $\zeta(x) \equiv 0$, a wave reflected in the specular direction gains an additional phase shift,

$$\delta\varphi(x) = 2k\zeta(x)\sin\vartheta, \quad k = 2\pi/\lambda, \tag{2}$$

where ϑ is the angle of incidence between $\mathbf{k}$ and the surface. From the Rayleigh criterion, if $2k\zeta(x)\sin\vartheta \ll \pi/2$, the roughness is not important. If we assume (Ziman, 1960) that the reflected waves are radiated by

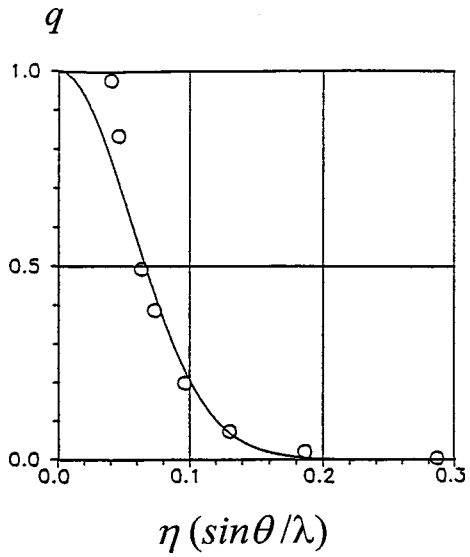

FIG. 8. The dependence of q, the probability of specular reflection, on the relative mean-square roughness height, $\beta = \eta/\lambda_{dB}$, for a Gaussian distribution of surface roughness heights. The solid curve is Eq. (3). The circles are $q(\theta)$ derived from the data of Fig. 17 (Sec. VI.C), normalized to mean-square roughness height η=338 Å. From M. Tsoi and V. Tsoi, 1995.

sources on the reference plane with constant density, and that the phase shift for each source is set by Eq. (2), then the diffraction pattern is set by the statistical properties of $\delta\varphi(x)$, and the statistical properties of $\delta\varphi(x)$ are determined by those of $\zeta(x)$, the surface structure of interest. If the surface height distribution is Gaussian with mean-square height η and correlation length—the length over which the mean of the product $\zeta(x_1)\zeta(x_2)$ decreases by a factor e—much less than η, then the probability density for specular reflection is (Ziman, 1960; Parrot, 1965)

$$q(\eta,\vartheta) = \exp\{-(4\pi\eta\sin\vartheta/\lambda_{dB})^2\} = \exp\{-(4\pi\beta\sin\vartheta)^2\}, \quad (3)$$

where $\beta = \eta/\lambda_{dB}$ (Fig. 8). Equation (3) confirms that, at normal incidence, specular reflection should occur in a normal metal with random Gaussian surface roughness only for atomically flat surfaces ($\beta < 0.1$).

Under arbitrary dispersion $\varepsilon(\mathbf{p})$, Eq. (3) must be generalized to a phase shift $\delta\varphi$ resulting from wave scattering at two scatters separated by a vector $\mathbf{r}$,

$$\delta\varphi = (\Delta\mathbf{k}\cdot\mathbf{r}) = 2\pi(\Delta\mathbf{p}\cdot\mathbf{r})/h, \quad (4)$$

where $\Delta\mathbf{p} = \mathbf{p}^- - \mathbf{p}^+$ is the change in electron momentum upon scattering. Equation (4) shows that what is important is neither the momentum alone nor its normal component, but its change. The ability of roughness to produce diffuse scattering must be determined by the change of momentum upon reflection.

2. Terracing and faceting

Within the last few years, STM studies of surface roughness on TEF samples (Bozhko *et al.*, 1984; Pryadkin and Tsoi, 1988; Bozhko, 1989; Hoevers and van Kempen, 1991; Hoevers *et al.*, 1992) have shown deviations from the random Gaussian roughness that we described. In Sec. V, we shall see that some surfaces either consist of atomically flat regions separated by steps, or else are faceted. For such non-Gaussian roughness, not only the mean-square roughness height, but also the form of the roughness must be given. In general, analysis of scattering from such roughness can only be done numerically. We shall call a surface "terraced" if it is composed of atomically flat regions that are large compared to λ_{dB}, separated by large ($\gg\lambda_{dB}$) steps. Here, assuming that step sizes are random, and neglecting small-scale roughness $\sim a_0$, geometrical optics can be used and the behavior of q depends upon details of the large-scale surface structure. (The situation is more complicated when the step size is $\sim a_0$.) Atomically flat regions that are aligned parallel to the median plane should give rise to specular reflection. Electrons collected after reflection are those specularly reflected from flat regions aligned within an angle $\Delta\Omega$ small enough that the reflected electrons fall within the finite area of C. In this case, q will not measure an average roughness η, as in the case of Sec. IV.B.1, but will measure the fraction of the surface that is atomically flat and aligned to within $\Delta\Omega$. In the samples studied so far, however, the atomically flat regions sometimes have size $\sim\lambda_{dB}$, and not all are aligned parallel to the median plane.

In TEF studies, the difference between random roughness and terracing will appear as different dependences of q upon λ_{dB}. For random roughness, the variation of q with λ_{dB} should be fit by Eq. (3) with a single value of η. For terracing with atomically flat regions, q should measure the fraction of the surface that is flat and properly aligned and thus be independent of λ_{dB}. The behaviors of real metals may of course, lie between these extremes.

C. Screening surface roughness—band bending

In semimetals, semiconductors, and superconductors, electron-interface scattering may be affected by changes of electronic potential near the surface of interest over distances $\gg a_0$. Radical changes in the electron-interface interaction can then occur. In particular, the potential may screen surface roughness. To show how, we characterize an electronic potential like that depicted in Fig. 9 by two parameters, V_0 and ζ_0, where V_0 is the change of the potential and ζ_0 is the distance over which the change occurs.

For the illustrated cases with $V_0 > \varepsilon_F^e$ and ε_F^h, A and B are turning points for holes reflected by downward band bending (dashed curve) before they reach the surface, and for electrons reflected by upward band bending (dotted curve). Upward (downward) band bending does not reflect holes (electrons), because such potentials hardly affect those current carriers at ε_F.

Importantly, surface roughness can still be screened even if V_0 is less than the kinetic energy ε of the particle. For an isotropic electronic spectrum, with fixed ki-

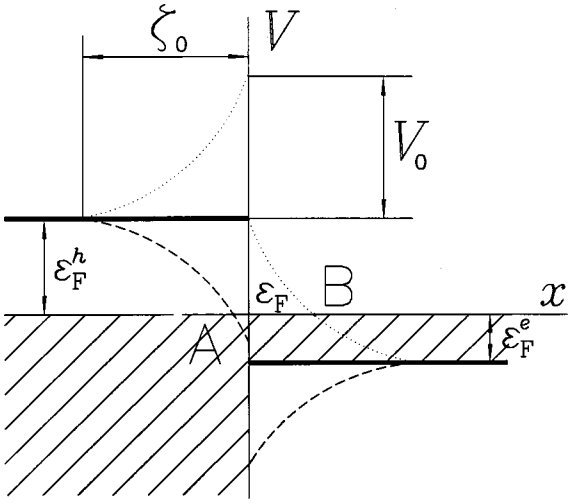

FIG. 9. Schematic drawings of electron and hole bands in a semimetal, showing the hole-band top (left heavy line), electron-band bottom (right heavy line), Fermi level ϵ_F and electron (ϵ_F^e) and hole (ϵ_F^h) Fermi energies, the semimetal/vacuum interface (vertical line), the magnitude of surface band bending ($V_0 > \epsilon_F^e, \epsilon_F^h$), and the distance over which it extends (ζ_0). The dashed curves show band bending down and the dotted ones up. A and B are the turning points for holes and electrons. Occupied electron states are hatched.

netic energy ε of the particle, only particles having $m\nu_\perp^2/2 \geq V_0$ can reach the surface, where $\nu_\perp$ is the component of particle velocity perpendicular to the surface. Particles with $m\nu_\perp^2/2 < V_0$ will be reflected by the potential barrier. Thus particles with kinetic energy $m\nu^2/2 > V_0$, but velocity directed outside the angle of incidence θ_0 between the velocity and surface given by the "cosine of reaching" formula

$$\cos\theta_0 = (1 - V_0/\varepsilon)^{1/2} \tag{5}$$

will be reflected by the potential barrier before reaching the actual surface. Since the roughnesses of the surface and potential barrier may be very different, the presence of surface band bending can radically change the character of electron reflection (Kravchenko and Rashba, 1969), cutting off diffuse scattering with decreasing incidence angle much more effectively than would occur for scattering of uncharged particles such as photons. We shall see how TEF reveals such behavior in Secs. VI.B, VI.D, VI.E, and IX.G.

D. What information is obtained from experiment?

In principle, different measured quantities (electrical resistivity, static skin effect, TEF spectra, etc.) should all be determined, at least partly, by scattering of electrons from the sample surface. Thus a complete analysis of each should provide the same information about such scattering. But most such quantities involve many electrons having different wavelengths and different angles of incidence onto the interface. It is difficult or impossible to determine the scattering of particular subsets. In this section we first define the fundamental quantities to be determined, then discuss briefly what one learns about them from measurements of other quantities such as electrical resistance and the static skin effect, and conclude with a more detailed discussion of the relation between the probability of specular reflection that one measures in TEF, q_M, and the intrinsic quantity of interest, q. The difference between q_M and q is negligible when $b/L \ll 1$ (b is the contact size), but can be significant when the Fermi surface of interest is cylindrical and when $b/L \geq 0.1$—which can occur in the semimetal Bi (Sec. VI) and in the 2D electron gas (Sec. X).

The quantity that characterizes the (spatially averaged) scattering of electrons of energy ε and momentum $\mathbf{p}^+$ from an interface is the probability $W(\varepsilon,\mathbf{p}^+;\varepsilon,\mathbf{p}^-)$ of reflection from state $\Psi(\varepsilon,\mathbf{p}^+)$ into state $\Psi(\varepsilon,\mathbf{p}^-)$. The quantity measured experimentally must be written as

$$\int B(\varepsilon,\mathbf{p}^+,\mathbf{p}^-)W(\varepsilon,\mathbf{p}^+;\varepsilon,\mathbf{p}^-)d\mathbf{p}^+, \tag{6}$$

where the integration is over all states of incident electrons, i.e., that part of the Fermi surface with a positive normal component of velocity $\mathbf{v}$. In Eq. (6), $W(\varepsilon,\mathbf{p}^+;\varepsilon,\mathbf{p}^-)$ is determined mainly by the structure of the surface of interest, and $B(\varepsilon,\mathbf{p}^+,\mathbf{p}^-)$ is determined by the quantity measured. Under specular reflection, $W(\varepsilon,\mathbf{p}^+;\varepsilon,\mathbf{p}^-) = W_0\delta(\mathbf{p}^{-*} - \mathbf{p}^+)$, where $\mathbf{p}^{-*}$ is the crystal momentum after specular reflection. An ideal experiment would have $B(\varepsilon,\mathbf{p}^+,\mathbf{p}^-) \sim \delta(\mathbf{p}^- - \mathbf{p}^+)$, allowing direct measurement of $W(\varepsilon,\mathbf{p}^+;\varepsilon,\mathbf{p}^-)$. In practice, neither $B(\varepsilon,\mathbf{p}^+,\mathbf{p}^-)$ nor $W(\varepsilon,\mathbf{p}^+;\varepsilon,\mathbf{p}^-)$ is ever a pure delta function. For integral measurements, such as resistance or the static skin effect, $B(\varepsilon,\mathbf{p}^+,\mathbf{p}^-)$ is nonzero over the whole integration area. For a differential measurement, like TEF, $B(\varepsilon,\mathbf{p}^+,\mathbf{p}^-)$ is nonzero only in a solid angle, $\Delta\Omega$, that depends on b/L. The smaller $\Delta\Omega$, the better for isolating $W(\varepsilon,\mathbf{p}^+;\varepsilon,\mathbf{p}^-)$.

Due to surface disorder and imperfections, $W(\varepsilon,\mathbf{p}^+;\varepsilon,\mathbf{p}^-)$ also differs from the delta function expected for fully specular reflection; i.e., there is an angular distribution of the intensity of reflected electrons—the "indicatrix." Fully diffuse (isotropic) scattering gives a cosine distribution, i.e., $I(\theta) = I_0\cos\theta$, corresponding to Lambert's law in optics and Knudsen's law in gas kinetics.

1. Techniques other than TEF

The first important analysis of conduction-electron sample surface scattering was made by Fuchs (1938), who characterized the scattering process by one constant—the Fuchs parameter q_{Fc}. Most subsequent analyses of electron-surface scattering used his approach. Only in the limiting cases $q_{Fc} = 0$ or 1 is the Fuchs parameter equal to the probability of specular reflection q. Otherwise, q_{Fc} and q have no simple relation. Green (1969) and Okulov and Ustinov (1979) relate q_{Fc} and $W(\varepsilon,\mathbf{p}^+;\varepsilon,\mathbf{p}^-)$.

Thin-film resistivities are easy to measure, aside from sample preparation (Schumacher, 1993). But it is hard to extract q quantitatively, because (1) all electrons con-

tribute to the conductivity and different ones may reflect differently—the angle and λ_{dB} dependences of q may be crucial (Fal'kovski, 1983; Parrott, 1965), and (2) the "bulk" conductivity of thin films need not be that of the sample material.

Static-skin-effect studies (Azbel' and Peschanskii, 1965; Panchenko, Lutsishin, *et al.*, 1973; Panchenko, Kharlamov, and Ptushinskii, 1974; Panchenko, Lutsishin, and Ptushinskii, 1974; Lutsishin *et al.*, 1975; Mitryaev *et al.*, 1978; Bozhko *et al.*, 1979) have some advantages over size-effect studies. They involve bulk samples. The skin depth is much larger than the thickness of size-effect films, so that possible changes in conductivity due to changing surface conditions (as opposed to surface scattering) are less crucial. The magnetic field enhances the effect by causing multiple collisions with the surface of those electrons that skip along the surface and determine the conductivity. But there is a problem. Kapeliovich (1988) argues that electron-hole collisions, rather than specular or diffuse scattering, control the static skin effect. Even a weak channel of electron-hole transitions due to point defects or atomic-scale surface roughness can predominate. The magnetoresistance can then behave as expected for diffuse Fuchs scattering, even if the surface scattering is highly specular.

Other phenomena such as magnetic surface states (Khaikin, 1960, 1969; Nee and Prange, 1967), Schubnikov oscillations in thin plates (Kosevich and Lifshitz, 1955; Gaidukov and Galyamina, 1976, 1978), and Sondheimer oscillations in thin plates under specular reflection (Kirichenko *et al.*, 1974) have been used to study $W(\varepsilon,\mathbf{p}^+;\varepsilon,\mathbf{p}^-)$. None seems to have the specificity or generality of TEF.

2. TEF

The amplitude of the first peak in a TEF spectrum is determined by electrons from within a solid angle $\Delta\Omega$, which sets the area of integration in Eq. (6) for TEF. In the usual geometry with $\mathbf{H}\perp\mathbf{L}$, the plane angle of $\Delta\Omega$ in the plane parallel to $\mathbf{H}$ is set by those electrons with velocity parallel to $\mathbf{H}$ small enough that they do not move out of the collector aperture during their travel time from E to C (Fig. 1). In $\mathbf{k}$ space, such electrons lie within a small band on the Fermi surface bordering the extremal orbit being focused. The plane angle of $\Delta\Omega$ in the plane perpendicular to $\mathbf{H}$ is set by those electrons emitted not quite perpendicular to the surface, which still return to the surface within the collector aperture. Both angles are functions of the ratio b/L.

One can calculate $\Delta\Omega$ via the geometric model noted in Sec. I, assuming collection of only directly focused electrons. For a spherical Fermi surface, a simple geometrical construction gives $\Delta\Omega\sim(b/L)^{3/2}$ with the axis perpendicular to the sample surface (V. Tsoi *et al.*, 1992). $\Delta\Omega$ is asymmetric with respect to this axis: in the plane perpendicular to $\mathbf{H}$, its plane angle is $\sim(b/L)^{1/2}$, whereas in the plane parallel to $\mathbf{H}$, the angle is $\sim b/L$. This asymmetry of $\Delta\Omega$ has been used to study the anisotropy of electron scattering (Bozhko, 1989; V. Tsoi *et al.*, 1992). For a cylindrical Fermi surface, $\Delta\Omega$ is $\sim(b/L)^{1/2}$, for no displacement of the electrons along the cylinder axis.

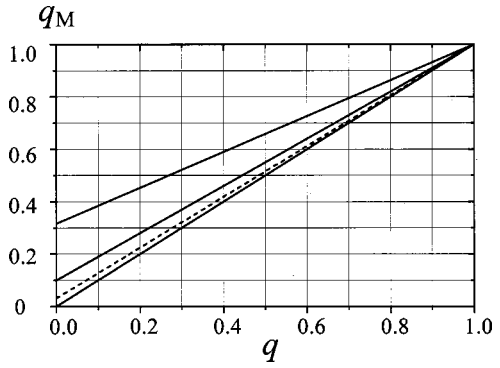

FIG. 10. Deviation of q_M from the straight-line $q_M=q$ for $b/L=0.1$ and 0.01 for Fermi surfaces that are cylindrical (solid lines) and spherical (dashed line for $b/L=0.1$ only—the dashed line for $b/L=0.01$ coincides with $q_M=q$).

If the electron mean free path l is not much larger than L, then the amplitude A_1 of the first TEF peak is proportional to $\exp(-s/l)$, where s is the path length of electrons moving from E to C [see Fig. 48(a)]:

$$A_1\sim f(b/L)\exp\{-s/l\}. \tag{7}$$

Here $f(b/L)$ accounts for the change of $\Delta\Omega$ with change in b/L, which depends upon the shape of the Fermi surface. For example, on a cylindrical Fermi surface, $f(b/L)=(b/L)^{1/2}$ and $s=(\pi/2)L$.

The amplitude A_2 of the second peak in a TEF spectrum is determined by only some of the electrons that form the first peak, mostly those reflected specularly from the surface within the angle $\Delta\Omega$ already described. It is important to emphasize that the ratio A_2/A_1 is independent of the ratio l/s, because the path lengths of direct and reflected electrons are the same (see Fig. 1).

For intravalley processes with $b\ll L$, few diffusely scattered electrons are collected, and the number of electrons determining A_2 is close to $N_0q(\pi/2)$, where N_0 electrons produce A_1. If, however, b is not $\ll L$, then the number of diffusely scattered electrons entering the collector can be significant, causing q_M to differ from q. The difference may be estimated as follows. The electrons forming the second TEF peak include (1) electrons reflected from the surface specularly and (2) electrons reflected from the surface diffusely, but moving within the solid angle $\Delta\Omega$. Separating these parts gives

$$q_M=q+(1-q)f(b,L). \tag{8}$$

The function $f(b,L)$ depends on the structure of the Fermi surface and the TEF geometry. If the Fermi surface is known, q_M may be corrected to give q. Figure 10 shows calculations for cylindrical (solid lines) and spherical (dashed line) Fermi surfaces for $b/L=0.01$ and 0.1. In the cylindrical cases, the difference between q_M and q is proportional to $(1-q)(b/L)^{1/2}$; in the spherical case, it is proportional to $(1-q)(b/L)^{3/2}$. For a typical

$b/L \leqslant 0.1$ and $q \ll 1$, the difference between q_M and q for a cylindrical Fermi surface will be $\geqslant 10$ times larger than for a spherical one.

In 3D samples, the "visual" b/L is usually $\ll 1$, which might mislead one to expect no problem. But defects produced during contact installation may greatly increase the effective contact size. To exclude such an effect, when the Fermi surface portion of interest is nearly cylindrical, so that $f(b,L)$ can be large, b/L should be estimated from the widths of the TEF peaks. We shall see in Sec. VI that resulting estimates of $b/L \sim 0.1$ in Bi are not unusual, and in Sec. X that most 2D electron-gas studies have even used visible values of $b/L \gg 0.1$.

V. METAL SURFACES

Prior to the TEF studies we describe, studies of electrical resistance (Schumacher, 1993), the static skin effect (Panchenko, Lutsishin *et al.*, 1973; Lutsishin *et al.*, 1975), and magnetic surface resonances (Khaikin, 1969) showed that electrons incident onto metal surfaces at glancing angles could be reflected with substantial specularity. The Gaussian roughness model of Eq. (3) could be used to understand such specularity, even with surface roughness larger than $\lambda_{dB} \sim a_0$. But about perpendicularly incident electrons nearly nothing was known. From Fig. 8, a high specularity probability q should be expected only for an atomically flat surface. However, in this section, we show that TEF observations of large q values (i.e., $q \sim 0.5$–0.9) in metals are more the rule than the exception. While this result was at first a puzzle, scanning tunnel microscopy (STM) studies have now shown that atomically flat regions often occupy a large fraction of low-index metal surfaces. In trying to maximize q, investigators presumably searched until they found flat regions.

Section V.A covers data on specularity of reflection from polished and roughened surfaces. Table I summarizes published values of q for such surfaces on a wide variety of metals. As just indicated, q is often large (~ 0.5–0.9) and, when it is, chemical etching reduces it only to ~ 0.3–0.4. Not only must large portions of the surfaces be initially flat, but also substantial flat regions must remain even after chemical etching. TEF allows the anisotropy of q on different crystal faces to be studied. The first question is whether any anisotropy exists. If so, the second question is whether it is due to anisotropy in the electronic or surface structure. Concerning the first question, for a given value of λ_{dB}, TEF studies show q to be the same for different crystal faces (isotropic) in some metals and to be different (anisotropic) in others. The physical source of the latter anisotropy is addressed in Sec. V.A.3. TEF also allows study of how q varies with λ_{dB}, a topic not previously addressed by any other technique. Clear-cut studies have been made so far only on W, where λ_{dB} varies from 6 to 51 Å. We shall see that different variations were found for the (011) and (001) surfaces, and that physical damage changes the variations for the (011) surfaces. These variations must thus result from different surface structures. Section V.A.2 concludes with an examination of how well the published results can be understood in terms of the random Gaussian roughness model of Eq. (3). When most of the published measurements were made, this was the accepted model for a metal surface. Interestingly, we shall see that most of the values of q in Table I are consistent with this model. However, Sec. V.A.3 will show that this consistency must often be accidental, since STM studies of two polished crystal faces each in Ag and W reveal different surface roughness profiles for different faces, none of which is Gaussian. Section V.A.3 shows that the combination of TEF and STM clearly establishes the physical source of the crystallographic anisotropies of q in Ag and W as anisotropy in the surface structure. Section V.A.3 concludes with an attempt to correlate anisotropy in q with anisotropy in the work function. Section V.A.4 reviews studies of surface contamination effects on q. In the only metal, W, for which detailed studies exist, q is large for an atomically clean (011) surface in UHV and for the same surface with a complete atomic overlayer of contaminant, but much smaller for a partial overlayer. A partial overlayer apparently destroys atomic flatness. Lastly, Sec. V.B shows that observations of specular hole reflection in TEF require an explanation involving Umklapp scattering.

A. Specularity of reflection from polished and roughened surfaces

1. Summary of experimental results

Most TEF measurements have been made on sample surfaces prepared and kept in air. Such surfaces are inevitably oxidized and saturated with adsorbed atoms and molecules. Table I contains what we believe to be an essentially complete collection of the probabilities of specular reflection at perpendicular incidence q found from TEF measurements on different crystal faces of metals and semimetals under such conditions. One set of measurements on W cleaned in UHV is also included. As described in Sec. I, the values of q were determined from ratios of the amplitudes of TEF peaks from data like those in Fig. 2. In this section, we focus on the metals, where the information available allows important conclusions to be drawn.

Aside from two smaller uncertainties for Ag (where measurements for a large number of locations were statistically averaged), the uncertainties in Table I are to be understood as $\pm$ 0.1 in the context that the values of q listed represent the largest values found for a given crystal face. Most investigators wished either to maximize q or to compare q's for different crystallographic directions, where taking the maximum value for each direction was perceived to minimize effects of differences in surface roughness (see, V. Tsoi *et al.*, 1979). Independent measurements of q for the same surface of the same metal give values that rarely differ by more than 0.2, the sum of the uncertainties of the two measure-

TABLE I. Values of q, the probability of specular reflection, for different metals, reflecting surfaces, de Broglie wavelengths λ_{dB}, directions of **H**, carriers (e=electrons, h=holes), and surfaces: po=polished, el=electropolished, me=mechanically polished, ce=chemical etched, io=ion etched, et=etched, da=damaged, di=dirty, at=atomically clean. λ_{dB} was calculated from the corresponding diameter of the Fermi-surface valley.

Metal	Face	q	λ_{dB}(Å)	**H**‖to	Carrier	Surface	Ref.
Ag	(011)	0.6	5.2	[1$\bar{1}$1]	e	po	a
	(011)	0.3	5.2	[1$\bar{1}$1]	e	po	b
	(011)	0.37±0.03	5.2	[1$\bar{1}$1]	e	po	c
	(011)	0.9	5.2	[100]	e	po	d
	(011)	0.3	9.6	[110]	e	po	d
	(001)	0.7	5.2	[1$\bar{1}$1]	e	po	a
	(001)	0.64±0.02	5.2	[100]	e	po	c
	(001)	0.5	5.2	[100]	e	po	b
	(001)	0.5	9.6	[100]	h	po	b
	(001)	0.8	5.2	[100]	e	po	d
	(001)	0.8	9.6	[100]	h	po	d
Al	(001)	~0	4.3	[100]	h	po	e
	(001)	0.5	4.2	[110]	h	po	e
	(001)	0.3	4.2	[110]	h	cl	e
	(011)	~0	4.6	[100]	h	po	e
	(011)	0.5	4.6	[01$\bar{1}$]	h	po	e
	(011)	0.25	4.7	[1$\bar{1}$1]	h	po	e
	(011)	0.3	4.7	[1$\bar{2}\bar{2}$]	h	cl	e
	(111)	0.6	6.1	[1$\bar{1}$0]	h	cl	e
	(111)	0.55	6.2	[$\bar{1}\bar{1}$2]	h	cl	e
Bi	(111)	0.6	900	[1$\bar{1}$0]	e	po	f
	(111)	1.0	900	[1$\bar{1}$0]	e	po	g
	(111)	0.6	140	[1$\bar{1}$0]	h	po	h
	(111)	<0.2	900	[1$\bar{1}$0]	e	io	i
	(111)	<0.2	900	[1$\bar{1}$0]	e	cl	j
	(1$\bar{1}$0)	<0.2	1200	[11$\bar{2}$]	e	po	g
	(1$\bar{1}$0)	0.9	450	[111]	h	po	h
	(11$\bar{2}$)	<0.2	1000	[1$\bar{1}$0]	e	po	k
Cu	(011)	0.35	4.6	[100]	e	po	l
	(011)	0.35	4.6	[1$\bar{1}$1]	e	po	m
	(001)	0.45	4.6	[100]	e	po	m
	(012)	0.9	6.6	[100]	h	po	n
	(012)	0.4	4.6	[100]	e	io	n
	(014)	~0.3	4.6	~[100]	e	po	o, p
In	(001)	~0	5	[110]	h	po	n
K		~0	8.4		e	cl	n
Na		~0	6.8		e	cl	n
Mo	(111)	0.3	10	[1$\bar{1}$0]	h	el	n
Sb	(111)	0.1	120	[1$\bar{1}$0]	e	el	q
	(111)	0.8	140	[1$\bar{1}$0]	h	el	q
Sn	(100)	0.5	8	[001]	e	cl	n
	(100)	0.5	8	[001]	h	cl	n
	(110)	~0	8	[001]	e	cl	n
W	(011)	0.65	51	[100]	h	el	l, r
	(011)	0.65	23	[100]	e	el	l, r
	(011)	0.65	10.5	[100]	h	el	l, r
	(011)	0.65	23	[2$\bar{1}$1]	e	el	l, r
	(011)	0.65	13.5	[2$\bar{1}$1]	e	el	l, r
	(011)	0.65	10.5	[2$\bar{1}$1]	h	el	l, r
	(011)	0.3	23	[2$\bar{1}$1]	e	et	l
	(011)	0.3	13.5	[2$\bar{1}$1]	e	et	l

TABLE I. (*Continued*).

Metal	Face	q	λ_{dB}(Å)	**H**∥to	Carrier	Surface	Ref.
	(011)	0.3	10.5	[2$\bar{1}$1]	*h*	et	l
	(011)	0.5	51	[100]	*h*	da	r
	(011)	0.3	23	[2$\bar{1}$1]	*e*	da	r
	(011)	0	13.5	[2$\bar{1}$1]	*e*	da	r
	(011)	0	10.5	[2$\bar{1}$1]	*h*	da	r
	(011)	0	10.5	[100]	*h*	da	r
	(011)	0.55	13.5	[0$\bar{1}$1]	*e*	at	s
	(011)	0.2	13.5	[0$\bar{1}$1]	*e*	di	s
	(011)	0.55	23	[100]	*e*	at	s
	(011)	0.2	23	[100]	*e*	di	s
	(011)	0.55	10.5	[0$\bar{1}$1]	*h*	at	t
	(011)	0.2	10.5	[0$\bar{1}$1]	*h*	di	t
	(001)	0.7	50	[100]	*h*	el	r
	(001)	0.3	26	[100]	*e*	el	r
	(001)	0.1	26	[100]	*e*	el	l
	(001)	0.1	8.2	[100]	*h*	el	l, r
	(001)	0	5.7	[100]	*e*	el	r
	(001)	0	8.2	[110]	*h*	el	r
	(001)	0	5.7	[110]	*e*	el	r
	(001)	0.3	26	[0$\bar{1}$1]	*e*	at	t
	(001)	0	26	[0$\bar{1}$1]	*e*	di	t
	(331)	0.5	13	[$\bar{2}$13]	*e*	me	n
	(331)	0.4	10	[$\bar{2}$13]	*h*	me	n
	(112)	0.3	13	[$\bar{1}\bar{1}$1]	*e*	me	n
	(112)	0.5	23	[$\bar{1}\bar{1}$1]	*e*	me	n
	(112)	0.5	50	[$\bar{1}\bar{1}$1]	*h*	me	n
	(112)	0.4	10	[$\bar{1}\bar{1}$1]	*h*	me	n
	(111)	0.2	10	[1$\bar{1}$0]	*h*	me	n
Zn	(0001)	0.6	15	[1$\bar{1}$00]	*e*	po	u
	(0001)	0.6	15	[11$\bar{2}$0]	*e*	po	u
	(0001)	0.35	15	[11$\bar{2}$0]	*e*	ch	u
	(1$\bar{1}$00)	0.5	6.3	[11$\bar{2}$0]	*e*	po	u
	(11$\bar{2}$0)	0	6.3	[1$\bar{1}$00]	*e*	po	u
	(11$\bar{2}$0)	0.3		[0001]	*h*	po	u
	(11$\bar{2}$0)	<0.15	various	[0001]	*e* & *h*	po	u

[a] Tsoi *et al.* (1979).
[b] Benistant *et al.* (1983).
[c] Benistant *et al.* (1986).
[d] Benistant (1984).
[e] Sato and Yonemitsu (1986).
[f] V. Tsoi (1974).
[g] V. Tsoi and N. Tsoi (1977).
[h] Sveklo and Tsoi (1993).
[i] Bozhko *et al.* (1982).
[j] Tsoi (1975a).
[k] Bozhko and Tsoi (1987).
[l] Tsoi and Razgonov (1977).
[m] Birker *et al.* (1978).
[n] Bozhko, Sveklo, and Tsoi (1988).
[o] Hoevers and van Kempen (1991).
[p] Hoevers *et al.* (1992).
[q] Tsoi and Razgonov (1976).
[r] Tsoi and Razgonov (1978).
[s] Mitryaev *et al.* (1978).
[t] Bozhko *et al.* (1979).
[u] Sato and Kimura (1984).

ments. It is not yet known if this agreement is intrinsic or due to similar sample-preparation techniques.

The first important point is that high specularity, i.e., $q \geqslant 0.5$, has been found for at least one crystal face of most of the metals studied, with the largest values, $q = 0.9$, reported for polished (011) Ag and (012) Cu. Such values mean that substantial portions of these crystal faces must be atomically flat. In contrast, values of $q \leqslant 0.1$ for polished surfaces are unusual, having been reported only for (001) and (011)Al, (001)W, and (1120)Zn. Completely diffuse scattering (i.e., $q = 0$) for polished surfaces seems to be rare, having been seen only in In, K, and Na. The extreme softness of these metals may contribute to the diffuse reflection, but the source of this behavior is not yet established.

Experimental values of q as high as 0.8–0.9 mean that the corrugation surface amplitudes discussed in Sec. IV.A, which determine the maximum possible value of q, must be $\leqslant$0.2 Å. Thus we shall not consider corrugation further. To see the effects of such small surface corrugation will require TEF measurements on nearly perfect crystals with atomically flat surfaces.

The value of q for scattering of excitations with close values of λ_{dB} from a given polished crystal face is usually the same for different crystallographic orientations of the TEF probes. Examples are (0001)Zn, (011)W, (011)Cu, and (011)Ag. Such results mean that q is usually determined by the structure of the crystal face, not by subtleties of the electronic structure. (001)Al and (011)Al are discrepant, since $\mathbf{H}\|[100]$ gives $q=0$, but $\mathbf{H}\|[110]$ or [011] gives $q\sim0.5$. Sharp edges on the Al Fermi surface might make the focusing orbits for $\mathbf{H}\|[100]$ sensitive to deviations of $\mathbf{H}$ and $\mathbf{N}$ from crystallographic directions, causing small misalignments to suppress higher-order peaks. Another possibility is strong anisotropy of surface scattering due to anisotropic surface terracing, such as occurs for the (012)Cu surface (Bozhko, 1989; V. Tsoi *et al.*, 1992). Further TEF measurements are needed to clarify this issue.

A fundamental question first addressed by TEF is whether q for a given value of λ_{dB} is isotropic over different crystal faces. The data in Table I suggest anisotropy in Sn, Zn, W, and Ag. We shall examine this issue further for Ag and W in Sec. V.A.3, invoking the aid of STM measurements.

Another fundamental topic about which TEF has given unique information is how q for a given crystal face varies with λ_{dB}. This issue has been examined in W (V. Tsoi and Razgonov, 1977, 1978), which has a complex Fermi surface containing one electron and a few hole "valleys" with λ_{dB} ranging from 6 to 51 Å. For electropolished (011) surfaces, $q\approx0.65$ was large and independent of λ_{dB}. Importantly, for this face, etching only reduced q by a constant factor (down to $\sim$0.3–0.4) for all λ_{dB} studied. However, physical damage produced by installing the TEF contacts under 200 V and 1 kΩ instead of the usual 100 V and 1 MΩ (see Table I) caused q to vary with λ_{dB}—from 0.5 for $\lambda_{dB}=51$ Å down to 0 for $\lambda_{dB}=10.5$ Å. On the electropolished (001) surface, in contrast, q varied with λ_{dB} from the start—it was large ($q\approx0.7$) for holes with $\lambda_{dB}=50$ Å, but much smaller for electrons with $\lambda_{dB}=26$ Å ($q=0.3$) and holes with $\lambda_{dB}=8$ Å ($q=0$). As these data were measured with fixed contact locations, all current carriers were reflected from the same surface area with the same surface roughness.

Comparisons of q after polishing and chemical etching have also been made on (001)Al (Benistant, 1984; Benistant, van Kempen, and Wyder, 1985), and (0001)Zn (Sato and Kimura, 1984) surfaces. For both metals, as for (011)W, when q began high ($q\geqslant0.5$)—indicating an initial surface that was mostly atomically flat—etching only partially suppressed it ($q\sim0.3$–0.35). Apparently, such etching produces terracing, with large atomically flat areas. Such studies show that the atomic order of a metal surface is not fully destroyed, even when the surface becomes dead (diffuse) for reflecting light.

2. Testing the random Gaussian roughness model

To try to synthesize these results, we ask how well they can be understood simply in terms of different amounts of surface roughness estimated from the Gaussian random roughness model [Eq. (3)]. For most metals, where $\lambda_{dB}\sim5-10$ Å, the highest values for polished surfaces, $q=0.9$, require mean-square roughness heights $\eta\sim0.1$–0.3 Å, and the lowest, $q=0-0.1$, require $\eta\geqslant0.6$–1.2 Å. The highest values of q thus correspond to atomically flat surfaces with only a small fraction of surface defects a few atomic layers high, and even the lowest values do not need η to be as large as a single atomic layer. Most of the observed changes in q upon etching require changes in η of only $\Delta\eta\leqslant1$ Å, a spacing of less than an atomic layer, as well. These data are thus consistent with the Gaussian roughness model, if the surfaces are atomically flat except for (usually) small numbers of randomly distributed defects one to a few atomic layers high.

The situation is more complex in W, where λ_{dB} ranges from 6 to 51 Å. If each value of q is uncertain to ±0.1, then the variations of q with λ_{dB} for both polished and "dirty" (001)W surfaces can be approximately fit by Eq. (3) with $\eta\sim2.5$ Å, the etched (011) surface can be fit by $\eta\sim1.5$ Å, and the "damaged" (011) surface roughly by $\eta\sim2.5$ Å, although in this last case Tsoi and Razgonov (1978) noted that trying to fit q vs λ_{dB} with a single η missed data points by more than the experimental error. These data, then, all appear to be roughly compatible with the Gaussian roughness model of Sec. IV.B.1. That model fails clearly only for the nearly constant values of $q=0.65\pm0.1$ for the polished (011)W surface, since there $\lambda_{dB}=50$ Å needs $\eta\cong2$ Å, but $\lambda_{dB}=8$ Å needs $\eta\leqslant0.6$ Å.

With this background, we now turn to what has recently been learned from STM studies.

3. Scanning tunneling microscopy and anisotropy of specular reflection

STM and TEF measurements have been combined to study the anisotropy of q in Ag (Benistant *et al.*, 1986) and W (Tsoi and Razgonov, 1977, 1978; Pryadkin and Tsoi, 1988).

In Ag, the usual nonsystematic measurements did not clearly establish any anisotropy in q (see Table I). To search for such anisotropy, mean square values of q were found by statistically averaging $\sim$100 measurements each over chemically polished (001) and (011) faces. This averaging revealed a clear difference: $q=0.64\pm0.02$ for (001) and $q=0.37\pm0.03$ for (011). Scanning tunneling microscopy images of the same surfaces were recorded under UHV. The (001) surface generally consisted of large, atomically flat terraces, 300–1000 Å across, with step heights between terraces varying from 4.0 Å (one unit cell) to $\sim$100 Å. The (011) surface was more hilly, with atomically flat regions curving smoothly

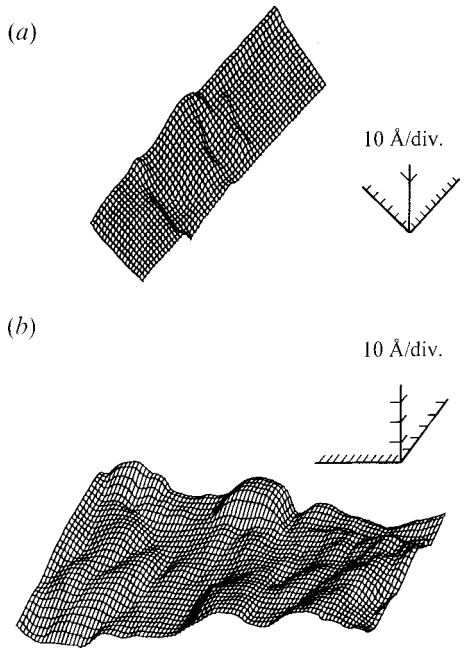

FIG. 11. Typical STM images: (a) the W (011) surface of an electropolished sample; (b) the W (001) surface of an electropolished sample. After Pryadkin and Tsoi, 1988.

into highly corrugated ones. For this surface, a simple geometrical optics analysis associated the observed q with a critical angle of $\theta_0 \sim 3°$ for collecting specularly reflected electrons. For the (001) surface, both the roughness profile and the nature of the electron orbits on the Fermi surface were more complicated. Here a complex 2D analysis was needed to approach the experimental results quantitatively (Benistant *et al.*, 1986).

The first evidence of crystallographic anisotropy of surface reflection in (001)W and (011)W came from static-skin-effect measurements (Panchenko *et al.*, 1973; Lutsishin *et al.*, 1975). The first TEF studies of these two faces were made by Tsoi and Razgonov (1977, 1978), with STM measurements and analysis by Pryadkin and Tsoi (1988). The STM images were made in air just after electrochemical polishing. The (001)W surface [Fig. 11(a)] consisted of atomically flat areas (500–1000 Å wide) with large steps (20–200 Å) along [011]. In contrast, the (001)W surface [Fig. 11(b)] was faceted, with faces mostly (013) or between (013) and (001). Averages over lengths of 500–1000 Å gave average roughness heights of 2–3 Å for the (011) W surface and 8–10 Å for the (001)W surface. The value of 8–10 Å for (001)W is 3–4 times the 2.5 Å estimated above for uncorrelated Gaussian roughness, and 2–3 Å for (011) W is at the high end of the range derived for such roughness. Thus Eq. (3) does not apply well to these data. For (011)W, the lack of dependence of q upon λ_{dB} was attributed to scattering from atomically flat surfaces, with q measuring the fraction of the surface that was flat and oriented nearly parallel to the median plane. For (001)W, the scattering process was modeled by wave optics in which a plane wave is scattered from a 1D triangular surface profile with a measured roughness of 8 Å, assuming specularity for reflections within an angle θ_0. Agreement with the observed variation of q with λ_{dB} was found for $\theta_0 \sim 5°$, comparable to the estimated collection aperture ($b/L \sim 0.1$ radians) and to $\theta_0 \sim 3°$ for Ag.

For all four surfaces, the observed values of q are consistent with simple geometrical or wave-optics analyses of the actual, non-Gaussian structures. The only case in which a random Gaussian surface structure might apply to W or Ag is artificially produced damage on (011)W (Tsoi and Razgonov, 1978), and even there, agreement of TEF data with a Gaussian roughness model is only fair.

We end this section by asking if the observed TEF anisotropies in Ag and W can be correlated with a physical parameter underlying crystallographic anisotropy. The obvious parameter is surface tension, since in thermodynamic equilibrium a surface not having the minimum tension energy should be stepped or faceted, because the surfaces of the steps and facets have smaller tension energy terms (Zangwill, 1988). Unfortunately, there do not appear to be reliable data on surface-tension anisotropy in Ag or W.

The closest parameter for which we have reasonable information is the work function, for which Smoluchowski (1941) developed a simplified analysis. Here, too, a rougher surface should lead to a lower work function and vice versa; hence a lower work function leads to lower specularity. We can test the proposal that the lower the work function, the lower the probability of specular reflection. In Ag, the work functions for (110) and (001) surfaces differ by less than 3%—4.52 ± 0.02 eV and 4.64 ± 0.02 eV (Holzl *et al.*, 1979). This small anisotropy is consistent with the need for careful mean-square value measurements of q to isolate any anisotropy (Benistant *et al.*, 1986). In contrast, the anisotropy in W is about 15%—5.30 ± 0.12 eV for (011) and 4.58 ± 0.08 eV for (001) (Fomenko, 1970)—and the differences in q for the different faces are also larger (Table I). This analysis needs further testing. Unfortunately, there are few accurate measurements of work-function anisotropy.

4. Effects of an adsorbed film

Little is yet known about the influence of adsorbed films on conduction-electron scattering from a sample surface. Such absorption causes changes in the electrical resistances of thin metal films (see Schumacher, 1993 and references therein), but it is difficult to determine the reason for these changes. The chemical nature of the adsorbate is usually not well known and changes in the character of surface electronic states may dominate over changes in electron scattering from the sample surface. Using bulk crystals decreases unwanted nonscattering effects, but suppresses the surface effects of interest.

The only systematic TEF studies of the effects of adsorbed films on q have been made on the (001) and (011) surfaces of W (Tsoi and Razgonov, 1977, 1978; Mitryaev *et al.*, 1978; Bozhko *et al.*, 1979). In W, techniques for making atomically clean crystal faces are well

developed, and behaviors can be compared for excitations with different λ_{dB}. Three surface conditions were examined: (1) Surfaces just electrochemically polished, presumed saturated by adsorbed gases. (2) Electropolished surfaces first treated in a complex way in UHV to give an atomically clean surface, then allowed to adsorb gases from the residual atmosphere (10^{-9}–10^{-8} Torr) of the UHV system. These surfaces are presumed to be unsaturated. (3) Atomically clean surfaces produced by flash-heating the sample to 2000 K by means of an electric current while submerged in liquid helium. The structure of an atomically clean W surface is well studied (van Hove and Tong, 1985).

Table I shows that reflections of two different electrons and one hole from the (110) surface of W were all highly specular and nearly the same when the surface was atomically clean ($q=0.55$) or saturated with adsorbed gas atoms and molecules ($q=0.65$). The unsaturated "dirty" W (110) surface, however, reflected all three carriers more diffusely ($q=0.2$). Such behavior agrees with the prediction in Lessie (1979) that roughness should be proportional to $c(1-c)$ where c is the fractional impurity coverage—i.e., q is maximum for both $c=0$ and $c=1$. However, that analysis assumed only monospecies absorption and monolayer substitution, whereas the real W surfaces were covered by a mixture of species. Apparently, such a mixture can also cause smoothing. One possible explanation is that the potentials of the different species are similar. Alternatively, oxidation might control the situation. Years of sample storage under open conditions where oxidation occurs without hindrance do not affect q (Pryadkin and Tsoi, 1988; Bozhko *et al.*, 1988). This result suggests that the shape of the interface between the metal and the native oxide layer must often reproduce the metal surface shape outside the oxide. Such a situation is found at semiconductor-oxide interfaces (Hasegava *et al.*, 1987).

B. Umklapp process

In a Peierls Umklapp process, the change in an electron's momentum $\Delta\mathbf{p}$ involves a reciprocal-lattice vector $\mathbf{G}$. In this section we show that such a process is required for the observed (Table I) intravalley specular reflection of electrons executing "hole" orbits (Sec. II.1) in metals (V. Tsoi, 1996).

Figure 1 shows the simplest TEF case—perpendicular emission from a horizontal surface, and specular reflection of conduction electrons moving on spherical arcs of spherical portions of the Fermi surface. When such an electron impacts the surface, a force $\mathbf{F}$ acts on it during a collision time Δt, changing its momentum by $\Delta\mathbf{p}=\mathbf{F}\Delta t$. For specular reflection upon perpendicular incidence, this force returns the electron to the momentum state it was in when it was first emitted. The electron's velocity must be directed toward the interface before reflection and away from it after reflection. $\Delta\mathbf{p}$ must be in the same direction as $\mathbf{F}$, pointing away from the interface. Figure 12(a) shows the resulting kinetics of electron reflection in $\mathbf{p}$ space. An incident electron in state I_i ($i=1,2,3$) is reflected into state R_i. Under scattering at a rough surface the wave phase shift $\Delta\varphi$ is proportional to $\Delta\mathbf{p}$ [Eq. (4)], which here is just the Fermi diameter. Figure 12(a) shows three Fermi spheres of different diameters. When $\Delta\mathbf{p}$ is small, $\Delta\varphi$ is small, giving specular reflection. Increasing $\Delta\mathbf{p}$ increases $\Delta\varphi$, reducing the specularity. For the spheres in Fig. 12(a), $\Delta\mathbf{p}$ increases in the order I_1, I_2, I_3, and we would expect $q_1>q_2>q_3$.

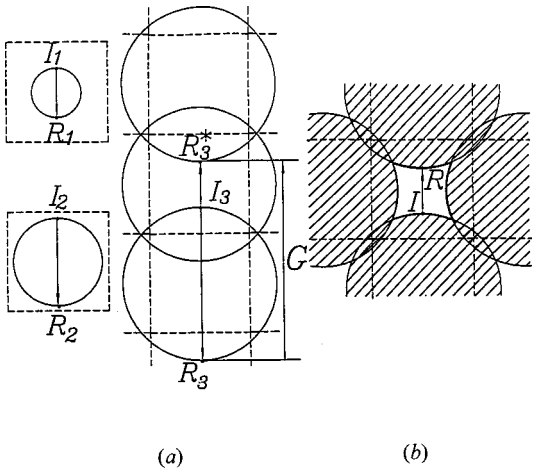

FIG. 12. Kinetics of electron reflection from a surface in $\mathbf{p}$ space. Momentum transfers are shown for specular reflection of (a) electrons and (b) a hole. The hole reflection requires an Umklapp process with reciprocal vector $\mathbf{G}$. Dashed lines indicate Brillouin-zone boundaries.

The situation changes, however, if the Fermi sphere is larger than the first Brillouin zone—case I_3 in Fig. 12(a). In this case, translation by a reciprocal-lattice vector $\mathbf{G}$ makes state R_3 equivalent to state R_3^*. The Umklapp transition from I_3 to R_3^* is then associated with the smaller $\Delta\mathbf{p}$ from I_3 to R_3^*. Figure 12(b) shows the Harrison construction that gives the hole orbit associated with this smaller $\Delta\mathbf{p}$. In hole terms, a hole incident onto a surface in state I is reflected into state R, with $\Delta\mathbf{p}$ equal to the vector IR. But from Fig. 12(a) and the remarks above, we see that the transition from I_3 to R_3^* must involve the reciprocal-lattice vector $\mathbf{G}$. This expectation is confirmed by measurements of q in W for electrons and holes of different valleys under reflection from rough surfaces [polished (001) and damaged (011) faces], which show that q is a monotonic function of valley diameter (see Table I and Sec. V.A.1), independent of whether the valley is electronlike or holelike (λ_{dB} in Table I was calculated from the diameter of the appropriate W Fermi-surface valley).

VI. SEMIMETAL SURFACES, ESPECIALLY Bi

The semimetals Bi, Sb, and As have lower conductivities than metals, due to their low current-carrier concentrations. These low concentrations yield values of $\lambda_{dB} \gg a_0$—e.g., in Bi, $\lambda_{dB}\sim 1000$ Å. For a free-electron gas, $q\approx 1$ would then be expected. Khaikin and Edelman

(1964) found a high probability of specularity for a large angle of incidence (~70°) in a unique Azbel-Kaner cyclotron-resonance experiment on a thin Bi single-crystal plate under conditions where the electron orbit was cut off by the sample surface. We shall see that TEF studies paint a more complex picture.

Most TEF measurements on semimetals have been made on Bi, a few on Sb, and none on As. Bi looks ideal for studying free-electron-like surface scattering, as cross sections of its Fermi surface give elliptical electron or hole orbits, with different values of the de Broglie wavelength λ_{dB} all greater than a_0. However, a main point of this section will be that surface scattering in Bi is quite different from that for a free particle. Surprisingly, Bi seems to be a model laboratory for manifesting differences between surface scattering of free electrons and scattering of those in a periodic potential. Instead of λ_{dB} controlling the probability of specular reflection q, in many cases q is controlled by an interplay between (1) intervalley scattering, originating from the multivalley structure of the Bi Fermi surface, which allows roughness on an atomic scale $\ll\lambda_{dB}$ to greatly reduce q, and (2) long-range charge screening due to band bending (Sec. IV.C), which screens such roughness, thereby increasing q.

A large number of interesting new phenomena have been seen for the first time in Bi by means of TEF. In Sec. VI.A, we briefly describe the crystal structure and the Fermi surface of Bi, which will be needed to understand the physics underlying TEF in Bi. In Sec. VI.B, we examine the crystallographic anisotropy of q in Bi for the standard TEF geometry. The q for electrons reflected from untreated, electropolished, or cleaved surfaces is high (~0.8) for scattering from the (111) plane, but much lower (~0.2) for $(1\underline{1}0)$. The q for holes is also fairly high (~0.6) for (111), but even higher (~0.9) for $(1\underline{1}0)$. Chemical and ion etching both drastically reduce the large q values for electrons on (111) and holes on $(1\underline{1}0)$, by as much as in metals, but only modestly reduce the somewhat smaller q for holes on (111) and actually increase the initially small q for electrons on $(1\underline{1}0)$. To complete the picture, we shall find that q in Sb is large for reflection of electrons from the (111) surface, but small for reflection of holes. This wide range of behaviors for Bi and Sb cannot be understood simply on the basis of free-electron-like intravalley scattering. Rather, they require a combination of effects due to intervalley scattering and band bending. In Sec. VI.C, we describe how an unusual measurement geometry (drift electron focusing, or DEF) allows the determination for Bi of $q(\theta)$, the dependence of q on the angle of incidence of electrons onto the (111)Bi surface. In Sec. VI.D, we describe experiments designed to measure intervalley scattering. Moving the *EC* line out of the planes perpendicular to the longest axes of the highly elongated electron ellipsoids in Bi makes it impossible for an electron to reach the collector without intervalley scattering. In Sec. VI.D.1, we show that increasing surface roughness increases electron-electron intervalley scattering to the point where the probability for such scattering can be comparable to that for intravalley scattering. This is just what is required for intervalley scattering to strongly affect the data of Sec. VI.B. In Sec. VI.D.2 we describe how three contacts have been used to determine the probability of electron-hole intervalley scattering. Increasing surface roughness also increases such scattering. Section VI.E describes two experiments on band bending. Section VI.E.1 shows how band bending can explain the unusual behavior of higher-order TEF peaks for the $(1\underline{1}0)$ Bi surface. Section VI.E.2 describes a successful experiment to change q by artificially inducing band bending.

A. Bi Crystal lattice, Fermi surface, and sample characteristics

The Bi lattice is rhombohedral, slightly distorted from body-centered cubic (bcc). Its symmetry elements are (1) A sixfold [111] glide axis, called trigonal $\mathbf{C}_3$; (2) three twofold axes (binary $[1\underline{1}0]$ axes—$\mathbf{C}_2$) perpendicular to $\mathbf{C}_3$; and (3) three mirror planes (bisector planes) perpendicular to $\mathbf{C}_2$. The Brillouin zone is slightly distorted from that for the bcc lattice, with two atoms per equivalent cubic unit cell. Bismuth is almost an insulator, but slight band overlap gives a compensated semimetal with small, equal numbers of electrons and holes. Its electronic spectrum is well known (Fal'kovskii, 1968; Edel'man, 1976).

The Fermi surface of Bi consists of three electron "ellipsoids" centered at points L and one hole ellipsoid of rotation centered at T. The hole ellipsoid is elongated along axis $\mathbf{C}_3$, and the longest axes of the electron ellipsoids are in the mirror planes and inclined from the basal plane by $6°23'$. The electron and hole concentrations are $n_e = n_h \approx 10^{-5}$/atom. Both electrons and holes have almost quadratic (p^2) dispersion, but different Fermi energies: for electrons, $\varepsilon_F^e = 0.0276$ eV relative to the bottom of the conduction band, and for holes, $\varepsilon_F^h = 0.0109$ eV relative to the top of the valence band.

Importantly for most TEF studies on bismuth, the electron ellipsoids are highly elongated and deviate from ellipsoidal shape toward cylindrical (Edel'man, 1976). Transverse electron focusing analysis is greatly simplified by replacing the ellipsoids with cylinders. Then, as shown in Sec. II.A, the electrons always move in real space in the plane perpendicular to the *cylinder* axis and, when the angle between $\mathbf{H}$ and the cylinder axis is nonzero, their displacement along the surface is $L = 2R_c(\varphi) = 2R_c/\cos\varphi$. Only when the ends of the ellipsoids are important (Sec. VI.C) must the ellipsoidal form of the Bi-electron Fermi surface be retained.

The Bi samples of the studies we review were single crystal discs of diameter 10 or 18 mm and thickness 0.2–2 mm, usually grown in a polished-quartz demountable form (Sharvin and Gantmakher, 1963). To get single crystals with flat surfaces coinciding with low Miller index planes, some crystals were grown by the Czochralski method (see, e.g., McKelvey, 1966). Most samples had the $\mathbf{C}_1$ or $\mathbf{C}_2$ axis, or both, parallel to the sample surface, denoted by its normal $\mathbf{N}$. The first sur-

faces studied were usually as grown, but some cleaved or electrochemically polished surfaces were also studied. Optical magnification to 1000 and electron magnification to 45 000 were used to check surface structure. Untreated surfaces were homogeneous—no structure was seen. Some surfaces were roughened by (1) chemical etching in different solutions or (2) Ar^+ ion etching (Bozhko and Tsoi, 1987; Sveklo and Tsoi, 1989b, 1992; V. Tsoi *et al.*, 1989). The surface structures obtained were very different: chemical etching gave faceting with flat areas a few μm across, whereas after ion etching neither optical nor electron microscopes showed any changes in surface structure—the surfaces still looked perfect.

B. Crystallographic and charge anisotropy and effects of surface treatment

The main objective of the first TEF studies on Bi was to see whether q varied with λ_{dB}, i.e., to look for any crystallographic anisotropy of q (V. Tsoi and N. Tsoi, 1977; Bozhko and Tsoi, 1987). The velocities and mean free path of holes in Bi are much shorter than those for electrons, necessitating much smaller contact separations ($\leqslant 50$ μm) for TEF studies (Sveklo and Tsoi, 1989a, 1993). The first studies thus focused on electrons. To present the available information most simply, we deviate from historical order and consider the data on electrons and holes together, along with data on electrons and holes in Sb.

In Sec. IV.D.2, we showed that, for a cylindrical Fermi surface and small q, b/L as large as ~ 0.1 gives a measured q_M significantly larger than the intrinsic q of interest. Most Bi TEF data on Bi are for nearly cylindrical electron Fermi-surface portions, and the TEF peak widths yield $b/L \sim 0.1$. Thus values of $q_M = 0.2$–0.3 for Bi electrons must be viewed as upper bounds on q.

1. Electron and hole reflections in Bi for (111) and (1$\bar{1}$0) surfaces

We start with TEF data for electrons q_e and holes q_h reflected from Bi(111) ($\mathbf{N} \| \mathbf{C}_3$) and (1$\bar{1}$0) ($\mathbf{N} \| \mathbf{C}_2$) surfaces, with and without etching. The chosen directions of **N**, **H**, and **L** allow intravalley scattering to bring both electrons and holes from E to C, but different orientations and treatments lead to different results for the two carriers. Figures 13(a), 14(a), and 14(b) show examples of data for untreated samples, and Fig. 13(b) is for an etched surface. The values of q_M for both untreated and etched samples are given in Tables I and II. To within uncertainties of ± 0.1, no differences were found in values of q_M for untreated samples grown in quartz forms, samples grown by the Czochralski method, or electropolished samples. We thus designate all three cases as "polished" or "untreated." Despite the very different surface structures they produced, chemical and Ar^+ ion etching both reduced q similarly (V. Tsoi, 1975; Bozhko, Tsoi, and Yakovlev, 1982; Bozhko, Sveklo, and Tsoi, 1989). In all the geometries shown, **H** is in the surface plane—$\mathbf{H} \perp \mathbf{N}$. Figure 13 shows examples for the untreated and chemically etched (111) surface $\mathbf{N} \| \mathbf{C}_3$ (V. Tsoi, 1975; V. Tsoi and N. Tsoi, 1977). Before etching, $q_e (\approx 0.7)$ was slightly larger than $q_h (\approx 0.6)$, and etching reduced both to ~ 0.2–0.4 (Table II). Figure 14(a) shows $U(H)$ for the geometry $\mathbf{N} \| \mathbf{C}_2$, $\mathbf{L} \perp \mathbf{C}_3$, and $\mathbf{H} \perp \mathbf{L}$, where the amplitude of the first hole peak is maximum. The hole focusing spectrum is very nice, but the electron spectrum is unusual in containing an irregular, multipeak structure in $U(H)$ which is not only nonperiodic, but also nonmonotonic with increasing peak number. This electron spectrum was very sensitive to the direction of the contact line with respect to the crystallographic axis of the sample; when **H** was rotated, some peaks shifted to higher field and others disappeared. This structure is probably due to focusing of electrons on nonextremal cross sections of the Fermi ellipsoid, and has not yet been studied in detail. Figure 14(b) shows data for $\mathbf{N} \| \mathbf{C}_2$, $\mathbf{H} \perp \mathbf{L}$, $\mathbf{L} \perp$ largest axis of electron ellipsoid for the same face as Fig. 14(a), but a different orientation of **L**. For this face, before ion etching q_h (≈ 0.9) was much larger than q_e (≈ 0.2), but etching reduced q_h by about half and increased q_e to almost as

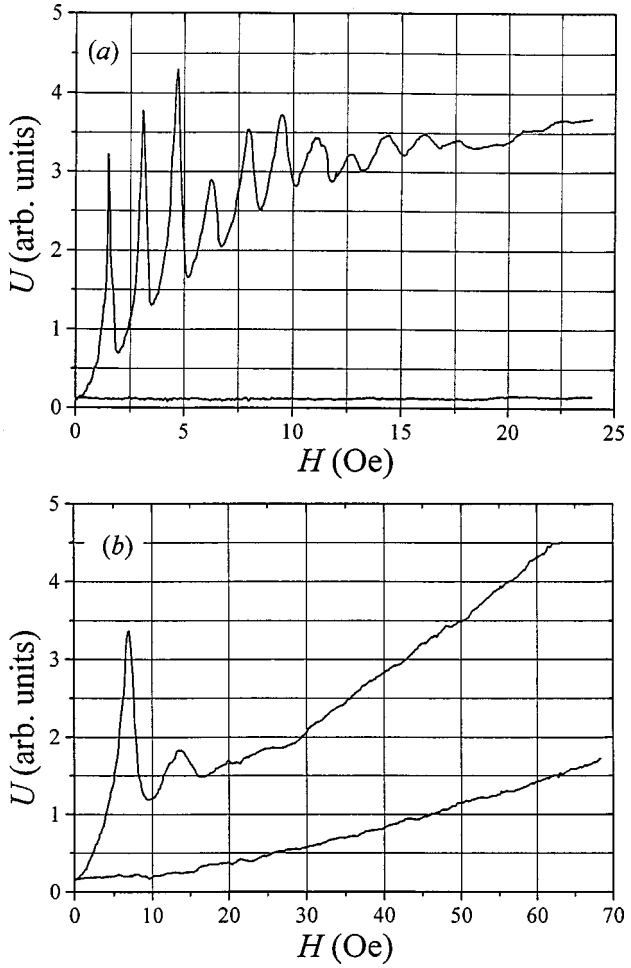

FIG. 13. Collector voltage U vs H for Bi surfaces with $\mathbf{H} \perp \mathbf{N} \| \mathbf{C}_3$, $\mathbf{L} \perp \mathbf{C}_1$: (a) polished surface (from V. Tsoi and N. Tsoi, 1977); (b) chemically etched surface (from V. Tsoi, 1975). The lower curves are for inverse field.

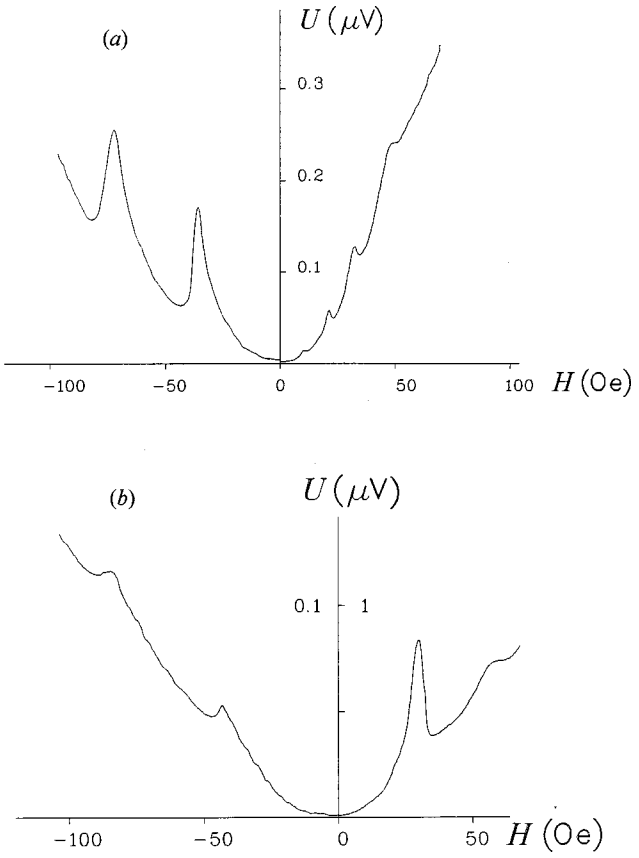

FIG. 14. Collector voltage U vs H: (a) For a polished Bi surface with $\mathbf{H}\perp\mathbf{N}\|\mathbf{C}_2$ and $\mathbf{H}\perp\mathbf{L}$ perpendicular to the largest axis of the hole ellipsoid. $+H$ focuses electrons and $-H$ focuses holes. (b) For a polished Bi surface with $\mathbf{N}\|\mathbf{C}_2$ and $\mathbf{L}$ perpendicular to the largest axis of the electron ellipsoid. The $\mathbf{H}$ direction is chosen to give similar H scales for electrons $(+H)$ and holes $(-H)$; note the reduced U scale for holes. After Sveklo and Tsoi, 1993.

large as q_h. Interestingly, the final values of q_e and q_h are very similar for both faces—$\mathbf{N}\|\mathbf{C}_3$ and $\mathbf{N}\|\mathbf{C}_2$ (see Table II).

Since electrons and holes scatter from the same places on the sample surface, it seems impossible for the results in Table II to be explained simply by intravalley scattering from surfaces with random roughness or terraced structures (see Sec. IV.B). For the polished $\mathbf{N}\|\mathbf{C}_3$ surface, Eq. (3) for random roughness would require $\eta\sim40$ Å for electrons, but only $\eta\sim8$ Å for holes, and chemical or ion etching would increase η to $\geqslant 90$ Å for electrons but only η to $\geqslant 10$ Å for holes. Terracing might fit with nearly equal values of q for electrons and holes for the polished surface, but not for the etched surface. For the polished $\mathbf{N}\|\mathbf{C}_2$ surface, for random roughness, electrons would need $\eta\geqslant 120$ Å, whereas holes would need only $\eta\leqslant 10$ Å and, after etching, electrons would need $\eta\approx 100$ Å, but holes $\eta\approx 30$ Å. Terracing cannot explain the disparate values for this surface of $q\approx 0.9$ for holes but ≈ 0.2 for electrons.

TABLE II. Probability of electron and hole specular reflection in Bi as a function of surface state and orientation.

	$\mathbf{N}\|\mathbf{C}_2$		$\mathbf{N}\|\mathbf{C}_3$	
	Before ion etching	After ion etching	Before ion etching	After ion etching
Electrons	0.22±0.09	0.31±0.07	0.71±0.09	0.24±0.03
Holes	0.94±0.06	0.42±0.2	0.57±0.1	0.4±0.1

The interpretation proposed (Sveklo and Tsoi, 1993) to explain the very different values of q in Table II for electrons and holes scattered from the same surfaces, along with the complex effects of etching, was a combination of intervalley scattering and electronic potentials at these Bi surfaces—equivalent to surface charge—that screen atomic roughness for only one charge sign (electrons or holes) at a time. As explained in Sec. IV.C (see Fig. 9), when $V_0>\varepsilon_F^e$, band bending upward (corresponding to negative surface charge) screens atomic roughness for electrons but not holes, and, when $V_0>\varepsilon_F^h$, band bending downward (positive charge) screens atomic roughness for holes but not electrons. This model will be elaborated upon in Sec. VI.B.4.

2. Electron and hole reflections in Sb for the (111) surface

The Sb samples were electropolished 2-mm-thick plates, with $\mathbf{C}_3\|\mathbf{N}$—i.e., (111) (V. Tsoi and Razgonov, 1976). The contact separation was 0.15 mm, $\mathbf{L}$ was perpendicular to one of three mirror planes, and the other orientations were $\mathbf{H}\perp\mathbf{N}\|\mathbf{C}_3$ and $\mathbf{L}\|\mathbf{C}_2$.

Antimony has the same lattice as Bi, and its electron Fermi surface is also similar to Bi's (Windmiller, 1966). However, its hole Fermi surface consists of three ellipsoids, with the largest axes in the mirror plane. The minor electron and hole axes in that plane are $p_e=0.54\times10^{-20}$ g cm/s and $p_h=0.48\times10^{-20}$ g cm/s. Figure 15(a) depicts the cross sections of effective electrons and holes set by the direction of $\mathbf{H}$. Note that the electrons and holes do not stay in the plane parallel to $\mathbf{N}$ as they move from E to C. Rather, the electron trajectories are tilted from $\mathbf{N}$ by a few degrees, and those for holes by approximately 40°. The most important feature of the Sb Fermi surface for the present purpose is that, under specular reflection, the changes in electron and hole momenta are almost equal. This near equality precludes any differences in q (see Table I) due to differences in λ_{dB}.

Figure 15(b) shows $U(H)$ for the specified geometry. The peak positions in H agree with predictions from Fig. 15(a). The amplitude ratios of the first and second peaks give $q_e=0.8$ and $q_h=0.1$. A combination of this result for Sb with those for Bi in Sec VI.B.1 strongly suggests that surface charge plays a fundamental role in surface reflection in semimetals (and, by analogy, also in semiconductors). Interestingly, Gaidukov and Galyamina (1978) found the (111) surface of a Sb whisker to reflect holes specularly, just the opposite of the TEF result of Tsoi and Razgonov (1976). The charge sign on a given surface thus may not be intrinsic—it may depend upon surface preparation, the nature of any adsorbed layer, etc.

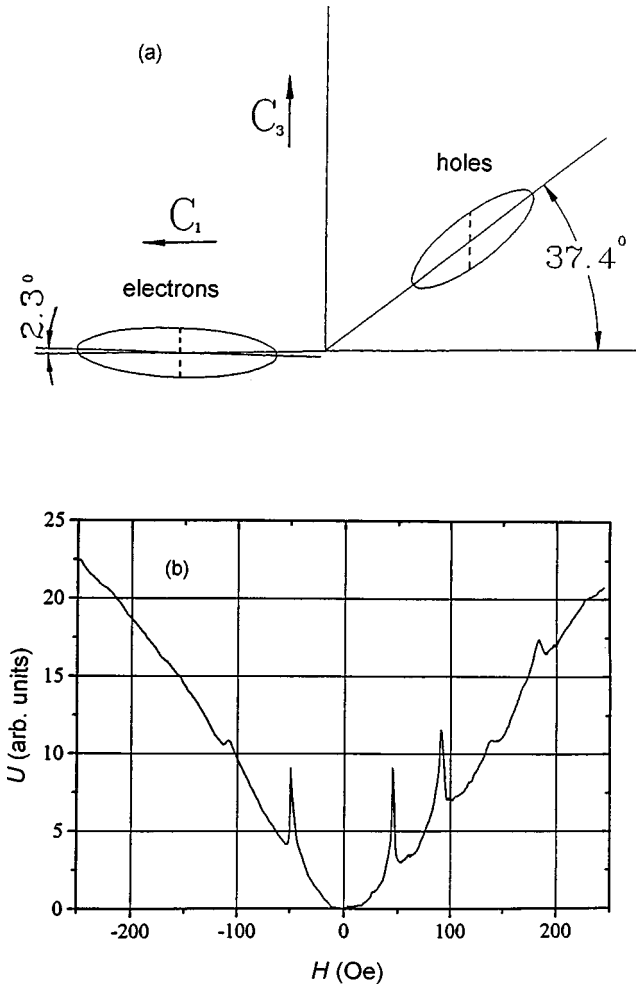

FIG. 15. Electron $(+H)$ and hole $(-H)$ focusing in Sb for $\mathbf{N}\|\mathbf{C}_3\perp\mathbf{H}$; $\mathbf{L}\|\mathbf{C}_2$; $L=0.15$ mm, $T=1.7$ K. (a) Cross sections of the electron and hole ellipsoids of the Sb FS cut by a mirror plane. Focused current carriers move on the cross sections indicated by dashed lines. (b) Focusing spectrum. The third electron peak is reduced by local surface defects. After Tsoi and Razgonov, 1976.

3. Electron reflections in Bi for surfaces tilted from the (111) surface

The last data in this section come from an early study of Bi in which effects of crystalline anisotropy were studied by varying the angle α between $\mathbf{C}_3$ and $\mathbf{N}$ from 0 to 90°. This procedure varied λ_{dB} and possibly the surface roughness systematically. Two sets of samples were studied, one with $\mathbf{C}_1$ in the surface plane and the other with $\mathbf{C}_2$ in this plane.

The variation of q_M with α for untreated surfaces is shown in Fig. 16, where each symbol denotes measurements for electrons on a given ellipsoid. The data in Fig. 16 were taken on several different samples and for a variety of contact placements on each. Care had to be taken to get comparable data, since contacts had to be shifted to measure q_M for different ellipsoids. When a surface plane is close to (111)—α near 0—the magnitude of q_M is close to unity ($q_M\sim0.8$). By the time α reaches 20°, q_M has decreased to 0.2–0.3, independent of

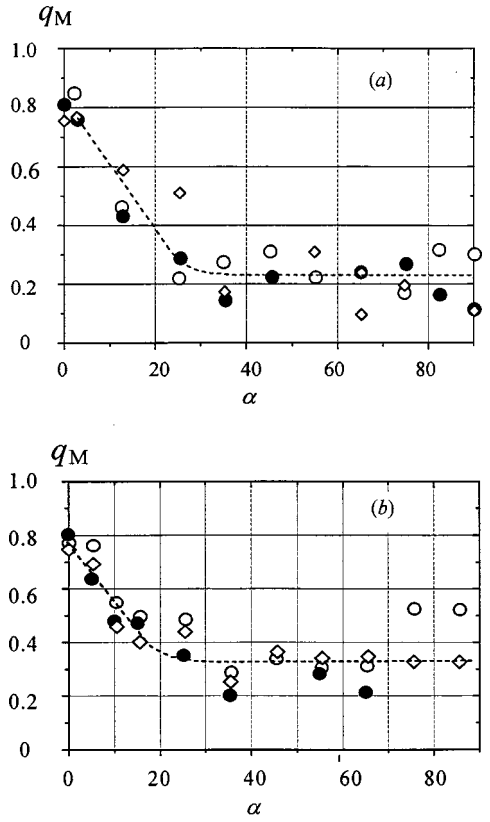

FIG. 16. Dependence of q_M on the deviation of $\mathbf{N}$ from $\mathbf{C}_3$ by angle α (in degrees): (a) in the plane (C_3C_2), (b) in the plane (C_3C_1). The dashed curves are to guide the eye. From Bozhko and Tsoi, 1987.

whether $\mathbf{C}_1$ or $\mathbf{C}_2$ is parallel to the sample surface. The differences between q_M for electrons of different ellipsoids generally lie within an accuracy of $q_M\pm0.1$. The change in momentum $\Delta\mathbf{p}$ under specular reflection is determined by the orientation of the electron ellipsoid relative to the sample surface. In Fig. 16, for the same surface, changes in $\Delta\mathbf{p}$ of >100% did not change q_M to within the measuring accuracy of ±0.1. These data cannot be explained by a simple intravalley free-electron model, with q_M determined simply by $\Delta\mathbf{p}$ [Eq. (4)].

4. Analysis of data on crystallographic anisotropy and charge sign

We first briefly summarize the results just described (Tables I and II).

(1) For electrons in Bi reflected from undamaged surfaces, q varies from 0.8 to 0.9 for the (111) surface, down to <0.2 for the $(11\bar{2})$ and $(1\bar{1}0)$ surfaces. Upon rotating an undamaged surface away from (111), one finds that q decreases out to about $\alpha=20°$, after which it stays constant to within the measuring uncertainty of ±0.1. For electrons in Sb, q is 0.8 on the (111) surface, the only surface studied so far.

(2) For undamaged (111) surfaces, $q_e>q_h$ in Bi, and $q_e\gg q_h$ in Sb, but $q_e\ll q_h$ for $(1\bar{1}0)$ in Bi. (3) The effects of etching are as follows: When $q=0.7$–0.9 for either electrons or holes in Bi, etching reduces it to ≈0.2–0.4. Such reductions are comparable to those for metals

(Table I, Sec. V). When $q=0.5$, etching slightly reduces q. When $q<q_M=0.2$, etching slightly increases q. In Bi, etching leads to nearly the same final value of q in all four cases (Table II).

As noted in Sec. VI.B.1, intravalley scattering alone, with any form of surface roughness, cannot explain such large differences in q_e and q_h for given surfaces and give $q_e \gg q_h$ on some surfaces but $q_e \ll q_h$ on others, independent of relative λ_{dB}. Both behaviors seem to require surface charge associated with band bending, with sign varying from surface to surface and affected by surface treatment (Sveklo and Tsoi, 1993). The Debye screening radii r_D of Bi (~500 Å) and Sb (~200 Å) are large enough to give the required screening. The band bendings needed are ~0.01–0.03 eV in Bi and ~0.1 eV in Sb.

It is also difficult to see how screening alone, with $\lambda_{dB}>100a_0$, could explain the data in Tables I and II, where values of $q=0.6$–0.9 are reduced by etching—in one case from 0.9 to 0.2—as strongly as in metals that have $\lambda_{dB}\sim a_0$, and yet a value of $q\approx 0.2$ can be slightly increased by etching. In addition to surface charge, a mechanism is needed to allow roughness on a scale $a_0 \ll \lambda_{dB}$ to affect q. Bozhko and Tsoi (1987), Bozhko *et al.* (1989), and Sveklo and Tsoi (1993) proposed intervalley scattering. The basic idea is that, in the usual TEF geometry, intervalley scattering reduces q by removing carriers from the specular beam, and that atomic-scale roughness enhances intervalley scattering to the point where it is comparable to intravalley scattering.

Combining surface band bending with intervalley scattering leads to the following proposed picture of surface reflection in Bi (and Sb) (Bozhko and Tsoi, 1987; Bozhko *et al.*, 1989; Sveklo and Tsoi, 1993). Bi is layered, composed of double atomic planes perpendicular to $\mathbf{C}_3$ (threefold axis). The atoms in these planes couple via covalent bonds. Van der Waals forces and weak metallic bonds supply the interactions between double planes. Any plane other than (111) has atoms with unsaturated covalent bonds. The greater the tilt of the surface normal away from (111), the larger the concentration of such atoms. Such atoms sharply increase at about 30°, after which the increase with increasing angle is much slower. These atoms result in atomic-scale surface roughness that enhances intervalley scattering, thereby decreasing q. The only exceptions are when the surface is initially very flat or when surface charge screens the roughness, thereby decreasing intervalley scattering and increasing q. Such screening can occur for only one charge sign at a time.

The (111) surface of Bi has no unsaturated covalent bonds. A small fraction of localized structural defects will change the specularity of reflection only slightly, thereby explaining why q is large and nearly independent of sample preparation techniques for undamaged (111) surfaces. Ion etching creates atomic disorder, producing unsaturated bonds that enhance intervalley and diffuse scattering. Chemical etching produces faceting that also gives unsaturated bonds and diffuse scattering. There are practically no areas on a chemically etched (111) surface for which the local normal $\mathbf{N}_{\rm loc}$ is parallel to $\mathbf{C}_3$; instead $\mathbf{N}_{\rm loc}$ is mostly tilted from $\mathbf{C}_3$ by 60°. Because $\mathbf{N}_{\rm loc}$ is not the normal $\mathbf{N}$ to the median plane, reflection becomes diffuse, whether reflection from the facets is specular or diffuse. Such diffuse reflection has two results: first, the measurements described above of the reduction in q as $\mathbf{N}$ is inclined from $\mathbf{C}_3$; second, the absence of an additional TEF peak at $H=0.56H_0$ (V. Tsoi, 1975; Bozhko and Tsoi, 1987). If a surface is terraced or faceted, and electron reflection from the terraces and facets is specular, additional TEF peaks must occur (see Korzh, 1981; Bozhko *et al.*, 1984; Tsoi *et al.*, 1992). Their absence indicates diffuse reflection. The only caveat is that the electrons giving such peaks must enter C at small angles, and roughness produced near C at installation could suppress this peak.

Of course, these qualitative ideas about the importance of bonding and surface charge still need detailed theoretical underpinning. For example, how is q affected by mutual bond saturation as the bond concentration increases, and what determines the surface charge?

To summarize, the observed values of q_e and q_h, on several fresh and damaged Bi surfaces and one polished Sb surface, cannot be understood simply in terms of intravalley surface reflection of free carriers, where q for each surface is determined by the ratio of atomic roughness to λ_{dB} for both electrons and holes. Rather, q_e and q_h display behaviors of carriers in a crystal lattice, where atomic-scale roughness greatly enhances intervalley scattering, thereby reducing q. Also important is the presence of surface charge associated with band banding, which, on a given surface, can screen such roughness for one charge sign only, reducing intervalley scattering and increasing q for that charge sign. In Secs. VI.D and E we describe experiments to look for evidence of intervalley scattering and surface charge associated with band bending.

C. Drift electron focusing and $q(\theta)$

In the previous section, the analysis of TEF experiments with the usual geometry focused upon the ratio of neighboring peak heights, which determines the probability of specular reflection at normal incidence, $q(\pi/2)$—designated by q. In principle, the shape of the TEF peaks contains information about the probability of specular reflection at all angles $q(\theta)$ (V. Tsoi, 1975; V. Tsoi and N. Tsoi, 1977), but it is hard to deconvolute the information. Derivations of $q(\theta)$ from analysis of higher-order peaks are described in Sec. VI.E.1, where it is concluded that band bending affects the results.

In this section we describe an experiment (M. Tsoi and V. Tsoi, 1995, 1996b) using an unusual TEF geometry, that lets q be directly measured for arbitrary $\mathbf{k}$ on the Fermi surface. If the applied field $\mathbf{H}$ is rotated away from perpendicular to the EC line, electrons incident at some θ will still be focused at the collector C after reflection from halfway between the emitter E and C. By rotating $\mathbf{H}$, it is thus possible to map out $q(\theta)$. In Bi, this technique requires very short EC separation, $L \sim 10\,\mu$m, as one must study the scattering of electrons in

the vicinity of the limit point of the Bi Fermi surface, the velocities and mean free paths of which are an order of magnitude less than those of electrons on the central cross section of the Fermi surface. We begin by explaining how this geometry allows $q(\theta)$ to be determined.

Consider the scheme in Fig. 4(c), starting with a metal with a spherical Fermi surface. The sample surface is in the (xz) plane, **H** is along the z axis, and nonequilibrium electrons are injected isotropically into the sample at the origin with the Fermi energy ε_F. The density $\rho(\mathbf{R})$ of electrons incident onto the sample surface without reflection is singular on the magnetoid curve (intersection of the caustic surface with the sample surface) that connects the point $(0,D=2R_c)$ with the points $(\pm\pi D,0)$. A collector C of area S placed at **R** registers a number N of electrons equal to the integral of $\rho(\mathbf{R})$ over S, which depends on the magnitude and direction of **H**. For a given **R**, N is maximal at the H where the magnetoid crosses C—a TEF peak occurs. This process is drift electron focusing (DEF) (Grishin, 1983; M. Tsoi and V. Tsoi, 1995, 1996b). The $\rho(\mathbf{R})$ of electrons incident onto the surface after one reflection is singular on the concentric magnetoid curve that connects the points $(0,2D)$ and $(\pm 2\pi D,0)$. When the magnetoid crosses C, a TEF peak occurs, with amplitude proportional to $q(\theta)$.

For analyzing the published measurements for $\mathbf{C}_3\|\mathbf{N}$, the electron Fermi surface in Bi can be approximated as an ellipsoid in the trigonal plane with its largest axis parallel to $\mathbf{C}_1$. The density function $\rho(\mathbf{R})$ for a spherical Fermi surface is transformed into that for an ellipsoid by simple expansion or compression along the z axis. In this way, one can find the magnetoid for arbitrary direction of **H** in the (xz) plane. Electrons focused onto different points on a magnetoid have different incident angles θ ranging from $\pi/2$ to 0. One can thus measure $q(\theta)$. In the published experiment, a contact line was fixed close to $\mathbf{C}_1$ with contact separation about 10 μm, and θ was changed by rotating **H**. The DEF spectrum involves a different point on the magnetoid for each direction of **H**—i.e., each angle φ between **H** and $\mathbf{C}_1$ corresponds to a different θ. φ was changed from $\pi/9$ to $\pi/2$ in steps of $\pi/36$. Focusing spectra with the contact line close to $\mathbf{C}_1$ are shown in Fig. 17(a). The focusing lines at H above 100 Oe are due to focusing of electrons after intervalley scattering (see Sec. VI.D.1). The locations of these peaks on the H axis allow the determination of the contact line direction with respect to $\mathbf{C}_1$. The focusing lines at $H\sim 40$ Oe and 80 Oe arise from drift electron focusing. For a given geometry, all parameters needed to calculate $q(\theta)$ are known. Figure 17(b) shows the DEF spectra of Fig. 17(a) after each curve has been rescaled to give the same amplitude for the first DEF peaks, shifted along the V axis arbitrarily for clarity, and the background has been compensated. The change in $q(\theta)$ is clear.

Tsoi and Tsoi (1995, 1996b) analyzed the data of Fig. 17 with Eq. (3), which assumes only intravalley scattering. The circles in Fig. 8 show that most of the $q(\theta)$ data points are compatible with Eq. (3) with η=338 Å. However, points at small θ are slightly higher than predicted.

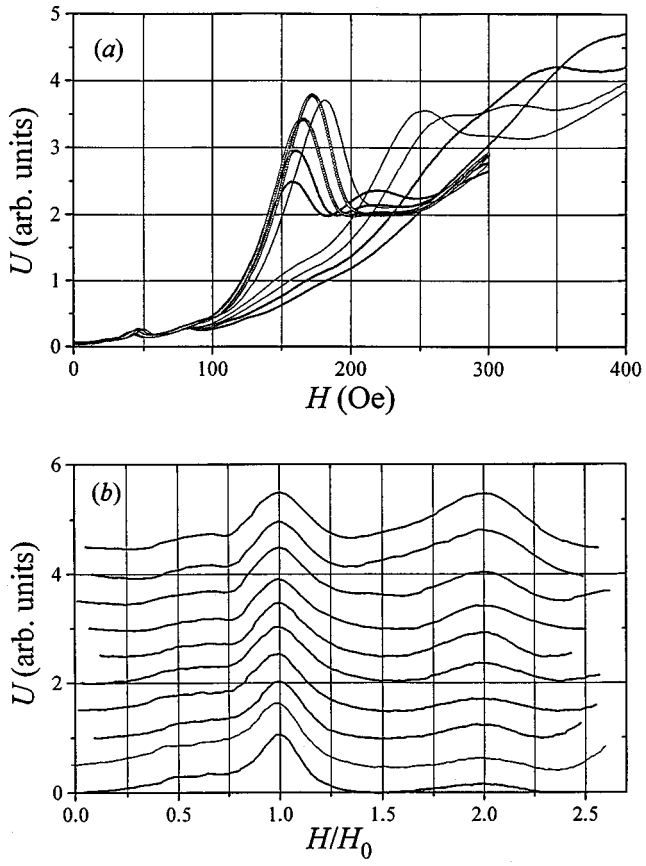

FIG. 17. Collector voltage U vs H for drift electron focusing. (a) Focusing spectrum with the angle between **H** and **L** varying from 20° to 85° in steps of 5°. From M. Tsoi and V. Tsoi, 1995. (b) The data rescaled to make the amplitudes of the first drift electron focusing peaks the same. The data have also been shifted along the U axis arbitrarily for clarity and the background has been compensated. After M. Tsoi and V. Tsoi, 1995.

This deviation could be due to shading effects that decrease the effective roughness height but are not accounted for in Eq. (3) or to screening of surface roughness at small angles of incidence by surface band bending (Secs. IV.C and VI.E). Tsoi and Tsoi suggested that the large value of η=338 Å might arise from irregularities in the mold in which the samples were grown. Damage from tip installation might also contribute.

D. Intervalley scattering

The electronic structure of metals and semimetals is usually multivalley, allowing the possibility of intervalley transitions. Intervalley scattering of conduction electrons at a surface is of great interest. It drastically modifies the electron kinetics in confined samples and results in anisotropic size effects (Rashba *et al.*, 1976). Switching on intervalley scattering can dramatically change electron kinetics in metals in a magnetic field (Kapeliovich, 1988). The multivalley electron spectrum of Bi is well suited to quantitative studies of intervalley scattering, because its geometry is simple and well known. As explained in Sec. II.A, the elongated electron ellipsoids

of the Bi Fermi surface can be well approximated as cylinders, where the electrons move in planes perpendicular to the cylinder axes. The presence of intervalley scattering can be demonstrated by aligning E and C so that C lies out of these planes, in which case surface intervalley scattering is required for injected electrons to reach C (hereafter, the word surface before intravalley reflection or intervalley scattering will be omitted). Other geometries will involve combinations of intravalley and intervalley scattering, allowing their relative importances to be found for different crystal faces and surface roughnesses. Such determinations can be complex, as they require knowledge of the relative contributions of processes with different path lengths, and thus different mfp corrections.

The Fermi surface structure of Bi precludes intervalley scattering from the (111) surface by the usual specular reflection process in which $\mathbf{p}_\tau$ is conserved. Intervalley scattering requires either participation of a surface reciprocal-superlattice vector (or an artificial surface reciprocal-lattice vector—see Sec. VII) or else diffuse scattering (Tsoi and Kolesnichenko, 1980). One would like to know the separate contributions of each alternative. The first is called a ''correlated'' transition, as the final momentum of the electron, $\mathbf{p}_\tau^- = \mathbf{p}_\tau^+ + \mathbf{G}_\tau$, is well defined. For transitions between electron valleys in Bi, the required $\mathbf{G}_\tau$ is half the usual $\mathbf{G}$ for the surface plane, necessitating a surface reconstruction (Tsoi and Kolesnichenko, 1980). The second, called an ''uncorrelated'' transition, involves no restrictions on $\mathbf{p}_\tau$, except that $\mathbf{p}_\tau^+$ and $\mathbf{p}_\tau^-$ lie on the sending and receiving cylinders, respectively. In the second case, $\Delta\mathbf{p}_\tau$ must be produced by surface roughness. Since the intervalley scattering transition takes the electron across a large fraction of the Brillouin zone, Δp must be $\sim h/a_0$, and only a roughness size $\sim a_0$ can be effective. To distinguish both transitions from ''specular'' ones, we designate their probabilities by the symbol h—i.e., h_c and h_{uc} for correlated and uncorrelated scattering.

Tsoi and Kolesnichenko (1980) note that h_c is limited in Bi by the overlap of the cross sections of the two electron ellipsoids involved, which is small since they are thin and oriented almost perpendicular to each other. The ratio of the number of electrons undergoing correlated intervalley scattering to the total number of electrons scattered is only $\sim$0.1. As the electrons can go to two valleys, the probability of going to either is $\sim$0.05.

In Sec. VI.D.1 we focus on electron-electron intervalley scattering, and in Sec. VI.D.2 on electron-hole intervalley scattering. For simplicity, we designate electron-electron scattering as just IVS, except where specificity is needed to avoid ambiguity. We shall see that the probability of electron-hole scattering is small, and thus usually negligible, except in geometries where it is explicitly selected.

1. Electron-electron intervalley scattering

Again approximating the electron ellipsoids in Bi by cylinders, we find that the skip lengths L_i along the sample surface for focused electrons on different ellipsoids are given by $2R_c(\varphi_i=0)/\cos\varphi_i$, with φ_i the angle between $\mathbf{H}$ and the largest axis of ellipsoid i. Figure 18 shows the ellipsoids (left side) and schematic drawings (right side) of the allowed skip paths for electrons to travel from emitter E to collector C as described in Sec. II.B. Here we need two cases for $\mathbf{N}\|\mathbf{C}_3$. Case 1, $\mathbf{H}\|\mathbf{C}_1$, $\mathbf{L}\|\mathbf{C}_2$, is shown in the upper half of Fig. 18 for fields that give focusing when the emitter E is located at E and the collector C is located at A, O, B (first peak), P (second peak, first IVS peak), M, K (first IVS peak), or C (third peak, second IVS peak). Case 2, $\mathbf{H}\|\mathbf{C}_2$, $\mathbf{L}\|\mathbf{C}_1$, is shown in the lower half of Fig. 18 for peaks: without reflections (C at A, B), after one reflection—IVS (C at O), specular reflection (C at M, K); after two reflections—one IVS and one specular reflection or two IVS (C at P, D); after three reflections—three IVS, two IVS and one specular, or one IVS and two specular (C at C). Circles and crosses denote points at which electrons are focused after intravalley reflection and intervalley scattering. At points with no signs, electrons are focused without surface reflection.

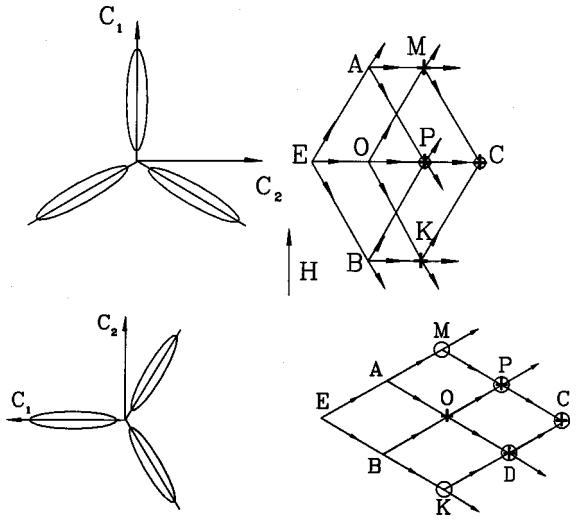

FIG. 18. Projections onto the sample plane $\mathbf{N}\|\mathbf{C}_3$ of the electron valleys of Bi (ellipsoids) and of the trajectories for the electrons that give focusing peaks in $\mathbf{H}\|\mathbf{C}_1$ (upper half=case 1) and $\mathbf{H}\|\mathbf{C}_2$ (lower half=case 2). E is the emitter. Focused electrons fall upon the surface at A, B C, D, K, M, O, and P. The arrows indicate possible electron directions after surface reflection. Symbols ○ and + indicate electrons focused after intravalley and intervalley scattering. After intervalley scattering, an electron changes its direction of motion.

In the cases we consider, $\mathbf{H}$ stays in the plane of the sample surface, perpendicular to $\mathbf{N}$. Bozhko and Tsoi (1987) describe supplementary studies of intervalley scattering with $\mathbf{H}$ out of this plane. The first direct isolation of intervalley scattering was reported by Tsoi and Kolesnichenko (1980) for polished Bi surfaces using the two crystal orientations shown in Fig. 18. We start with the experimental data in the upper curve in Fig. 19(a), which is for case 1. This curve gives $q_M \sim 0.65$. From the schematic in Fig. 18 for case 1, we see that the first peak in the upper curve of Fig. 19(a) occurs for the field at which electrons are collected at O, and involves only

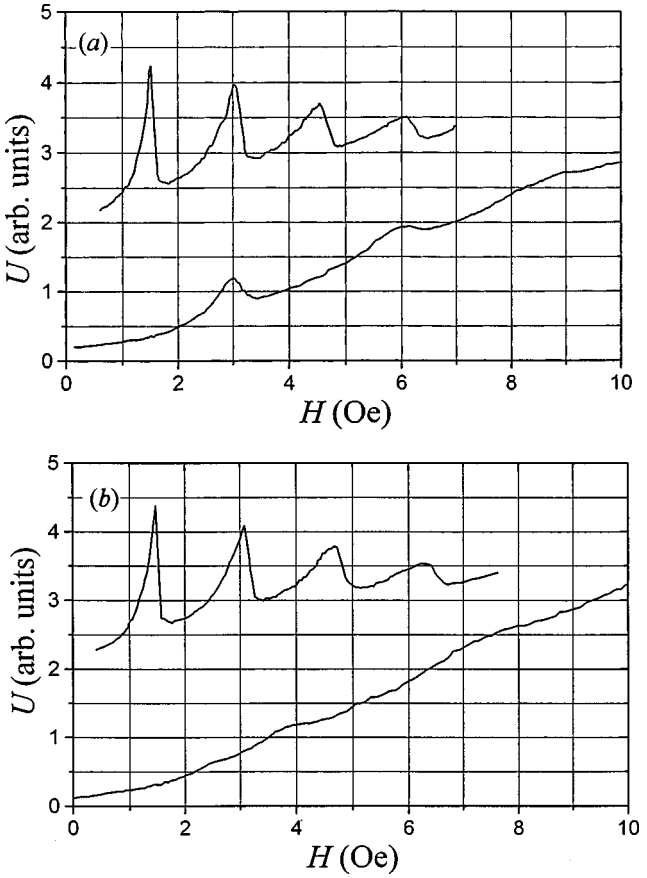

FIG. 19. Collector voltage U vs H for a Bi sample with $\mathbf{N}\|\mathbf{C}_3$: (a) $\mathbf{H}\perp\mathbf{L}$; (b) $\angle\mathbf{HL}=70°$. The upper curves are for $\mathbf{L}\|\mathbf{C}_2$ and the lower ones for $\mathbf{L}\|\mathbf{C}_1$. For the lower curves, the gain of the system was increased fivefold. These data are plotted for a different value of L than those in V. Tsoi and Kolesnichenko, 1980.

electrons on one ellipsoid that reach O without being scattered. The height of this peak, which we call A_1, sets the scale for all other peaks. For a cylindrical Fermi surface, $A_1=D\times I\times R\times(b/L)^{1/2}$, where I is the current, R the contact (E) (tip) resistance, and D a constant associated with the Bi Fermi surface (Tsoi and Kolesnichenko, 1980). The amplitudes of the subsequent peaks in this geometry (the second and third peaks occur for the higher fields for which electrons are collected at P and C, respectively) involve both intravalley and intervalley scattering. If intervalley scattering is weak, the second peak will be dominated by the contribution from intervalley scattering of electrons on one ellipsoid traveling along path EP, so that $q_M\approx q$ for such scattering. But this peak will also contain small contributions from intervalley scattering of electrons starting on other ellipsoids and traveling along EAP and EBP, respectively. Both intravalley and intervalley scattering are present at P, C, etc., causing the amplitudes of the second and higher peaks to depend upon both the relative probabilities of intravalley and intervalley scattering and, via Eq. (7), the different path lengths involved in different itineraries from E to C.

Fortunately, case 2, leading to the lower curve in Fig. 19(b), allows a more direct isolation of intervalley scattering. In this geometry, Fig. 18 shows that electrons on one ellipsoid must travel around that ellipsoid's long axis. The specific characteristics of the Bi electronic spectrum preclude such electrons' contributing to the peak amplitudes. Thus electrons emitted at E can move only along lines EM or EK. For the first peak, which occurs at the field where the collector C is located at O, there is no direct path from E to O without surface reflection, and specular intravalley reflection alone cannot bring these electrons to C. Observing TEF, when it is prohibited under intravalley scattering alone, provides a direct proof of intervalley scattering, and the amplitude of the first peak directly measures its probability. Defining h for this peak as the ratio of the peak amplitude A_1' to that of A_1 defined above (for the same I and R), Tsoi and Kolesnichenko (1980) derived $h\approx 0.05$. Since electrons can come to the final valley from two other valleys, the probability of scattering from one valley to another is $h\approx 0.025$. As this value is comparable to the maximum probability of coherent scattering noted above, Tsoi and Kolesnichenko could not decide whether h was more coherent or incoherent. From the lower curve in Fig. 19(a) the ratio of the amplitudes of the first and second peaks in this geometry is 0.5. Arguing that this amplitude would be dominated by the paths $EAMPC$ and $EBKDC$, which involve two intravalley processes and only a single intervalley one, the authors estimated the ratio of the second peak to the first (which involves only a single intervalley process), as simply the product of two intravalley processes, finding decent agreement between the measured value, 0.5, and calculated value $0.65\times 0.65=0.42$.

To check their attribution of the peak in the lower curve of Fig. 19(a) to intervalley scattering, Tsoi and Kolesnichenko (1980) rotated $\mathbf{H}$ by 20° away from the perpendicular to $\mathbf{L}$ (but still with $\mathbf{H}\perp\mathbf{N}$). Since the orientations of $\mathbf{L}$ and the ellipsoids do not change, the directions of motion of the electrons remain the same (Fig. 3). However, the step lengths change as $1/\cos\varphi$ as the angle φ between $\mathbf{H}$ and the cylinder axis changes. From Fig. 18, for $\mathbf{L}\|\mathbf{C}_2$, taking intravalley scattering from one ellipsoid as dominant, one expects no change in the relative amplitudes of the peaks in the upper curves of Fig. 19 and a change in the H scale by only $(1/\cos 20°)$—since $\mathbf{H}$ was initially parallel to the cylinder axis ($\varphi=0°$). Indeed, the only difference between the upper curves of Figs. 19(a) and (b) is this minor change in H scale. For $\mathbf{L}\|\mathbf{C}_1$, in contrast, Fig. 18 predicts more radical changes. The ability of intervalley scattering to focus electrons at O was contingent upon the skip lengths for EA and AO (EB and BO) being the same—both proportional to $(1/\cos 30°)$. But rotating $\mathbf{H}$ by 20° makes the ratio of the step lengths noninteger $(\cos 10°/\cos 50°\approx 1.5)$. Only when the ratio of the step lengths is a prime number can intervalley scattering give weak peaks, the locations of which depend upon φ. The

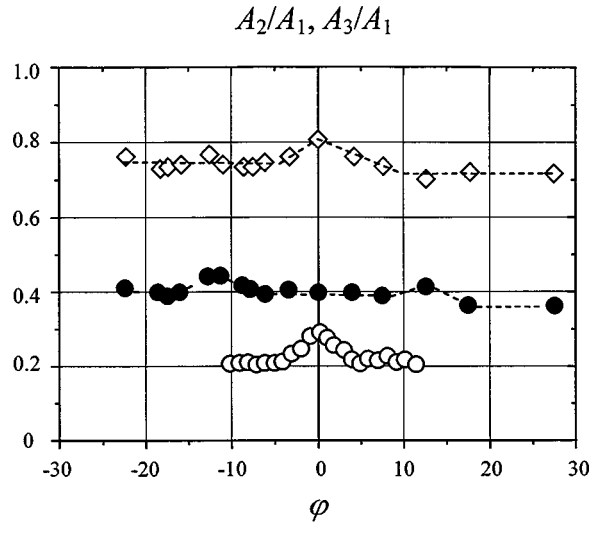

FIG. 20. Dependence of A_2/A_1 ($\diamond$ and $\bigcirc$) and A_3/A_1 ($\bullet$) on tilt angle φ (in degrees) of **H** from $\mathbf{C}_1 \perp \mathbf{L}$, $\mathbf{H} \perp \mathbf{N} \| \mathbf{C}_3$. From Bozhko *et al.*, 1989.

two weak peaks in the lower curve in Fig. 19(b) agree with this analysis; for details see Andrievskii *et al.* (1985) and Bozhko *et al.* (1989).

Two subsequent studies set out to address the two main questions left unanswered by Tsoi and Kolesnichenko, namely, (a) is intervalley scattering mostly correlated or uncorrelated? and (b) how does h depend upon surface roughness? Andrievskii *et al.* (1985) also used a polished (111) surface. Bozhko *et al.* (1989) used both a polished (111) surface and an ion- and chemically etched one, along with surfaces of other orientations. We briefly outline the strategy followed and the main results obtained.

These studies involved more complex analyses of how peak heights changed as **H** was rotated to change its angle φ with **L**. Such rotations allow different intervalley scattering processes to be turned on and off. The analyses required correcting the contributions from electrons taking different paths from E to C for effects of the finite mean free path l. In Bozhko *et al.* (1989), l was measured simultaneously in the same sample. Figure 20 shows examples of TEF data as a function of φ. The ratio of the height of the second peak to the first, (A_2/A_1), is shown as open diamonds for the polished surface and open circles for the etched one, and the ratio of the third peak (A_3/A_1) is shown as filled circles for the polished surface. Note that the fractional decrease in A_2/A_1 is larger in the etched case and that the ratio A_3/A_1 is a nonmonotonic function of φ. From analysis of data such as those in Figs. 19 and 20, Andrievski *et al.* (1985) and Bozhko *et al.* (1989) both concluded that uncorrelated intervalley scattering usually dominated h. Bozhko *et al.* (1989) found that when the (111) surface was artificially roughened—compare the open circles and diamonds in Fig. 20—q for intravalley scattering dropped from 0.65 to ~0.2, while h for intervalley scattering grew from ~0.05 to ~0.2. As 0.2 exceeds the upper limit for correlated intervalley scattering (Sec. VI.D), they concluded that intravalley and intervalley processes were about equally probable for the roughened (111) surface.

2. Electron-hole intervalley scattering

Transverse electron focusing has also been used to investigate electron-hole intervalley scattering transitions, which are especially interesting because they apparently determine a wide variety of anisotropic size effects (Rashba *et al.*, 1976), as well as the sample resistance in the static skin effect (Kapeliovich, 1988). Magnetoresistivity measurements (Murzin, 1982) show that the probability of electron-hole transitions is very small, $\sim 10^{-2}$–10^{-3}. Directly observing these transitions with TEF was not easy, but was done using a special geometry that gives focusing only after electron-hole transitions. To fully characterize the subprocesses involved, Sveklo and Tsoi (1989a) noncollinear point contacts, with the electron-hole transitions occurring at intermediate locations between emitter E and collector C.

Since the separation between electron and hole ellipsoids in the Bi Brillouin zone is comparable to the basic reciprocal-lattice vector **G** of the Bi lattice, electron-hole intervalley scattering involves a large $\Delta \mathbf{p}_\tau$, which requires surface roughness on an atomic scale. Electron-hole intervalley scattering thus requires such surface roughness.

Figure 21 shows the measurement geometry. To obtain the largest TEF amplitudes for both hole and electron peaks, the samples are oriented with $\mathbf{N} \| \mathbf{C}_2$, so that the largest axes of the hole ellipsoid and one of three electron ellipsoids are in the plane of the sample surface. If an emitter is installed at point 2, then for the best electron focusing, the collector must be installed on the line 2-1, perpendicular to the largest axis of the electron ellipsoid. For the best hole focusing, in contrast, the collector must be installed on the line 2-3, perpendicular to $\mathbf{C}_3$. Since R_c depends upon the angle between **H** and the ellipsoid axis (for the electron ellipsoid, see Sec. II.A), electron and hole focusing can be seen at the same value of H, despite the large difference in their ellipsoid sizes. As the mean free path of holes is much shorter than that of electrons, the contact separation must be small (~50 μm) to see hole focusing.

If surface scattering induces electron-hole transitions, then one should be able to produce transverse electron focusing using this three-point contact geometry with the alternative choices of contact 1 (3) as the emitter and contact 3 (1) as the collector. This is the geometry actually used. Contacts 1 and 2 were fixed on one support, about 100 μm apart, with facilities to place them simultaneously on the sample surface. By rotating the sample, the contact line was adjusted as desired, using the amplitude of the TEF peak as reference. Contact 3 was then installed so that the line 2-3 (1-2′) was orthogonal to $\mathbf{C}_3$, using the hole TEF peak as a reference. The separation of contacts 2 and 3 was about 50 μm. By rotating **H** in the surface plane, it was possible to reach a

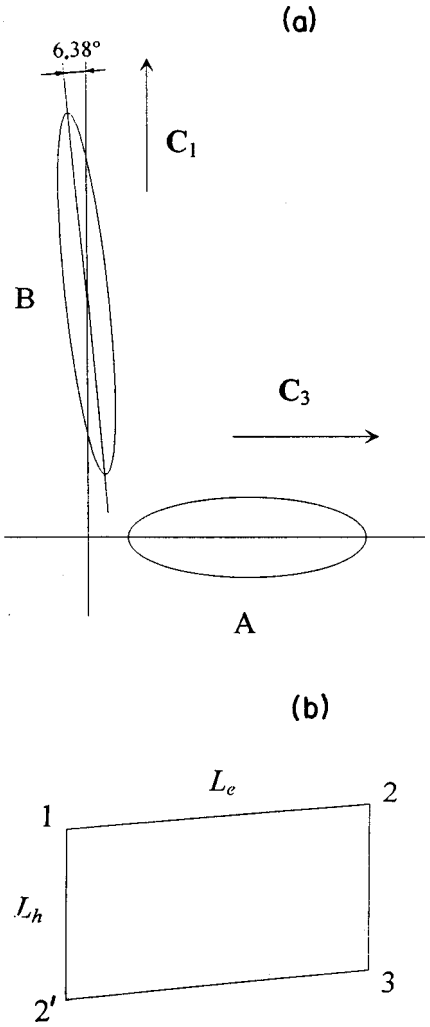

FIG. 21. Geometry for observing electron-hole and hole-electron surface transitions. (a) Projection of the hole ellipsoid (A) and one electron ellipsoid (B) of the bismuth Fermi surface onto the plane perpendicular to C_2; (b) Projection of the orbits of focused electrons (1-2; 2′-3) and holes (2-3 and 1-2′) onto the sample plane. The contacts are located at points 1, 2, and 3. Lines 1-2 and 2′-3 are perpendicular to the largest axis of the electron ellipsoid; lines 2-3 and 1-2′ are perpendicular to the major axis of the hole ellipsoid. $\mathbf{H} \perp \mathbf{N}$.

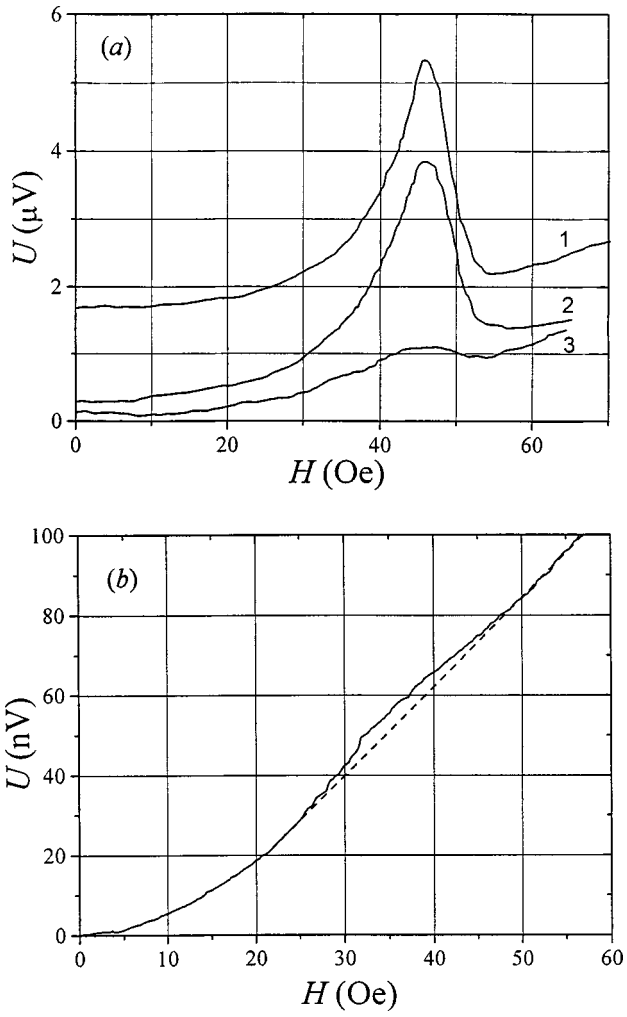

FIG. 22. Collector voltage U vs H for a Bi sample with the geometry of Fig. 21: (a) 1, focusing of electrons (contact 1 is the emitter E and 2 is the collector C); 2, focusing of holes (contact 2 is E and 3 is C); 3, focusing of electrons (holes) that have undergone an electron-hole (hole-electron) transition (contact 1 is E and 3 is C). The gain was increased by a factor of 6.32 for curve 2 and 31.6 for curve 3. (b) Case 3 of (a), but with only contacts 1 and 3 on an otherwise perfect surface, and U scale in nV. From Sveklo and Tsoi, 1989a.

situation in which the electrons emitted by contact 1 were focused onto 2, and simultaneously holes emitted by 2 were focused onto 3 for fixed **H** size and direction. At the same time, holes emitted by contact 1 were focused onto 2′, and electrons emitted by 2′ were focused onto 3. The collected current is the sum of excitations arriving by these two paths.

This scheme allowed the following: (1) observation of the electron TEF peak with contacts 1 and 2; (2) observation of the hole TEF peak with contacts 2 and 3; (3) observation of focusing of electrons (holes) after hole-electron (electron-hole) surface transitions with contacts 1 and 3—with the capability to shift each transition between 2 and 2′ by reversing the direction of **H** and interchanging contacts 1 and 3; (4) simultaneous observation of focusing of electrons and holes onto the same contact at the same magnetic-field value with contact 2 as collector, contact 1 as electron emitter, and contact 3 as hole emitter (Sveklo and Tsoi, 1989a). Here, we focus on cases (1)–(3).

Figure 22(a) shows TEF spectra for electron focusing with $E=1$ and $C=2$ (curve 1)—TEF amplitude 3.1×10^{-6} V; hole focusing with $E=2$ and $C=3$ (curve 2)—TEF amplitude 0.42×10^{-6} V; and electron-hole intervalley scattering, with $E=1$ and $C=3$ (curve 3)—TEF amplitude 0.01×10^{-6} V.

Two other potential mechanisms must be examined for the TEF peak in curve 3 of Fig. 22(a), focusing of current carriers on nonextremal orbits on the Fermi surface (drift electron focusing, Sec. VI.C), and trajectory reproduction of the electric field of a point contact (Kolesnichenko *et al.*, 1982). The first is excluded by the Fermi surface shape and the mfp's of the current carriers. The second would produce a signal two orders of magnitude too small. Thus electron-hole intervalley

scattering transitions must produce the TEF peak in curve 3 of Fig. 22(a).

A further check of the TEF peak source was made by examining how its amplitude varied when **H** was rotated. The signal dropped off rapidly away from the maximum, because to see the hole and electron TEF lines at the same value of H requires an **H** direction within about 10° of the line between contacts 1 and 2. A small deviation δ from this direction causes a large displacement $[2R_c=2R_c(\varphi=0)/\cos(\varphi+\delta)$, with φ about 80°] of the point onto which electrons are focused, thereby shifting the focused electrons away from the collector.

Thus curve 3 of Fig. 22(a) is due to electron-hole intervalley scattering processes. As noted above, this curve contains contributions from excitations following two different paths in Fig. 21(b), electrons emitted from $E=1$, converted to holes at 2 and focused onto $C=3$, and holes emitted from $E=1$, converted to electrons at 2 and focused onto $C=3$. The difference lies in the presence of the contact at 2 that produces local damage, but none at $2'$, where the surface is "perfect." Inverting **H**, and simultaneously inverting the roles of the contacts to $E=3$ and $C=1$ shifts the electron-hole transitions to $2'$ and the hole-electron transitions to 2. Such an inversion did not change the amplitude of the TEF peak, showing that $h_{eh}=h_{he}$ (Sveklo and Tsoi, 1989a).

As noted above, surface roughness is required for electron-hole intervalley scattering to occur. In the processes described so far, roughness was produced at point 2 by damage due to contact installation. The importance of such damage was studied by fixing the relative orientation of contacts 1 and 3 while moving them to a different part of the surface, where contact 2 was absent, so that both locations 2 and $2'$ were undamaged. Figure 22(b) shows that the TEF peak amplitude for such undamaged surfaces was much smaller than that for one damaged surface and one undamaged one, and that the peak was also much broader [note that the U scale is μV in 22(a) but only nV in 22(b)]. Clearly the probability of electron-hole (hole-electron) surface transitions is enhanced by the defects produced during contact installation.

Converting h_M to h (see Sec. IV.D.2) using the TEF peak shapes in curves 1 and 2 of Fig. 22(a) to estimate the ratio b/L led to the following estimates of the probabilities of electron-hole intervalley scattering transitions h_{eh} and hole-electron transitions h_{he} for undamaged and damaged surfaces (Sveklo and Tsoi, 1989a): $h_{eh}+h_{he}\approx 0.02$ for the undamaged area, and $h_{eh}\approx h_{he}\approx 0.04$ for the damaged area.

E. Surface band bending

1. $q(\theta)$: TEF at multiples of H_0

If surface band bending is present in Bi, then it should exert a profound influence upon the scattering of electrons incident on a rough surface, by producing a long-range ($\gg a_0$) potential that stops electrons from reaching the surface (Sec. IV.C.). The minimum scale of the potential roughness is approximately the Debye screening radius, $r_D \gg a_0$, so this screening stops electrons from feeling any atomic roughness. The electrons then see a smoother potential that should suppress the intervalley scattering channel that requires atomic-scale roughness to occur, and should cause the electrons to be scattered more specularly. Higher-order TEF peaks, at multiples of the first TEF peak field H_0, involve electrons impinging at normal incidence. These peaks are the focus of the present section. An abrupt steplike cutoff of diffuse scattering when the incident angle decreases, due to band bending, can shift higher-order TEF peaks to lower fields and decrease the separation between them (V. Tsoi and N. Tsoi, 1977). The physics is that electrons incident at the high angles that usually dominate the multiple TEF peaks are greatly reduced by diffuse scattering, leaving mostly the low-field tail of specularly reflected electrons incident at smaller angles. The higher-order TEF maxima then occur at smaller values of H than the usual multiples of H_0.

The heavy curve in Fig. 23(a) is a TEF spectrum for $\mathbf{N}\|\mathbf{C}_2$ (V. Tsoi and N. Tsoi, 1977). Note that the decay of amplitude is sharp, the higher-order TEF peaks shift to

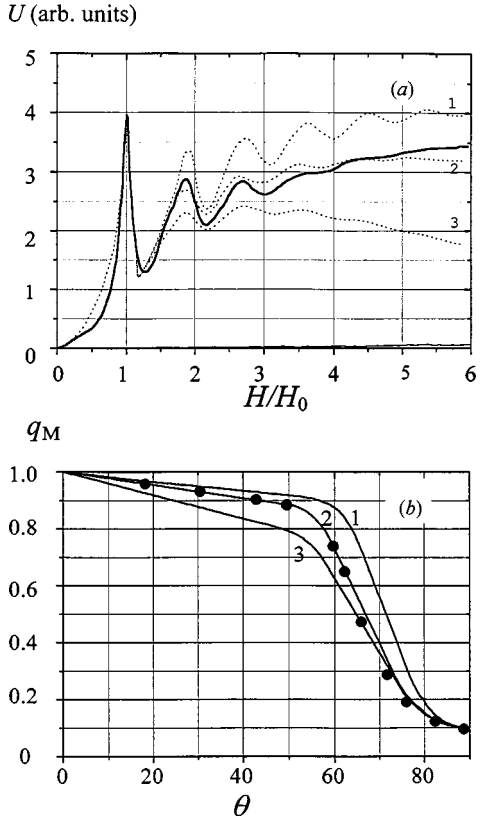

FIG. 23. Evidence for band bending. (a) Collector voltage U vs H/H_0. The solid curve depicts data for $\mathbf{H}\perp\mathbf{N}\|\mathbf{C}_2$ with $\mathbf{L}\perp\mathbf{H}\|\mathbf{C}_1$ and $L=0.15$ mm. The dashed curves 1–3 are calculated for $q(\theta)$, the probability of specular reflection at all angles, with the forms of curves 1–3, respectively, in (b). (b) Probability of specular reflection at all angles, q_M vs θ (degrees). The solid circles in (b) show the ability of band bending to reproduce the $q(\theta)$ of curve 2 using parameters given in the text. After V. Tsoi and N. Tsoi, 1977.

lower fields, and the separation between peaks 2–5 is less than H_0. For comparison, for $\mathbf{N}\|\mathbf{C}_3$ [Fig. 13(a)] the decay of amplitude is much slower, and the higher-order peaks are located very closely at multiples of H_0. As noted in Sec. VI.A, no evidence of differences in surface roughness for these two surfaces was seen by either optical or electron microscopy.

Tsoi and Tsoi (1977) used the solid curve of Fig. 23(a) and the geometrical model of TEF (see Sec. I) to derive the $q(\theta)$ given by curve 2 in Fig. 23(b). As the derivation is complex, we refer the reader to that paper for details. When we reverse the process, the dotted curve 2 in Fig. 23(a) shows that this derived $q(\theta)$ fits the experimental data rather well. The sensitivity of the fits in Fig. 23(a) to variations in the curve in Fig. 23(b) is illustrated by the alternative coupled curves labeled 1 and 3.

We conclude by asking how well the $q(\theta)$ of curve 2 in Fig. 23(b) can be explained by band bending. To do this, we estimate the band bending needed to reproduce that $q(\theta)$. We assume only intravalley scattering and include refraction by requiring conservation of electron energy as the electron approaches the surface. Taking $q(\pi/2)=0.13$ from Fig. 23(a) and assuming $q(\theta)=1$ for θ below the cutoff, we are left with only one adjustable parameter, V_0/ε_F. Curve 1 in Fig. 24 shows the $q(\theta)$ derived assuming $V_0/\varepsilon_F=0$—no band bending. Curves 2–6 show the cutoff of diffuse scattering with decreasing θ for $V_0/\varepsilon_F=0.1$, 0.2, 0.4, 0.6, and 0.8. Comparing these curves with curve 2 in Fig. 23(b) we see that $q(\theta)=1$ below the cutoff will not do. If, instead, we take $q(\theta)$ for scattering from the potential barrier to have the form of the dashed curve in Fig. 24, corresponding to $q(\pi/2)=0.8$ [i.e., $\eta\sim 50$ Å in Eq. (3)] and $V_0/\varepsilon_F=0$, and choose for the physical surface itself $V_0/\varepsilon_F=0.7$ [(i.e., $V_0\approx 15$ mV) and $q(\pi/2)=0.13$ ($\eta\sim 130$ Å)], we predict the solid circles in Fig. 23(b). These show that band bending with reasonable parameters can fit the derived $q(\theta)$ of curve 2.

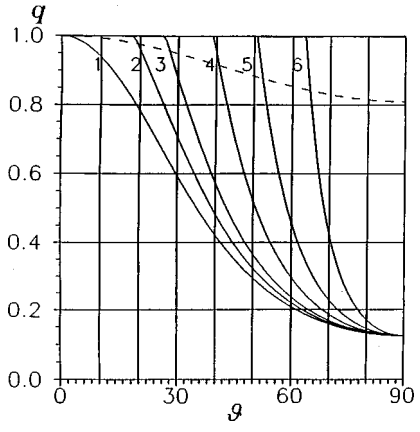

FIG. 24. Calculated angular variation of q, $q(\vartheta)$, ϑ in degrees, using Eq. (3) and taking account of refraction. Curves 1–6 use $q(90°)=0.13$ from Fig. 23(a) with band-bending parameters $V_0/\varepsilon_F=0$, 0.1, 0.2, 0.4, 0.6, and 0.8. The dashed curve is for $q(90°)=0.8$ and $V_0/\varepsilon_F=0$, appropriate for helping to fit the data of curve 2 in Fig. 23(b).

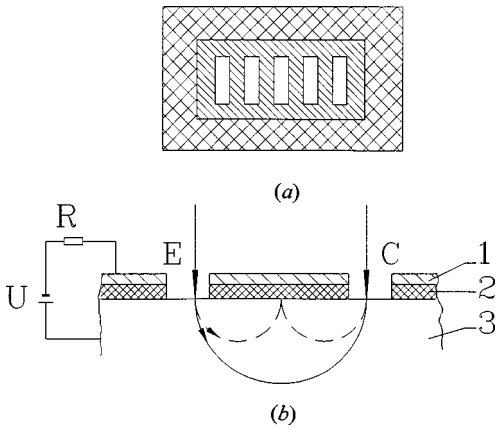

FIG. 25. Setup for observing the effect of an external electric field on the reflection of conduction electrons from a sample surface. The deposited Al film is hatched, the insulating film is cross hatched: (a) Top view. (b) Sectional view of the capacitor: *E*, emitter; *C*, collector; 1, Al film; 2, insulating film; 3, Bi sample; *U* voltage source; *R*, ballast resistance. Two trajectories are shown, one without reflection (solid curve) and one after a single reflection (dashed curve). From Sveklo and Tsoi, 1992.

2. Artificial band bending

Here we describe an experiment that further strengthened the case for band bending and surface charge in Bi when it suppressed intervalley scattering by changing the charge on a surface. Since, in the usual TEF geometry, intervalley scattering contributes only part of the reflection, isolating its contribution was not trivial.

The usual TEF scheme was used to focus electrons in a Bi single crystal with $\mathbf{N}\|\mathbf{C}_3$ and $\mathbf{L}\|\mathbf{C}_2$ (Sveklo and Tsoi, 1992, 1993). To maximize the change in reflection due to an external electric field, the surface was Ar^+ ion etched to maximize the initial probability of intervalley scattering. An external electric field was created with a special capacitor, shown in Fig. 25, in which one electrode was the sample and the other a thin Al film evaporated onto a dielectric insert. A thin layer of insulator was first deposited onto the sample surface, and rectangular slits $100\times 1000\ \mu m^2$ were made in the insulator using photolithography. Then the Al film was evaporated onto the insulator through a mask. Any short circuit was removed by applying a voltage ~10 V between the film and sample, giving a current large enough to burn out the film along the slit edges. Electrical connection was made to the Al film with conducting glue. Photoresist and SiO were tried as alternative insulators. A centrifuge was used to create a photoresist film ~1-μm thick. The SiO was evaporated thermally to a thickness of ~0.5 μm.

An emitter and collector were placed in neighboring slits in the insulator [Fig. 25(b)], and TEF spectra were taken with and without a voltage on the capacitor. The voltage was near the limit of the insulating material. After SiO was evaporated onto the sample surface, q increased by ~0.1–0.15 relative to the q for a reference area on the sample surface, but applying an electric field did not affect the TEF spectrum. With the photo-

resist, however, a voltage of −30 V (electric field $\sim -6\times10^5$ V/cm) gave a noticeable effect.

Figure 26 compares TEF spectra with −30 V (heavy curve) and with 0 V (light curve) on the capacitor. Applying +30 V did not affect the spectrum. Applying −30 V, in contrast, led to the appearance of the third peak, which was unresolved at 0 V. The rest of the TEF spectrum hardly changed.

The crucial point in explaining such behavior is that, under diffuse scattering, a change in q, δq due to intervalley scattering does not affect the amplitude of the second TEF peak (seen when the collector C is placed at point P in the upper half of Fig. 18) because the Fermi surface consists of three identical ellipsoids (except for rotation in the plane of the sample surface). A change δq due to intervalley scattering at point O onto two other ellipsoids is completely compensated by intervalley scattering back from these other two ellipsoids at points A and B. The height of the second peak is thus independent of whether intervalley scattering is present. For the third peak, in contrast, C must be located at C in the upper half of Fig. 18. There are now many more possible paths from E to C, and no cancellation is required (for details see Sveklo and Tsoi, 1992, 1993).

To summarize, the electric field should produce a change in peak amplitude that depends upon the field polarity, and this crucial test is satisfied. The two most prominent features of the data of Fig. 26, no change in A_2 and a significant increase in A_3, can be explained by a simple model involving intervalley scattering on the electron Fermi surface of Bi. The small probability of specular reflection inferred from the experiments does not allow the amplitudes of TEF peaks beyond the third to be observed.

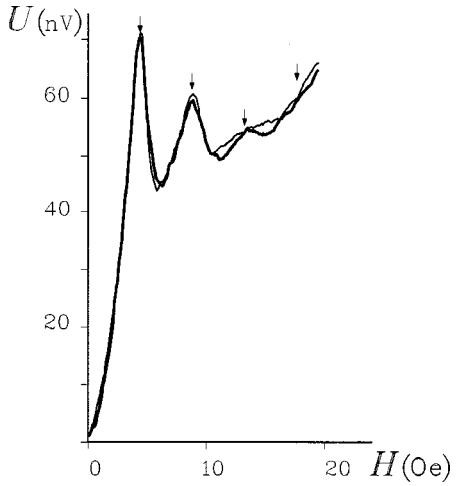

FIG. 26. Collector voltage U vs H for zero voltage across the capacitor (light curve) and for −30 V (heavy curve). Arrows indicate expected TEF peak locations. From Sveklo and Tsoi, 1992.

VII. CONDUCTION-ELECTRON SURFACE RESONANCES

In previous sections, we have shown how different perturbations can change the magnitudes and locations of the usual TEF peaks in metals and semimetals. In this section we show how a singularity in the scattering of electrons in a particular state can lead to new peaks.

In quantum mechanics, the capture of an incident particle by a target to form a compound state, which later decays to release the particle (Landau and Lifshitz, 1965), so profoundly affects the scattering cross section that it is given a special name: resonant scattering or resonance. Surface resonances in solids have been seen with several external probes. In molecular-beam scattering the phenomenon is called "selective adsorption" (Heinz *et al.*, 1982; Benedek and Valbusa, 1987). For electrons, surface resonances were first seen in high-energy scattering (Kikuchi and Nakagawa, 1933) and later in low-energy scattering (McRae and Galdwell, 1964). McRae (1979) reviewed the excitation of electronic surface resonances by low-energy electrons. Excitation of electronic surface resonances by conduction electrons is similar, but has features specific to a degenerate Fermi system.

Here, we describe the use of TEF (Tsoi, de Wilde *et al.*, 1996) to see conduction-electron surface resonances (CESR)—resonant transitions of conduction electrons into and back out of electron surface states in the presence of **H** aligned parallel to the surface. The trick is that such resonances produce new TEF peaks. The surface states can be of two kinds: (1) Surface magnetic (edge) states such as those seen in metals with **H** parallel to the surface (Khaikin, 1960, 1969; Nee and Prange, 1967), where electrons skip closely along the sample surface under specular reflection. The electron must make several skips before being scattered diffusely—i.e., q must be ≈ 1 for orbits intersecting the surface at small angles. (2) Electron quantum levels in a potential well produced by surface band bending (Secs. IV.C and VI.E). It is not yet known which of these controls the behavior we describe.

As in the other resonant situations mentioned above, singularities in the scattering indicatrix can occur for conduction-electron surface scattering if an incoming electron can make transitions into and out of a surface state while conserving $\mathbf{p}_\tau$—i.e., under resonance conditions. In the TEF experiments, a surface grating provided the surface reciprocal-lattice vector **G** needed for such conservation. Conduction-electron surface resonance can occur with either intravalley or intervalley scattering (Sec. VI.D), but the new peaks due to intravalley contributions must lie on the slopes of much larger standard TEF peaks and have not yet been seen. In contrast, the new peaks due to conduction-electron surface resonance and intervalley scattering have been isolated by clever use of the contact geometry and field orientation to eliminate the much larger standard intravalley and IVS TEF peaks.

In Sec. VII.A we describe the physical grounds for the observed behavior of conduction-electron surface resonances and explain where one expects new peaks if intervalley scattering processes are dominant. In Sec.

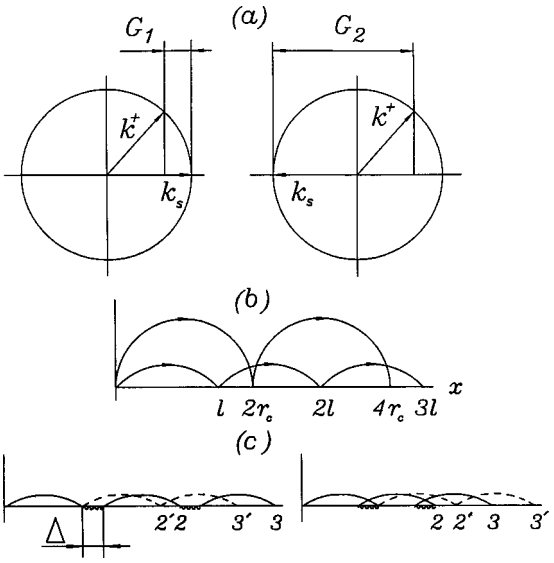

FIG. 27. Surface resonance geometries. (a) Trapping of an electron $\mathbf{k}^+$ into a surface state $\mathbf{k}_s$ via reciprocal vector $\mathbf{G}_1$ or $\mathbf{G}_2$. (b) Skipping orbits in an applied magnetic field that give the usual TEF at distances $2r_c$ and $4r_c$, and focusing via resonant scattering into a surface state at $2l$ and $3l$. (c) Skipping orbits for trapping into surface states with a finite lifetime, adding a correction Δ to the skipping length with focusing now at 2 and 3 ($2'$ and $3'$ for $\Delta=0$) for the two cases with opposite $\mathbf{k}_s$.

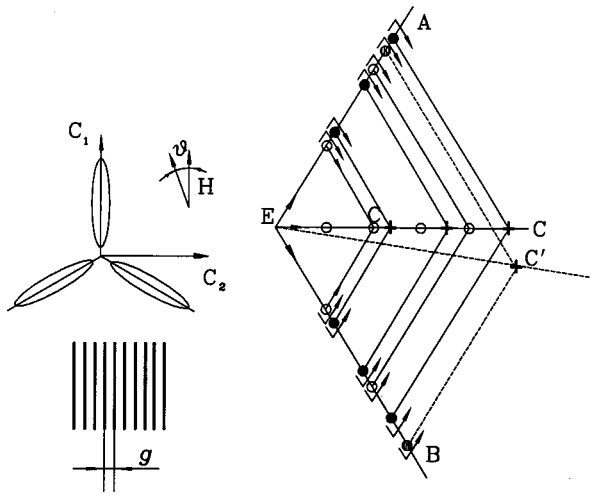

FIG. 28. Projection of the electron valleys (ellipsoids) of Bi onto the $(k_x k_y)$ plane, along with the expected focusing locations for the indicated orientation of the magnetic field and the grating grooves. Open circles denote ordinary focusing locations, solid circles surface resonance singularities, and crosses surface resonances involving intervalley scattering (denoted by bent arrows). Tilting the field away from $\mathbf{C}_1$ shifts the surface-resonance intervalley scattering singularities away from EC (dashed lines). Contact installation along EC' (slightly tilted from EC) reduces intravalley TEF peaks because the focusing location then only slightly overlaps the collector, but a proper ϑ restores the intervalley scattering peaks (dashed lines).

VII.B we shall see that the data display both the qualitative and the semiquantitative behaviors expected.

A. Physics underlying conduction-electron surface resonances

Figure 27(a) shows how a surface reciprocal-lattice vector $\mathbf{G}_\tau=\mathbf{G}_1$ or $\mathbf{G}_2$ can conserve tangential momentum [Eq. (1)] in trapping a particular incident bulk electron $\mathbf{k}^+$ at the Fermi energy ε_F into a surface state in which $\mathbf{k}_s$ is parallel to the surface. We treat elastic scattering (i.e., conservation of electron energy) and, for simplicity, assume $k_S=k_F$, thereby neglecting the depth of any surface level below ε_F. The surface-state dispersion is also taken to be the same as in bulk. Because in Bi, $\lambda_{dB}\approx 100$ nm, $\mathbf{G}_\tau$ could be provided by an artificial grating on the Bi surface much larger than atomic scale.

Figure 28 illustrates the intravalley and intervalley processes that can contribute to the TEF signal of interest, showing the steps taken by electrons in moving along the Bi surface when the electron ellipsoids are replaced by cylinders. As the electrons on each cylinder move in a plane perpendicular to the cylinder axis (Sec. II.A), electrons emitted at E move along lines EA, EB, and EC. Arrows with kinks indicate changes in planes of motion upon intervalley scattering (compare to Fig. 18). Open circles indicate the usual transverse electron focusing locations along the three lines of electron emission (one for each electron ellipsoid), with both intravalley and intervalley contributions. Solid circles indicate the focusing locations for resonant scattering. Note that it takes two skips (at least one scattering from the interface before detection) to give a singularity in the resonant processes. In Fig. 28, the first solid circles along EA (or EB) are shown further out than the first open circles. Thereafter, the separation between solid circles along EA is smaller than that between open ones, because a skip length is less than the cyclotron diameter that determines the separation between those open circles. The lengths of the skips are compared with those of the usual intravalley semicircles along EC in Fig. 27(b), showing resonant electrons jumping along the surface in an applied field $\mathbf{H}$. For $\mathbf{k}_s^+=\mathbf{k}_s-\mathbf{G}_\tau$ and $k_S=k_F$, the skip length for an intravalley process along EC is $l=2R_c((2k_F G_{\text{eff}}-G_{\text{eff}}^2)/k_F^2)^{1/2}$, where G_{eff} is the component of $\mathbf{G}_\tau$ perpendicular to the cylinder axis, as only that component is effective (for paths along EA and EB, R_c is twice that for the path along EC). Conduction-electron surface resonance singularities in $\rho(x)$ along EC (Sec. II.B) would then occur at $x=2l$, $3l$, etc. As in ordinary focusing, these singularities should give collector voltage peaks as a function of H when $x=L$. However, for the intervalley scattering processes actually studied, where L is along EC, the conduction-electron peaks after scattering occur at the locations indicated by crosses in Fig. 28. The resulting length along EC, $l^*=4R_C\{[2k_F G_\tau/2-(G_\tau/2)^2]/k_F^2\}^{1/2}$ and $x=2l^*$, $3l^*$, etc., should give collector voltage peaks as a function of H whenever $x=L$. Lastly, since the resonance skipping orbits of Figs. 27 and 28 involve correlated absorption and remission of electrons, they do not require specular reflection. Hence multiple TEF peaks occur independently of whether reflection is specular or diffuse.

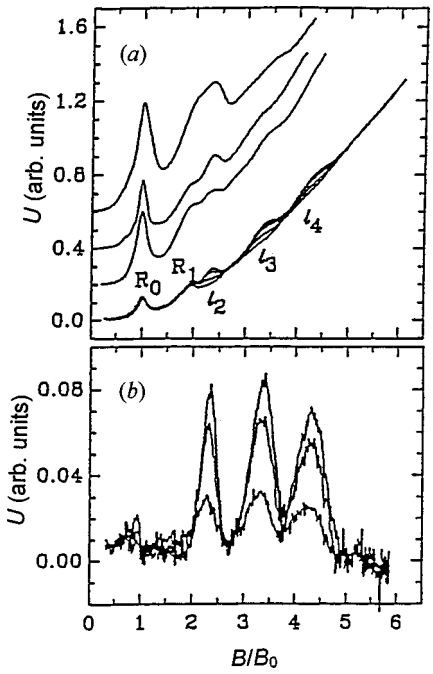

FIG. 29. Transverse electron focusing signals for different distances between E and C parallel to $\mathbf{C}_2$: (a) The field is normalized to the focusing field H_0. Both **H** and the grooves of the surface grating are parallel to $\mathbf{C}_1$. R_0 and R_1 indicate the usual TEF signals, and l_2, l_3, and l_4 surface-resonance signals. The lowest TEF curve shows the strong suppression of surface resonances in a rotated magnetic field (ϑ changes by 2 degrees between curves). (b) The curve with the largest ϑ has been subtracted from the others, to better show the decrease in collector signal with increasing ϑ. From M. Tsoi *et al.*, 1996.

B. Samples, data, and analysis

The measurements were made with the otherwise standard TEF geometry of Fig. 1, with emitter current $\approx 1\,m$A. Photoresist was applied to the surface of a Bi crystal perpendicular to the threefold $\mathbf{C}_3$ axis, and holographic interferometry was used to make a grating with period $g=170$ nm (surface reciprocal vector $G_\tau = 2\pi/g$) and **L** slightly off parallel to $\mathbf{C}_2$ (x axis). A grating on the Bi crystal surface was reactive ion etched to a groove depth ≈ 100 nm.

The electron mfp was comparable to the contact separations $\geqslant 100\ \mu$m. Thus (Sec. IV.D.2), the usual intervalley scattering contributions to TEF in Bi are suppressed relative to intravalley ones, because the intervalley scattering path length is twice as long. However, electrons hopping via surface resonances have shallow trajectories [Fig. 27(b)], with shorter path lengths that enhance their TEF signal. These factors aid in seeing the conduction-electron surface resonance signals.

Figure 28 shows that the slight misalignment of EC from $\mathbf{C}_2$ noted above should switch off the usual intravalley TEF contributions, but a small rotation of **H** can then bring intervalley scattering back.

Figure 29(a) shows typical TEF recordings vs H at 1.5 K for the alignment of **H** needed to give intervalley scattering and for rotations ϑ of **H** away from this alignment. Because the position of the first peak R_0 is proportional to $1/\cos\vartheta$, and different values of L were used in the measurements, the abscissas were rescaled to bring the first peaks together—$H/H_0=1$. All the curves then show similar features. Peaks R_0 and R_1 are the usual first two TEF peaks at H_0 and $2H_0$, with q too small for the peak at $3H_0$ to be seen. The peaks labeled l_2, l_3, and l_4 are anomalous and are not seen without a surface grating. They are not located at $3H_0$, $4H_0$, $5H_0$ but are approximately related as $2l$, $3l$, and $4l$, as expected from the model described above.

Rotating **H** through small angles ϑ around the best alignment provides a check that these anomalous peaks are due to intervalley scattering, since such rotations should switch off intervalley scattering, but hardly affect the already reduced intravalley scattering. Figure 29(a) shows that the surface resonances are strongly suppressed for $\vartheta \neq 0$, but the two usual intravalley TEF peaks are not.

In Fig. 29(b), the surface-resonance singularities (l_2, l_3, l_4) have been enhanced by subtracting the curve in Fig. 29(a) with the smallest resonance peaks. The attenuation of these singularities with increasing peak number is clearly much less than that of the ordinary TEF peaks (R_0, R_1). Such behavior also supports the picture of enhanced specular reflection of selected electron states resonantly coupled to surface states, since such a correlated process should give little loss of electrons from one peak to the next.

The observed behaviors all qualitatively agree with expectations for intervalley scattering. The resonance peaks should be at $x=2l^*$, $3l$,* and $4l^*$ with $l^* = 4R_C\{[2k_F G/2-(G/2)^2]/k_F^2\}^{1/2}$. Using $k_F = 0.530 \times 10^{-8}\,\mathrm{m}^{-1}$, one expects the first focusing peak for surface resonances at $3.4H_0$. The actual first peak occurs about 25% lower. The difference in fields between the peaks at l_2 and l_3 (or l_3 and l_4) is also not exactly half the field of peak l_2. Both disagreements can be removed (Tsoi, de Wilde *et al.*, 1996) by assuming that a finite lifetime for the electrons trapped in surface states requires adding a distance Δ to the skipping orbit length l^* under focusing conditions [Fig. 27(c)]. $\Delta \cong (0.3)l^*$ gives the observed focusing fields of $2.3H_0$, $3.4H_0$, and $4.4H_0$ to within experimental accuracy. However, since possible surface band bending and differences in dispersion of surface and bulk states have been neglected, the agreement is not definitive. A more complete theory including higher-order diffraction effects is still needed.

VIII. INTERCRYSTALLINE BOUNDARY

A general theoretical analysis of conduction-electron transmission through an intercrystalline boundary is not trivial, because the **p** spaces of the adjacent crystals are rotated relative to each other, giving many possible electron states after transmission. Theoretical principles for the problem were given by Pippard (1965), and some aspects were treated by V. Tsoi *et al.* (1992), but the topic is still in an early stage where experimental guidance is crucial. For fundamentals of interfaces, see Sutton and Balluffi (1995). Experimentally, transmission

and reflection of electrons from intercrystalline boundaries are essentially unstudied. The only direct study known to us is that by Sharvin and Sharvin (1979), who used the symmetry of a twinning plane in Al to obtain a radio-frequency size effect (the Gantmakher effect) that required correlated transmission of electrons through the interface plane, with the two sample surfaces and the interface all parallel to each other. TEF studies should thus be fruitful.

The possibility of using TEF to study reflection and transmission of conduction electrons at an interface between two conductors was recognized early on (V. Tsoi *et al.*, 1992), but only recently carried out. Section IX describes TEF studies of reflection at an N/S interface. In the present section we describe the first results of a TEF study of transmission and reflection at a $\sim 30°$ intercrystalline boundary of a Bi bicrystal (M. Tsoi *et al.*, 1997). The measurements were made with the technique of laser-induced electron excitations described in Sec. III, with the emitter E scanned and the collector C fixed. By allowing visualization of a two-dimensional nonequilibrium electron distribution, this technique greatly simplifies the problem of determining the behavior of electrons after transmission or reflection. However, it also brings complications. Since a real surface is inhomogeneous, and the EC distance changes as the emitter moves, quantitative data analysis is not simple. Moreover, differences can occur between the situation described and the more natural case to analyze in which E is fixed and C is scanned. The pattern structures are essentially the same, but the way they come about is different. For ease of exposition, we describe the data as if E were fixed and C scanned. We shall see evidence that the boundary usually transmits electrons with high probability, but sometimes does not transmit them at all. This latter behavior may indicate that the Bi boundary can become superconducting under as yet unclear conditions.

Studying electron transmission and reflection at an intercrystalline boundary is especially easy in Bi, because the electron valleys of the Fermi surface are cylindrical. As described in Sec. II.A and illustrated in Figs. 3(c), 30(a), and 30(b), if **H** is applied at an angle φ to the axis of a cylindrical Fermi surface, the motion of an electron is a circle of Larmor radius $R_c = p_F c/(eH\cos\varphi)$ in the plane perpendicular to the cylinder axis. Electrons specularly reflected from the surface skip along the surface, staying in the same plane, independent of the direction of **H**. Changing the direction or magnitude of **H** changes only R_c. In Fig. 30(b), the sample surface is taken to be the (xy) plane, the intercrystalline boundary is the (yz) plane, and **H** lies in the (xy) plane. When **H** is parallel to the cylinder axis, the motion of an injected electron in **p** space [Fig. 30(a)] is cyclical along the line a'-b'-c', corresponding to motion in **r** space [Fig. 33(b)] along the line E-b-c, etc., repeating the previous skip along the x axis. When **H** is tilted from the cylinder axis by φ, the electron moves along the line a'-b*-c' in **p** space [Fig. 30(a)] and along the line E-b*-z*-c, etc., [Fig. 30(b)] in **r** space.

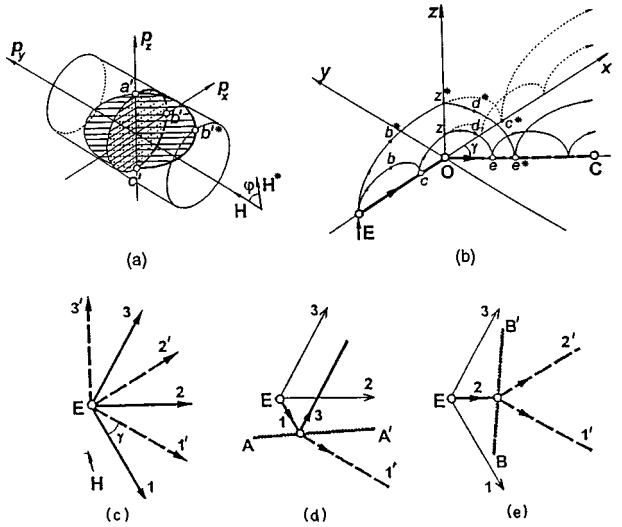

FIG. 30. Motion and skipping paths of electronic excitations injected through emitter E on the surface [(xy) plane] of a conductor with a cylindrical Fermi surface: (a) In **p** space, two thick lines (a'-b'-c' and a'-b'*-c') represent two different directions of the magnetic field **H** lying in the $(p_x p_y)$ plane. (b) In real space, without the intercrystal boundary, lines E-b-c, etc., and E-b*-z*-c*, etc.; refracting at the intercrystal boundary [(yz) plane]—lines with and without asterisks indicate two directions of the magnetic field **H**. The heavy line E-O-C shows the refracting skipping path. (c)–(e) Schematic drawings of the skipping paths (1–3 and $1'$–$3'$ in adjacent crystals), propagating along the sample surface (arrows indicate the direction of propagation for a given orientation of **H**). The three paths for each crystal are due to the three "cylinders" of the Bi Fermi surface (see text). (c) No interface (all paths—1–3 and $1'$–$3'$—shown coming from one emitter). (d) and (e) electron transmission through a boundary [paths 1-$1'$ in (d) and 2-$2'$, 2-$1'$ in (e)] and electron reflection from the boundary [path 1-3 in (d)] for two different boundary orientations, AA' and BB'].

To treat electron transmission through an intercrystal line boundary, we assume that the half-spaces $x<0$ and $x>0$ are occupied by the same material, but that the Fermi-surface cylinders in adjacent crystals are transformed into each other by rotation around the p_z axis through an angle γ. Transmission through the boundary thus results in rotation of the plane of electron motion [Fig. 33(b)]. The skipping paths in adjacent crystals are shown as the thick lines E-O and O-C. The incident electron hits the interface at point z (or z* depending upon the direction of **H**) and follows a possible path z-d-e, etc. (z*-d*-e*, etc.). Note that in the half-space $x>0$, **H** is tilted from the axis of the Fermi-surface cylinder by the angle $\varphi+\gamma$.

In Bi, the electron Fermi surface consists of three cylinders. Hence in each crystal there are three planes of electron motion. The intersections of these planes with the surface—skipping paths—are shown in Fig. 30(c) (solid lines depict skipping paths in one crystal, dashed in the other). In an applied magnetic field, depending upon the orientation of **H** and the intercrystalline boundary, it is possible to observe both electron trans-

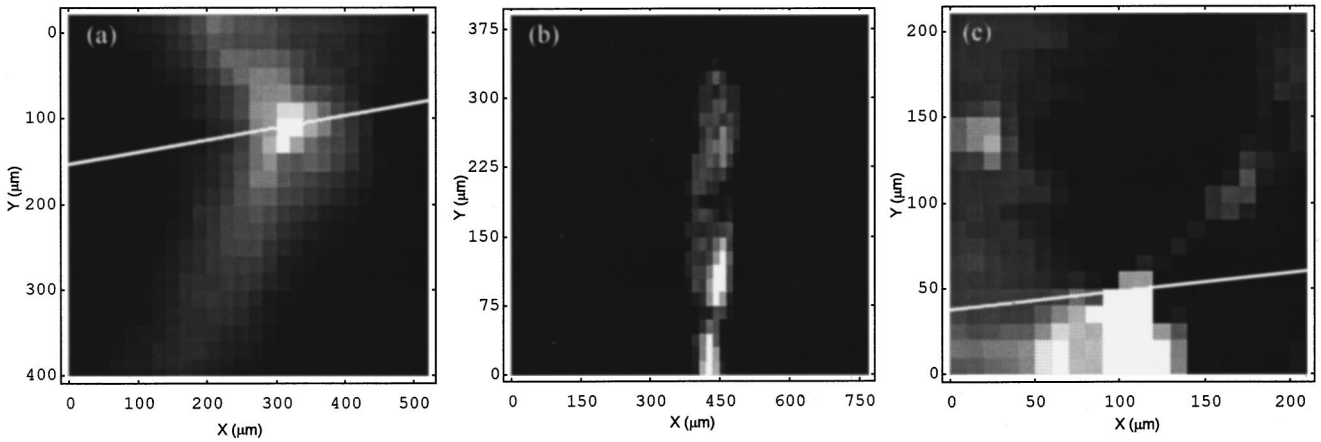

FIG. 31. Drift flux and ballistic TEF transmission through a bicrystal interface: (a) 2D grey scale density plot of the drift flux through the interface (indicated as a white line), with $H=50$ Oe about in the x-axis direction. Lighter color indicates higher flux. For (x, y), the flux enters from about (200,0) and exists at about (150,400). (b) and (c) Density plots for ballistic TEF, (b) with no interface and $H=10$ Oe about in the x-axis direction—three ordinary TEF peaks are visible centered at roughly (430,10), (440,120), and (450,240), and the emitter position is about (420,110)—out of the scanned area; (c) transmission through the interface (indicated as a white line) with $H=6$ Oe in the x-axis direction. Two broad, weak TEF peaks are visible after electron transmission through the interface, one at about (25,135) and one at about (170,110); the emitter position is out of the scanned area at about (130,–50). The white squares within (90–130, 0–50) are due to the enhanced contrast needed to make the two weak peaks visible.

mission through a boundary and reflection from it. Figures 30(d) and 30(e) illustrate these possibilities for boundary orientations AA' and BB' with $\gamma \approx 30°$, near the value in the experiments.

The measurements (M. Tsoi *et al.*, 1997) were made on an accidentally grown Bi bicrystal, the surface of which was etched to make the intercrystalline boundary visible. Electron reflection from that surface at large angles of incidence was diffuse, with a high probability of electron-electron intervalley surface scattering (Sec. VI.D). The $\mathbf{C}_3$ axes of the two single crystals were parallel to each other and tilted by 12° to the normal to the sample surface. X-ray diffraction showed that the orientation of the single crystals was such that they transformed into each other by a rotation of about 30 degrees around the $\mathbf{C}_3$ axis.

The emitter and the collectors for reflected or transmitted signals were located on the same face of the bicrystal slab. Two sets of measurements were made, one involving *drift flux* and one *ballistic flux*. To observe drift flux, the energy relaxation mfp l_ε must be greater than or equal to the E-C separation. For observation of ballistic effects, the ballistic electron mean free path l_b must be long enough to give ballistic motion from E to C.

A. Drift flux

For this case, the setup was optimized to visualize refraction of the conduction electrons at the intercrystalline boundary. A drift (nonballistic) flux was created by increasing the magnetic field H to make R_c only about half the emitter size. In this case, the series of ballistically produced focusing peaks on the sample surface that one would expect for a smaller H collapse together, and one expects to see just the propagation of excitations along the sample surface in directions perpendicular to the axes of the electron ellipsoids [skipping paths in Figs. 30(b)–(e)]. The flux consists of two parts: (1) electrons reflected specularly from the surface; and (2) electrons that undergo random (diffuse) intravalley reflection, but with excitation energy$\neq 0$. The electrons stay in the same plane in **r** space and continue to skip along the same line, forming the drift flux after either specular or diffuse scattering, but not after intervalley scattering, which results in spreading and damping of the flux. Far enough from the emitter, mostly glancing electrons contribute to the flux for two reasons. First, these electrons have much shorter path lengths (they move almost in a straight line, and contributions of other electrons are suppressed because of inelastic scattering events). Second, the reflection of glancing electrons is highly specular (Sec. VI.C).

Since E is scanned, in principle, both transmission and reflection could be detected by a single collector for correct geometries. M. Tsoi *et al.* (1997) set the direction of **H** so that relatively high electron fluxes could propagate along the surface for two ellipsoids: propagating from E to the boundary on one ellipsoid, and then, after transmitting through the boundary, propagating to C on a different one. For this direction of **H**, any reflection was too weak to be clearly resolved.

One might have expected the initially highly directed flux on each ellipsoid to deplete rapidly as it propagated, due both to intervalley scattering (Sec. VI.D), which transfers electrons from the flux for one ellipsoid to those for the other two, and to finite-lifetime effects, which take excitations out of the directed flux. The surface etch used to make the intercrystalline boundary visible might even have exacerbated such effects. The observation of focused signals means that intervalley scattering is less effective for grazing incidence reflections.

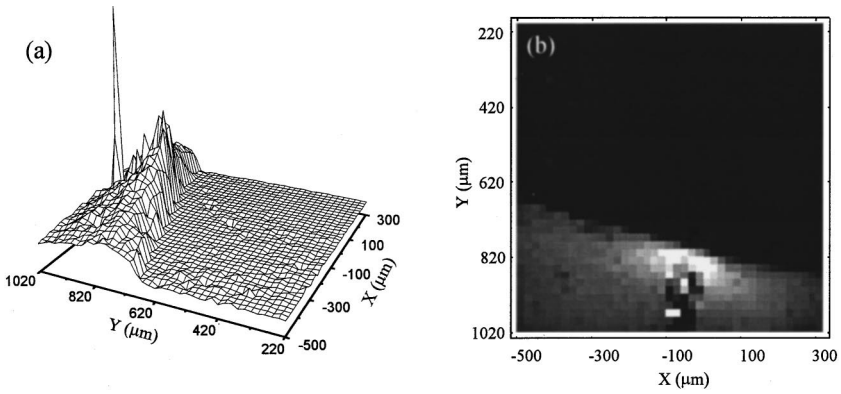

FIG. 32. Two plots for ballistic TEF of attempted transmission through an unusual plane: (a) topological graph, rotated by over 90° from (b) the grey scale one to make its features more visible; (b) two-dimensional grey-scale density plot of a plane located at the boundary between the darker (low) and lighter (higher) areas. Both figures show three TEF peaks before the flux reaches the plane, and no transmission.

Figure 31(a) shows a typical experimental 2D grey-scale pattern of the diffusive flux. The white line indicates the position of the interface and the white rectangle indicates where the incident and transmitted fluxes encounter it. The incident flux comes from the bottom center, and the transmitted flux exits at the top, left of center. The transmitted flux is clearly rather high under these conditions.

B. Ballistic flux

For the ballistic flux, H was chosen to make R_c about the point-contact/interface separation, much larger than the microcontact size. The ballistic trajectories project into the sample as shown schematically in Fig. 30(b). Preliminary measurements involving drift flux were used to find the best positions for observing TEF peaks due to interface transmission. Once the directions of incident and transmitted flux were established, C was set ~100 μm from the interface and E was scanned to determine the value and the direction of **H** that gave the most intense focusing peaks due to transmitted electrons.

Results for the ballistic fluxes are depicted in Figs. 31(b) and (c), which compare the behaviors seen with and without an interface. Figure 31(b) shows three gradually broadening and weakening focusing peaks for no interface. Figure 31(c) shows, on a magnified scale, just two peaks (due to two different electron ellipsoids) after transmission through the interface (indicated as a white line), one fairly well defined at about (25,135) and one less well defined at about (170,110). This picture clearly shows focusing peaks after electron refraction at the boundary. The concept of extremal displacement can be used to analyze TEF under electron transmission and reflection at a boundary (V. Tsoi *et al.*, 1992). We omit detailed analysis of the origin of the TEF peaks after transmission, only indicating, first, that the focused electrons impinge upon the boundary at about normal incidence and, second, that after refraction (a correlated transmission—not random or chaotic, which would destroy focusing under the conditions specified) the electrons are focused onto the sample surface. Such focusing was made possible by proper choice of the magnitude and direction of **H**.

Sometimes (M. Tsoi, 1997), a different pattern was seen, with no transmission at the interface. As shown in Fig. 32, there was the usual TEF pattern when E and C were on the same side of the interface, but only a flat background when they were on opposite sides. Such patterns were stable for a few days over a long portion of the interface (~1 mm), but then disappeared. Such sporadic behavior must be connected with changes in sample characteristics, but conditions for its appearance were not established. Boundary scattering has to be inelastic and very strong to shorten the elastic electron mfp so drastically. The problem is to isolate a source that can be present sporadically, with no deliberate action taken to change the sample. This sporadic behavior was tentatively attributed to interface superconductivity. As will be discussed in Sec. IX, an N/S interface has a very high resistance to energy flux (low thermal conductance). Thus nonequilibrium excitations cannot be transmitted through the interface. Superconductivity of stressed Bi (Chester and Jones, 1953) or Bi films evaporated onto a cold substrate (Buckel and Hilsch, 1954) is well known, and changes in stress might change the grain boundary from superconducting to nonsuperconducting. A tip crash onto the interface might also do so. If a superconducting plane can be clearly established in a conducting system, this TEF technique would allow study of its reflection and transmission of excitations—i.e., study of two-dimensional superconductivity.

IX. NORMAL-METAL/SUPERCONDUCTOR INTERFACE

The reflection of conduction electrons from the N/S interface between a normal metal (N) and a superconductor (S) involves a novel phenomenon, called Andreev reflection, which is fundamentally different from the scattering of an electron from a non-S interface. Andreev reflection was introduced by Andreev (1964) to explain the observation of strong interface thermal resistance, but practically no interface electrical resistance, when a magnetic field forces a superconductor into the intermediate state where N and S layers alternate (Zavaritsky, 1960). When an electron from N hits an N/S boundary, a Cooper pair is created in S and a hole is reflected back into N. The momenta of the incoming electron and outgoing hole are almost the same. Momentum is thus conserved, as well as current, since the sum of the (equal) currents of the incoming electron and reflected hole is carried away by the Cooper pair that

propagates into the superconductor. There is thus practically no interface electrical resistance, but there is a large interface thermal resistance, because the energy of the reflected hole is equal to that of the incoming electron—i.e., there is "energy flux reflection." For perpendicular incidence onto the N/S interface, the velocity of the outgoing hole (opposite to that of the incoming electron) is the same as that for a specularly reflected electron. However, for any other angle of incidence, the directions of the velocities of the hole and the specularly reflected electron will differ, and the difference grows as the angle of incidence decreases.

A number of indirect observations of Andreev reflection have been made by means other than TEF: electrical and thermal conductivities, single-point-contact resistances, etc. (see references in Krylov, 1980; V. Tsoi *et al.*, 1989). Usually, an alternative explanation for the observed behavior is possible, making proof of Andreev reflection inconclusive. One experiment that unambiguously showed the presence of Andreev reflection was carried out by Krylov and Sharvin (1970), using the radio-frequency size effect.

A fundamental feature of Andreev reflection is that the current carrier in N changes the signs of its charge and mass and inverts its velocity. Because TEF can register the effects of the kinetic behaviors of a small group of current carriers, both before and after reflection from an N/S interface, and is also sensitive to the sign of the charge of the carrier, it was recognized early on (V. Tsoi, 1975) as having a unique capability for directly observing these changes under Andreev reflection. In Sec. IX.B we describe two different TEF geometries used to investigate Andreev reflection, each with its advantages. In Sec. IX.C we show how one geometry of TEF was used to observe the change in sign of charge directly and the change in sign of mass indirectly, and in Sec. IX.D how the other was used to directly observe the change in sign of velocity. In Sec. IX.E we describe how TEF can be used to study the probability of Andreev reflection from an N/S interface, and in Sec. IX.F we briefly note studies of the dependence of Andreev reflection on energy and temperature and the difficulties incurred. An observation (Sec. IX.G) that the first negative Andreev reflection peak at temperatures well below T_c can be much larger than the equivalent positive TEF peak at temperatures just above T_c shows that screening strongly affects intravalley scattering. Analysis of effects of screening on TEF under intervalley scattering shows that the Bi/Sn interface studied contained patches of N/S interfaces and bare N surfaces.

A. Andreev reflection

In the ground state of a Fermi system at $T=0$ K, all electron states below the Fermi energy ε_F are filled and all states above are empty. An excitation may occur in two ways. First, an electron with ε_F can gain energy ε'—"electron excitation." Here the prime ($'$) distinguishes excitation energy ε' (>0) from electron energy $\varepsilon=\varepsilon_F\pm\varepsilon'$. Such an excitation will respond like an electron to electric and magnetic fields. Alternatively, an electron with $\varepsilon=\varepsilon_F-\varepsilon'$ can go up to a state with ε_F. The system again gains energy ε', but its kinetics will be that of the empty hole state, or hole "excitation." Increasing the momentum of such an excitation results in decreasing energy, so the excitation's mass is negative; the excitation's velocity is directed opposite to its momentum. Thus to get a hole excitation with energy ε' and momentum $\mathbf{p}$, we must put into the electron state $\{\mathbf{p},\varepsilon=\varepsilon_F-\varepsilon'\}$ a quasiparticle with a positive charge to compensate for the electron charge and a negative electron mass so that it will then move like an electron.

Under Andreev reflection, an excitation changes its signs of charge, mass, and velocity—i.e., an electron excitation turns into a hole excitation with opposite velocity, and vice versa (Andreev, 1964). For perpendicular incidence onto the N/S interface, the velocity of the outgoing hole is the same as that for a specularly reflected electron. However, for any other angle of incidence, the directions of the velocities of the hole and the specularly reflected electron will differ, and the difference grows as the angle of incidence decreases. In this review we limit ourselves to the usual superconductors ($\Delta\leqslant 10\,\mathrm{K}\ll\varepsilon_F$), so the incident and reflected excitations move oppositely (Andreev, 1964).

B. TEF techniques for studying Andreev reflection

Two different TEF geometries have been used to study Andreev reflection, each with its advantages.

Bozhko *et al.* (1982) created the N/S interface at the same surface on which the microcontacts were installed [Fig. 33(a)]. In this case, one must avoid superconducting short circuits between the contacts, and between each contact and the superconductor. This geometry is advantageous for seeing the change in sign of charge and mass and for measuring the probability Q_A of Andreev reflection.

Benistant *et al.* (1983) fabricated the N/S interface on the opposite side of a single-crystal plate from the microcontacts [Fig. 33(b)]. This geometry automatically isolates the microcontacts from the superconductor. However, the thickness of the plate must be smaller than the electron mean free path, so that excitations can reflect from S and reach the collector without being otherwise scattered, the probability of which depends strongly on the excitation energy. If the plate thickness is less than half the contact separation, then for the usual electron scattering from the opposite surface of the plate, the TEF peak is cut off when the electron orbit no longer fits inside the plate, i.e., when the Larmor radius is larger than the plate thickness. Such behavior, observed by Sato and Yonemitsu (1986), generates no new TEF peaks, but does give a small singularity in the dependence of $U(H)$ when the largest possible orbit just fits into the plate (Korzh, 1975; Kolesnichenko, 1992). The configuration of Fig. 33(b) allows a nice illustration of the concept of extremal displacement (V. Tsoi *et al.*, 1992). Figure 34 shows how the displacement of a reflected electron changes with incident angle under

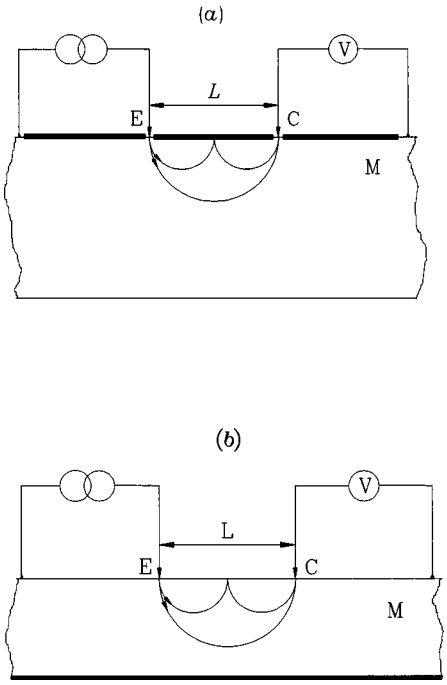

FIG. 33. Schematic drawings of the TEF arrangement for Andreev reflection with (a) the superconducting (S) film (thick lines) between the emitter E and collector C on M, and (b) the S film on the opposite side of M. The quasiparticle paths that produce electron-focusing peaks are shown for $H=H_0$ and $2H_0$.

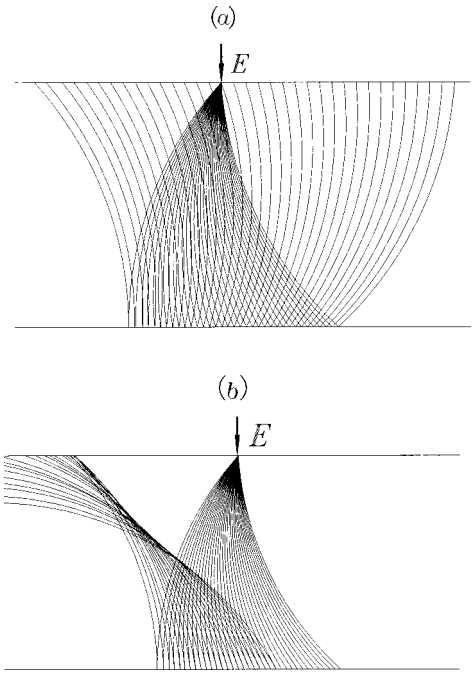

FIG. 34. Electron trajectories in a thin plate under (a) specular reflection or (b) Andreev reflection from the opposite surface of the sample. The arrow indicates the emitter location.

specular reflection [Fig. 34(a)] and under Andreev reflection [Fig. 34(b)]. Specular reflection from the opposite side of the plate produces no extremal displacements and thus no new focusing peaks. Andreev reflection from the opposite surface of the plate, in contrast, does. The reversal of all velocity components in Andreev reflection leads to an extremal displacement—''pileup'' of reflected orbits—at a distance L from the source, the value of which is determined by the ratio d/R_c, where d is the plate thickness and R_c the Larmor radius. Decreasing d/R_c increases the amplitude of the TEF peak, which is largest when $d/R_c=0$—when all electrons have zero displacement along the surface under Andreev reflection from the opposite surface of the plate. TEF then occurs in zero magnetic field with zero emitter-collector separation—one microcontact is both emitter and collector.

The first *single* point-contact TEF measurements were made by Benistant, van Gelder, *et al.* (1985). The method is analyzed by Benistant (1984). This scheme has subsequently been tried to study high-T_c superconductors (Gray, 1988; Hoevers *et al.*, 1988; Hoevers, van Bentum *et al.*, 1989; Jing *et al.*, 1989; Hoevers, 1992), where the gap can be comparable to ε_F (thus $\Delta p/p_F \sim 1$) and the mfp's are very short. Detailed discussion of this topic is outside the purview of the present review, but we warn the reader that not all experimental and theoretical problems are as yet resolved. The most important experimental problem is creating a perfect N/S interface. High T_c also introduces new phenomena into Andreev reflection, e.g., excitation velocities are not always in just the opposite direction. The peak amplitude will then depend on the excitation energy, even for an Andreev reflection probability of 1. Transverse electron focusing theory has yet to be modified to take proper account of such features.

C. Change in sign of charge

The type of excitation injected into a metal by an emitter—electrons or holes—is determined by the polarity of the applied voltage, and the polarity of the potential spike at the point onto which the excitations are focused is determined by the type of focused excitation. Thus, for a fixed field direction, injection and detection of electrons gives potential spikes at the collector of one polarity, and injection and detection of holes gives the opposite polarity. These polarities are independent of whether reflection from the surface is specular or diffuse, so long as the type of excitation does not change under reflection. If, however, the sign of the excitation charge changes upon reflection, as in Andreev reflection, then the charge of the entity detected will be opposite to that emitted, and the polarity of the TEF peak will reverse. It is this characteristic, along with others that we reiterate in the next paragraph, that allows TEF in the usual geometry to directly detect a change in sign of charge under Andreev reflection.

In the TEF geometry with the S metal between the two contacts, the reversal of velocity upon normal incidence onto the N/S interface is the same for Andreev reflection and for specular reflection. Moreover, as described in Sec. II, the motion of a charged particle under

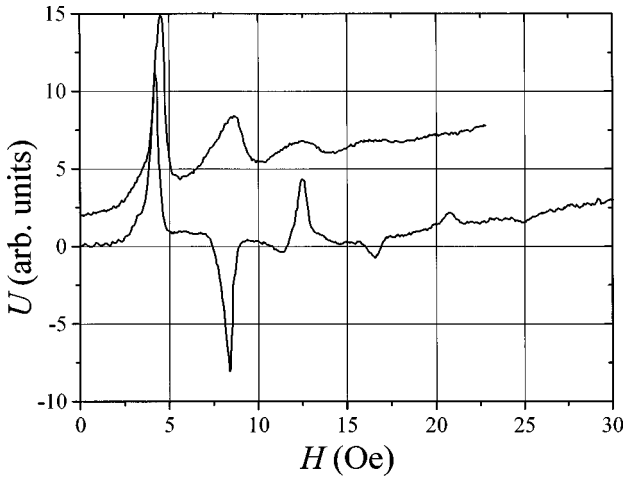

FIG. 35. Collector voltage U vs magnetic field H under multiple Andreev reflection for a Bi sample with a surface Sn film. $\mathbf{N}\|\mathbf{C}_3$, $\mathbf{H}\perp\mathbf{L}\|\mathbf{C}_2$. The curves are shifted along the U axis for clarity. The upper curve is for $T=4.2\,\mathrm{K}>T_c=3.7\,\mathrm{K}$, and the lower one for $T=1.7\,\mathrm{K}<T_c$. The polarities of odd and even TEF peaks differ because of Andreev reflection. From V. Tsoi *et al.*, 1989.

a uniform **H** depends upon the ratio e/m. Thus if under Andreev reflection the velocity is reversed, and the signs of both the charge and mass also reverse, the reflected particle should move along a path similar to that of the incident particle. With this geometry we thus expect Andreev reflection to give a TEF spectrum with the peaks located at the usual places, but with the fundamental change that the polarities of neighboring peaks alternate—i.e., odd TEF peaks (produced by an even number of reflections, and thus by "detected electrons") have the same polarity as the first TEF peak, and even TEF peaks (produced by holes) have opposite polarity (Kolesnichenko, 1992).

Bozhko *et al.* (1982), Tsoi and Yakovlev (1987), V. Tsoi *et al.* (1989), and Sveklo and Tsoi (1989b) directly observed this sign change under Andreev reflection using a Sn film deposited between the two point contacts on a face of a Bi crystal. The major experimental problems to be solved were isolating the contacts from the Sn film and making the Sn-free regions around the contacts much smaller than the separation between the contacts. When photolithography was used to make a large contact separation over a thick Sn film, the N/S interface was stable for more than a year. However, when the Sn film was very thin ($\sim$500 Å), so that installing the contacts under high potential burned off the Sn film around the contacts, the interface degraded in a few weeks. We shall see in Sec. IX.D that the alternative geometry of Fig. 33(b) also gives negative Andreev peaks, but in a reversed field (Benistant *et al.*, 1983).

Figure 35 shows a six-peaked TEF spectrum under Andreev reflection, in agreement with the picture just described. The alternating positive and negative peaks are direct evidence of the sign change in the charge of the carrier during reflection. The fact that the negative peaks occur halfway between the positive ones, with the field in the same direction, is at least indirect evidence that the sign of the mass also changes.

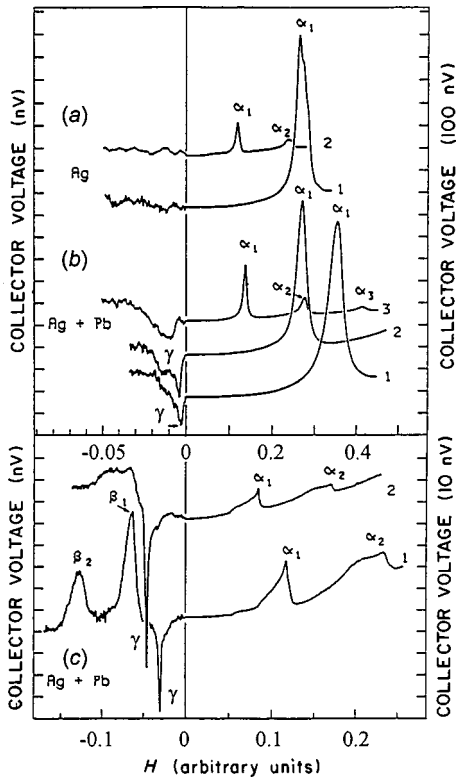

FIG. 36. Collector voltage U vs magnetic field H at 4.2 K for Ag single crystals under different conditions. (a) and (b) are for sample 1 with and without a Pb layer on the bottom surface. (c) is for sample 2 with a Pb layer, showing focusing of electrons and holes on different types of orbits: (α) "electron" (belly) orbits, focused directly (α_1) or after one or more reflections from the upper Ag surface (α_2,α_3); (β_1,β_2) "hole" (four-cornered rosette) orbits; (γ) Andreev-reflected particles on belly orbits. Increasing numbers label curves with increasing point-contact distances; different distances give different focusing fields. The voltage and field scales differ for $+H$ and $-H$. After Benistant *et al.*, 1983.

D. Change in sign of velocity

The TEF scheme of Fig. 33(a) is not suitable for proving the change in sign of velocity, because at normal incidence the velocities after specular reflection and Andreev reflection coincide. Isolating the change in sign of velocity under Andreev reflection requires using glancing incidence, where specular and Andreev reflection result in almost opposite directions of velocity. Observing TEF with a thin sample in the geometry of Fig. 33(b) allows an elegant demonstration of the inverse velocity direction after Andreev reflection (Benistant *et al.*, 1983), which gives a new extremal displacement and thus an additional TEF peak. As this peak involves only a single Andreev reflection, its polarity is opposite to that of the usual TEF peaks.

Figure 36 shows the TEF peaks seen at 4.2 K on thin single-crystal Ag plates before (a) and after (b) and (c) a

Pb film was evaporated onto the opposite surface from the point contacts. When the sample temperature is below $T_c = 7.2$ K for Pb the Pb film gives an S/N interface at the Ag surface. The peaks α and β are ordinary TEF peaks. Their positions in the magnetic field agree with the Ag Fermi surface and the experimental geometry. The dip γ, which has opposite polarity to the other peaks, occurs only after applying the Pb film. Its location and behavior agree with the expectations for Andreev reflection given above. For a detailed analysis of the spectrum see Benistant *et al.* (1983) and Benistant (1984).

The data of Fig. 36 are direct evidence for the change in sign of velocity. Combining the results of Figs. 35 and 36 shows that both velocity and charge change sign.

E. Probability of Andreev reflection

For specular reflection from a surface, $q = A_{n+1}/A_n$ for $n > 1$. The determination of the probability of Andreev reflection, Q_A, from A_{n+1}/A_n is less straightforward. Under the usual specular reflection, the velocity component parallel to **H** is not reversed. Thus only electrons on the Fermi surface with velocity components in this direction small enough that they do not drift beyond the outer edge of the collector will be collected. In Andreev reflection, however, every time an initially injected electron is transformed into a hole, its velocity parallel to **H** is reversed, and the drift of the hole parallel to **H** after reflection cancels that of the electron before reflection. On a spherical Fermi surface, this process allows injected electrons that would have missed the collector under specular reflection to be collected under Andreev reflection. The increase in collection is especially strong for even peaks (odd number of reflections), since total drift is completely canceled. For odd peaks, the "last" electron or hole skip is always the same as the first one, and a drift remains.

Analysis for a spherical Fermi surface, based upon simple geometry, predicts that the amplitudes of the even peaks should be proportional to $(b/L)^{1/4}$, while those for the odd peaks should be proportional to $(b/L)^{3/2}$ as for specular reflection, but with different prefactors (Bozhko *et al.*, 1982; V. Tsoi *et al.*, 1989; Kolnesnichenko, 1992). If Q_A is near unity and b/L is small, the even peaks for Andreev reflection should thus be gigantic compared to the usual TEF peaks. This prediction has not yet been tested.

For a cylindrical Fermi surface (such as for electrons in Bi), in contrast, the TEF peaks for Andreev reflection behave similarly to those for specular reflection. There is no distinction between odd and even peaks, and Q_A should be given by $Q_A = A_{n+1}/A_n$ (V. Tsoi *et al.*, 1989), so long as the N/S interface is homogeneous. If it has patches of bare N, the situation becomes complex. Andreev reflection screens surface roughness, since the velocity direction of the reflected excitation is opposite to that of the incident excitation, independent of surface roughness (Andreev, 1964). It can thus be described by "geometric optics" and a perfectly flat surface. For a bare N surface, in contrast, q is determined by the statistical structure of surface roughness. If the N/S interface has patches of bare N surface, one will see a combination of ordinary reflection and Andreev reflection, with the Andreev reflection proportional to the N/S percentage. Moreover, specular reflection from a bare N surface contributes to each TEF peak oppositely in sign to Andreev reflection. If $q + Q_A = 1$—i.e., reflection is either specular or Andreev—the peak polarity is determined by the sign of $(q - Q_A)$, and if $q = Q_A$, only the first TEF peak remains (V. Tsoi *et al.*, 1989). Section IX.G contains evidence that Bi/Sn samples with a thin Sn film can have patched surfaces. The best estimate for Q_A for a given surface is, then, the largest value measured at a variety of different places on the surface. The possible presence of a potential barrier at some N/S interfaces (Blonder *et al.*, 1982) adds still further complications (see V. Tsoi *et al.*, 1989 and references therein). V. Tsoi *et al.* (1989) estimated $Q_A \approx 1$ for a Bi/Sn sample with a patchy thin Sn surface.

F. Dependence of Andreev reflection on energy and temperature

Since increasing the emitter voltage U_0 increases the energy of injected excitations, it seems apparent that TEF should allow studies of the energy dependence of Andreev reflection, giving $\Delta(\mathbf{k})$, the anisotropy of the energy gap Δ in $\mathbf{k}$ space. In practice, however, such studies are not straightforward. This topic is outside the purview of the present review, but we briefly describe some problems. For details see V. Tsoi *et al.* (1989).

The first problem is that, unless L is smaller than the electron mean free path l, which decreases rapidly with increasing ε', excitations decay rapidly to near ε_F before reaching C. Transverse electron focusing still occurs (V. Tsoi *et al.*, 1989), but the desired effects become exponentially small and can be masked by other effects having nothing to do with highly nonequilibrium electrons. Thus one can only reliably investigate $Q_A(\varepsilon')$ for energies ε' for which $l(\varepsilon') < L$. Figure 37 depicts the effect of changing U_0 on the TEF spectrum under Andreev reflection for Bi/Sn, using a modulation technique with an accelerating bias voltage (V. Tsoi and Yakovlev, 1987). In Bi with $L < 100\,\mu$m, the focused excitations had energy $\varepsilon' \sim 1$ meV (V. Tsoi *et al.*, 1989). In Bi/Sn, only for $L < 100\,\mu$m ($U_0 < 1$ meV) did the experimental results show a dependence of Q_A upon U_0 (V. Tsoi *et al.*, 1989). Figure 38 shows examples of the energy dependences found from figures such as Fig. 37 for $L < 100\,\mu$m and for different polarities of U_0. Unexpectedly, the data turned out to be strongly affected by the polarity of U_0. The falloff in Fig. 38 is much faster for electrons (solid circles) than for holes (open circles). That this difference is not due to a difference in relaxation rates between electrons and holes was shown recently in TEF studies of highly nonequilibrium excitations using $L \sim 5\,\mu$m (M. Tsoi *et al.*, 1996). In that paper, focusing of electrons with energy 0.7–1.5 ε_F was seen. Such a short L should allow quantitative TEF studies of

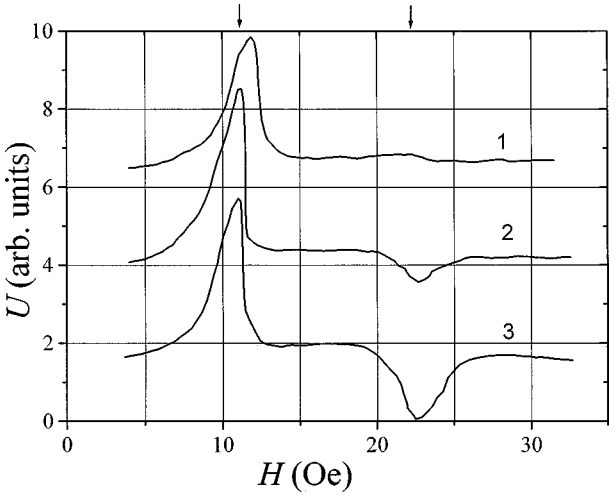

FIG. 37. Variation of Bi/Sn TEF spectra with reference voltage: curve 1, $V_0=3.9$ mV, curve 2, $V_0=0.7$ mV, curve 3, $V_0=0$ mV. $\mathbf{N}\|\mathbf{C}_3$, $\mathbf{L}\|\mathbf{C}_2$, $L=82\,\mu$m. Arrows show H_0 and $2H_0$. From Tsoi and Yakovlev, 1987.

the energy dependence of Andreev reflection at Bi/S interfaces, including interfaces with high-T_c materials.

The second problem is that finite $T>0$ K must be taken into account in analyzing TEF data on the energy dependence of Q_A, since excitations with $\varepsilon' \sim k_B T$ are generated, some with $\varepsilon'<\Delta$ and some with $\varepsilon'>\Delta$. Importantly, Joule heating raises the local emitter temperature to higher than the bath temperature, and the emitter temperature changes with U_0.

G. Screening of surface roughness by the electronic potential

Experiments on screening of surface roughness at an N/S interface for both intravalley and intervalley scattering were performed on Bi/Sn interfaces produced by thermal evaporation of ~500-Å-thick Sn films in UHV onto surfaces of Bi crystals with $\mathbf{N}\|\mathbf{C}_3$ that had first been cleaned by Ar^+ ion etching (V. Tsoi *et al.*, 1989). By analogy with the screening of surface roughness by surface charge described in Sec. VI.E, surface irregularities in the N/S interface must be screened by the electron pair potential in S, with screening length of order the coherence length $\xi \gg a_0$.

1. Intravalley and intervalley scattering

Figures 35 and 39 show TEF spectra above and below T_c for $\mathbf{H}\|\mathbf{C}_1\perp\mathbf{L}$-oriented Bi, with a Sn film between E and C. Under normal reflection ($T>T_c$), q_M is low (≈0.2). Presumably, as discussed in Sec. VI, surface roughness suppresses specularity. Decreasing T to below T_c both inverts the polarity of the second peak—due to the change in charge sign under Andreev reflection—and strongly increases its amplitude to nearly that of the first peak. This increase cannot be due to compensation of electron-hole drift along **H** (Sec. IX.E), because the Fermi surface of Bi is cylindrical. Rather, it seems to be clear evidence for screening of roughness under Andreev reflection for both intravalley and intervalley scattering. From Sec. VI, we recall that only when both are screened can the height of the second TEF peak (one reflection) be close to that of the first peak (no reflec-

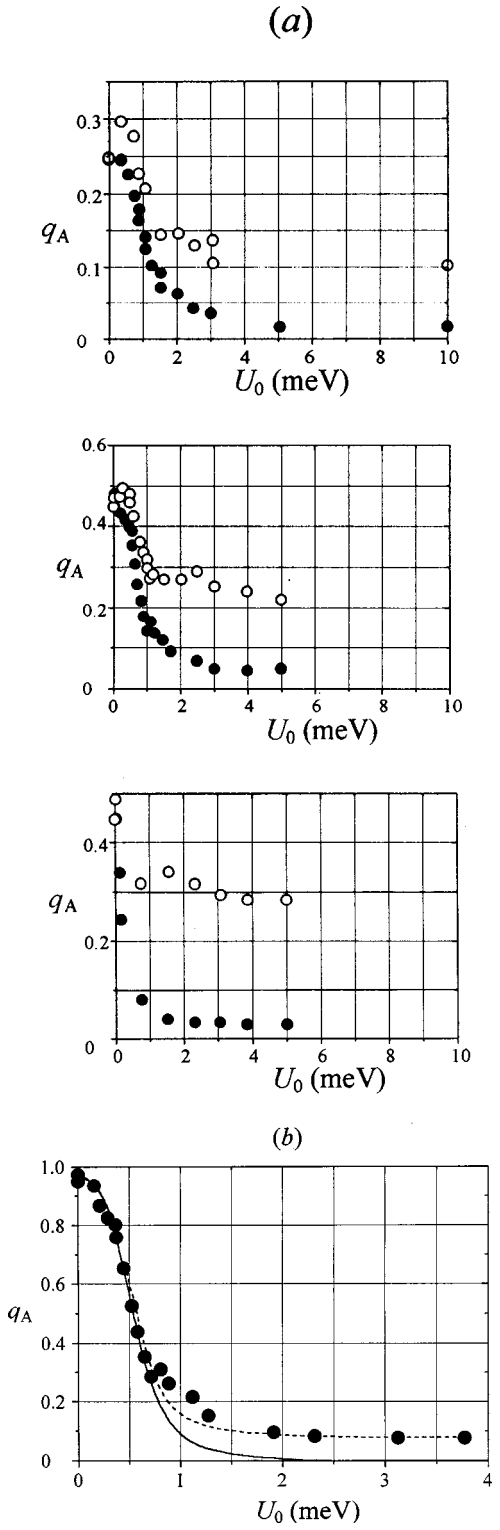

FIG. 38. Probability of Andreev reflection, q_A ($=Q_A$ as measured by TEF), vs emitter voltage U_0 for different polarities of U_0 under Andreev reflection. Different graphs indicate measurements on different areas of the sample surface: ●, $U_0<0$; ○, $U_0>0$. After V. Tsoi *et al.*, 1989.

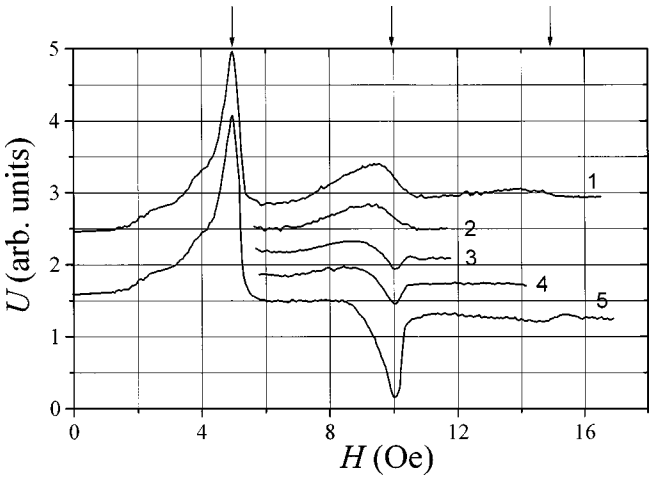

FIG. 39. Collector voltage U vs magnetic field H for a Bi sample with a surface Sn film for $T=3.80$ K, 3.78 K, 3.74 K, 3.70 K, and 2.78 K (curves 1–5). The curves are shifted along the U axis for clarity. Arrows indicate the usual TEF peak positions. From Bozhko *et al.*, 1982.

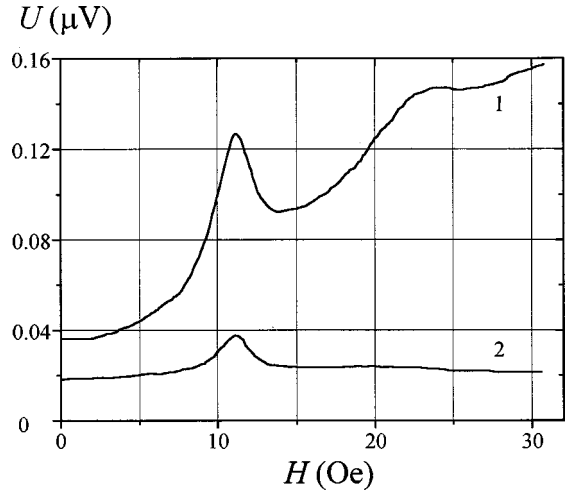

FIG. 40. Collector voltage U vs magnetic field H in a Bi sample with $\mathbf{N}\|\mathbf{C}_3$, $\mathbf{L}\|\mathbf{C}_1$, and $\mathbf{H}\perp\mathbf{L}$, and covered by a Sn film having $T_c=3.7$ K: curve 1, $T=4.2$ K; curve 2, $T=1.7$ K. The curves are shifted along the U axis for clarity. From Sveklo and Tsoi 1989b.

tion). In addition to screening small-scale roughness ($\eta \ll \xi$) that would usually produce diffuse intervalley scattering, Andreev reflection has the unique ability to screen even large-scale roughness ($>\lambda_{dB}$), because the inversion of the excitation velocity is independent of the direction of the local surface normal.

2. Intervalley scattering alone

The geometry of the lower half of Fig. 18—$\mathbf{L}\|\mathbf{C}_1\perp\mathbf{H}$—where the first TEF peak is due solely to intervalley scattering—was used to investigate whether the N/S interface was partly bare N, i.e., patched (Sveklo and Tsoi, 1989b). If the first TEF peak is still seen below T_c with unchanged polarity, then part of the interface must be bare N, and the decrease in amplitude of this peak when T goes below T_c measures the bare N fraction (Sec. IX.E). Figure 40 shows TEF scans above and below T_c.

(1) The presence of the first electron-focusing peak for $T<T_c$ means that intervalley scattering must still be occurring, but such scattering is incompatible with a fully N/S interface, which must screen intervalley Andreev reflection ($\xi \gg a_o$; Sec. VI.D), thereby eliminating coupling between different valleys.

(2) The peak's polarity does not change, even though it is produced by electrons reflected from the surface. Thus the reflection does not involve a change in the type of excitation and, again, its presence requires ordinary intervalley scattering from a bare N surface that is rough on an atomic scale.

(3) The peak's amplitude drops by about 75%, a behavior very different from intravalley scattering, where A_1 hardly changes as T_c is crossed (Figs. 35 and 39). The surface must thus be patched. Either the Sn film is composed of islands, or there is an insulating layer at the Bi/Sn interface, or both conditions coexist. The first alternative is consistent with the presence of a fairly large Bi Auger peak after deposition of the Sn (Sveklo and V. Tsoi, 1989b). For the second, the small ε_F of Bi (=0.027 eV), causes an insulating layer with a thickness of only one monolayer to have a low transparency: $\sim 10^{-2}$. Stringent cleanliness of the N/S interface is essential.

(4) The background $U(H)$ markedly weakens for $T<T_c$. Such weakening is reasonable, since below T_c there are both electron and hole backgrounds that contribute oppositely to the total (V. Tsoi *et al.*, 1989).

From the ratio of the amplitudes of the first TEF peak in Fig. 40 for $T<T_c$ and $T>T_c$, Sveklo and Tsoi (1989a, 1989b) derived a bare-N fraction of about $\frac{1}{4}$. The specularity is low enough to correctly yield the practically complete disappearance of the second peak for $T<T_c$. These conclusions were independently confirmed by Sveklo and Tsoi (1989b) using an alternative geometry, $\mathbf{L}\|\mathbf{C}_2\perp\mathbf{H}$, and measuring changes in amplitude of the second peak as $\mathbf{H}$ was rotated.

X. ELECTRON REFLECTION FROM THE 2D ELECTRON-GAS CHANNEL EDGE

Recent improvements in lithographic and focused-ion-beam (FIB) techniques for making complex micron- and submicron-sized structures, combined with enhanced transport mobilities of electrons in the 2D electron gas in GaAs-$Al_xGa_{1-x}As$ heterojunctions (giving mfp, l_μ, up to 100 μm), have made possible TEF studies of the 2D electron gas. The first such studies were those of Beenakker *et al.* (1988) and van Houten *et al.* (1988, 1989). Beenakker and van Houten (1991) have reviewed studies published through 1990. We update that review, following it in using $\mathbf{B}$ for the magnetic field, directed perpendicular to the plane of the 2D electron gas.

Reasoning from the simple geometrical model of TEF, one might expect analysis of TEF in the 2D electron gas to be simpler than in the 3D electron gas, since the 2D Fermi surface is just a circle. In practice, however, most published TEF studies of the 2D electron gas do not meet the conditions $W \ll L < l_F$ needed for the geometrical model to apply. When this geometry is combined with situations in which quantum effects can be crucial, analysis becomes complex and is, as yet, uncertain. At least the following issues must be considered: (1) As described in Sec. IV.D.2, even when the geometrical model is applicable, a two-dimensional Fermi surface, such as that of the 2D electron gas can lead to large differences between the quantity measured by TEF, q_M, and the real probability of specular reflection, q. (2) The combination of a circular Fermi surface plus $W/L \sim 1$ leads to very large densities of focused electrons at the first TEF peak location—the collector voltage for directly focused electrons can be only a factor of 10 or so less than that across the emitter, about 10^3 times larger than is found for the cylindrical Fermi surface of Bi (Sec. VI). The resulting large local disturbance of the electrochemical potential due to electron "pileup" can act as an additional electron emitter, contributing TEF amplitudes at just those fields where the condition $l_F < L$ leads to reduction of the usual specular TEF peaks. (3) If the temperature is low, the contact separation L is small, and the contact width W is reduced to $\sim \lambda_{dB}$, then TEF in the 2D electron gas can be dominated by quantum effects. Simultaneously, there are only a few conduction channels in such contacts due to lateral confinement ($W \sim \lambda_{dB}$), and not many Landau levels in the 2D gas because of the high focusing field. Transverse electron focusing must then involve nonadiabatic conditions, in which transitions occur between different Landau levels. Lack of ability to rigorously combine these various phenomena leads to larger than usual uncertainty in inferring q from measured values of q_M.

We shall see the following: scattering of electrons from the channel edge seems to be more specular for edges defined electrostatically by Schottky gate depletion than for edges made by ion beams; the mfp measured by TEF is several times smaller than that measured from transport (mobility) measurements, but has a similar temperature dependence; hot electrons can propagate long distances in a 2D electron gas; and quantum effects predominate at very low temperatures or when the point-contact widths are comparable to λ_{dB}.

Because the Bi electron Fermi surface is almost cylindrical, and the electron Fermi energy, mass, and λ_{dB} are all comparable to those of the 2D electron gas given below, we expect electrons in the 2D gas to behave rather like those in Bi. We shall sometimes use Bi as a comparison standard.

A. Samples and experimental techniques

The 2D electron gas is confined at the GaAs-$Al_xGa_{1-x}As$ interface within a heterostructure wafer grown by molecular-beam epitaxy. Typical 2D electron-gas parameters in a high-mobility heterostructure are as follows: sheet carrier density, $n_s \sim 1-5\times10^{15}$ m^{-2}; Fermi wave vector, $k_F \sim 0.08-0.15$ nm^{-1}; Fermi velocity $\sim 3 \times 10^5$ m/s; and GaAs effective mass$=0.067\ m_e$, where m_e is the free-electron mass. Zero-field resistivity measurements yield transport mfp's $l_\mu \sim 10-100\ \mu$m. n_s can be varied either by exciting "persistent" photocarriers by illumination, or electrostatically by applying a voltage to a separate gate placed above the 2D electron gas, thereby depleting the electron gas under the gate (Thornton *et al.*, 1986).

Two different wafer-patterning techniques (and their combinations) have been used to obtain 2D electron-gas channel boundaries with contacts for TEF studies: (1) electron beam lithography, and (2) focused-ion-beam implantation.

(1) Lithography is followed by a wafer surface treatment through a mask, usually with wet or ion etching. The contacts are defined electrostatically by means of a split gate on top of the heterostructure. Increasing negative gate voltage depletes the electron gas under the gate, until beyond the depletion threshold ~ -0.6 V no mobile carriers are left under the gate. The 2D electron-gas boundary between the two point contacts is a depletion potential well below the gate which, for large negative gate voltages, extends beyond the gate pattern by up to a few tenths of a μm. This process gives constrictions of variable width W, down to widths comparable to λ_F (quantum point contacts). The precise dependence of W on gate voltage is typically history dependent (van Houten *et al.*, 1988)—thermal cycling and large positive gate voltages shift the depletion threshold—but transport measurements seem to be reproducible if the sample is kept cold and the gate voltage not strongly varied.

(2) An advantage of focused-ion-beam techniques is their ability to draw directly without a mask. The implanted ions greatly increase the resistance of the exposed regions, both by disrupting the lattice of the heterostructure and by implanting acceptors into the donor layer. Channeled ion implantation can be used to pattern a more deeply buried 2D electron gas (Hornsey *et al.*, 1993a).

Some measurements have used an equivalent of the standard TEF scheme, with two or more point contacts beside each other on the 2D electron-gas boundary. Others used a grid scheme (Nakamura *et al.*, 1990) with multiparallel quasi-one-dimensional channels to observe TEF. The electron transmission probability of such a grid varies with B, as cyclotron motion returns the electrons to the grid, reducing the transmission probability and increasing the resistance. The result is peaks in resistance for grid spacings that are multiples of the cyclotron diameter $2R_c$. This scheme allows smaller contact separations than the scheme described above, since terminals do not have to be attached to each channel. However, quantitative analysis is more complicated.

Transverse electron focusing spectra have also been seen using only optical lithography (Gao *et al.*, 1994) and with small ($W=5\ \mu$m) ohmic contacts diffused 25

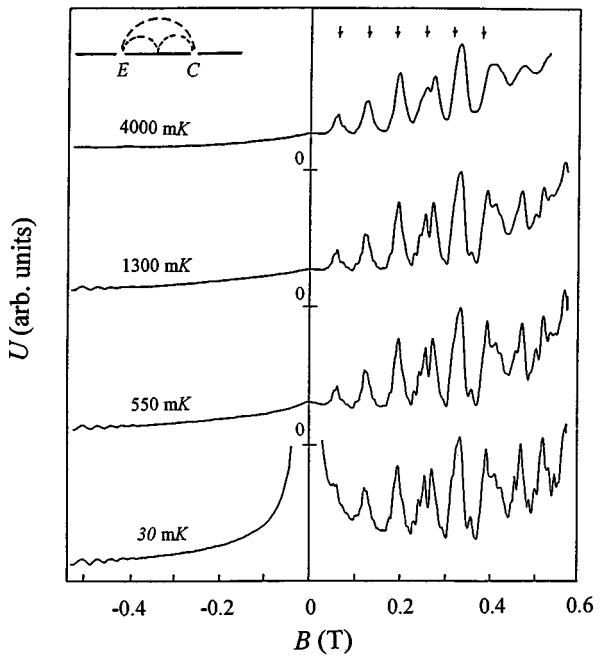

FIG. 41. Transverse electron focusing spectra for $2W/\lambda_F \approx 1$ and $L \sim 3$ μm, 4 K$>T>$30 mK. Expected TEF peak positions are shown by arrows. As T is reduced from 4 K, fine structure is resolved, and small Shubnikov-DeHaas oscillations appear at high reversed fields. The large negative peak near $B=0$ at 30 mK is a series magnetoresistance effect—see van Houten *et al.* (1989). From van Houten *et al.*, 1988.

μm apart into the edge of a 2D electron-gas mesa (Spector *et al.*, 1990b), a process that simplifies the fabrication steps. In principle, TEF should be seen with needle point contacts to bulk doped semiconductors (Trzcinski *et al.*, 1987), but no such studies have yet been reported.

B. Results and analysis

1. Focusing spectra

Representative examples of experimental TEF spectra for electrostatically produced channel boundaries and contacts, as well as these produced by focused-ion-beam techniques, are given in Figs. 41–45.

Figures 41–43 show spectra for electrostatically defined contacts measured using a structure equivalent to the standard TEF scheme. At 1–4 K, there are a large number of the usual TEF peaks at the usual locations. However, the peaks initially grow larger with increasing peak number and do not seem to become wider as H increases. As T decreases, a strong fine structure develops and grows in size down to about 300 mK. This fine structure is insensitive to injection voltages up to values comparable to 300 mK, but injection voltages$\gg k_B T/e$ smear the fine structure in a manner analogous to a temperature increase. Figure 42 shows that both the TEF peak heights and the fine structure depend upon the gate voltage and thus upon the point-contact widths. The geometrical contact widths for the samples of Figs. 41 and 42 were $W \approx 0.25$ μm. In Fig. 43, the electrostatically limited widths were estimated to range from W

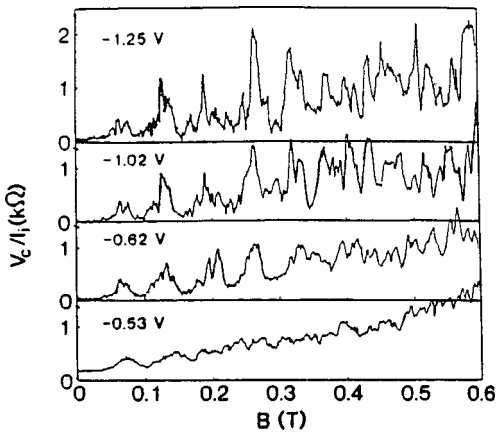

FIG. 42. Dependence of TEF spectra on gate voltage (and thus on point-contact width) for an electrostatic sample with $L \sim 3$ μm at 50 mK. A large negative gate voltage corresponds to narrow emitter and collector contacts. From van Houten *et al.*, 1989.

~ 0.25 μm for the lowest gate voltage, $V_g = -0.53$ V, to $W \sim 0.02$ μm for the emitter and ~ 0.08 μm for the collector—quantum contacts ($W \sim \lambda_{dB} \approx 0.04$ μm) for $V_g = -1.25$ V. Those in Fig. 43 were estimated to stay at about $W \sim 1$ μm.

Data for samples prepared with a focused ion beam, which have fixed geometrical contact widths, are shown in Figs. 44 ($W \sim 1$ μm) and 45 ($W \sim 0.4$ μm). The spectra in Fig. 44 are for a Hall configuration. The data of Fig. 44(a) taken at 1.7 K, look similar to normal TEF data for Bi or a metal—peaks occur only at the usual focusing locations, and the peak heights decrease and widths increase with increasing peak number. In contrast, the data of Fig. 44(b) taken at 0.12 K, are like those at the lowest temperatures in Fig. 41—there is fine structure on the usual TEF peaks, the peak heights initially grow, and the widths are usually almost independent of peak number. Figure 45 shows that a multiple-grid geometry with a sample prepared by a focused ion

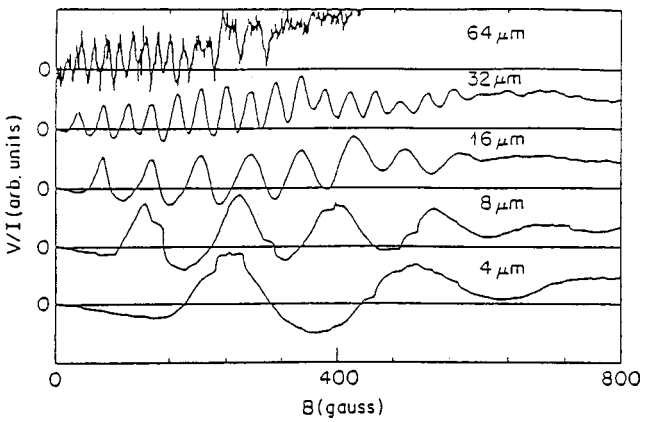

FIG. 43. Collector voltage vs B for five emitter-collector distances from $L = 4-64$ μm as a function of magnetic field for an electrostatic sample. The vertical scale varies among the curves to facilitate comparison of their periods. From Spector *et al.*, 1990a.

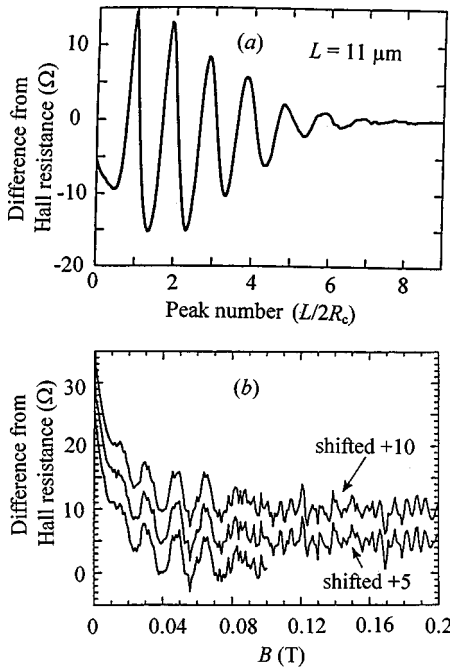

FIG. 44. TEF signal after removal of Hall resistance for a focused-ion-beam sample measured with a two-point contact structure with leads in a four-terminal Hall configuration: (a) The sample was at 1.7 K after illumination. The field axis is normalized to peak number. (b) Similar signal, but at $T=0.12$ K in the dark. Three sweeps (offset for clarity) show reproducibility of the fine structure. After Hornsey *et al.*, 1993.

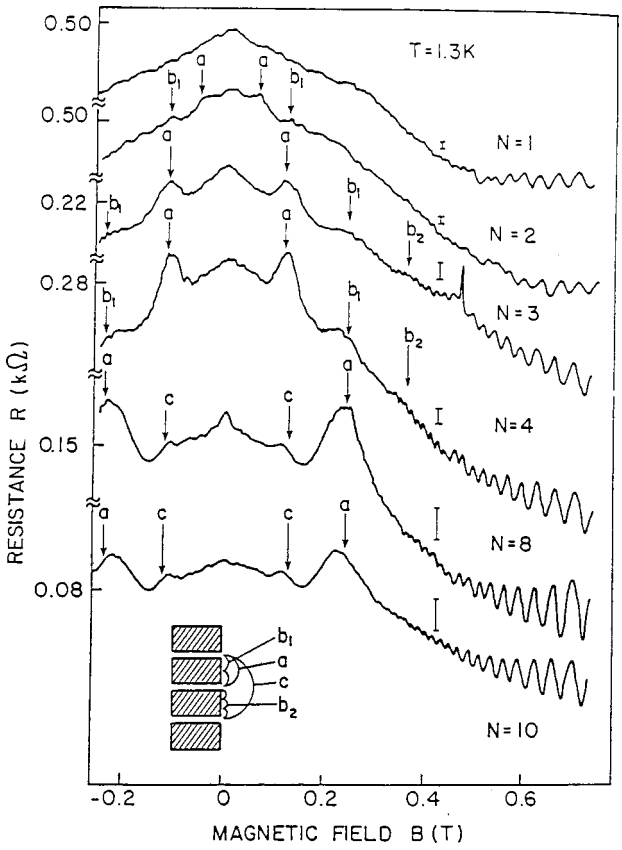

FIG. 45. Low-field magnetoresistance at $T=1.3$ K for six focused-ion-beam samples with different numbers (N) of channels, using grid geometry in the inset. Arrows indicate expected locations of TEF peaks for electron trajectories in the inset: a (fundamental), b_1 (first harmonic), b_2, (second harmonic), and c (subharmonic). From Nakamura *et al.*, 1990.

beam yields peak locations that correlate well with TEF expectations.

Most published 2D electron-gas TEF spectra fall within the range of behaviors shown in Figs. 41–45. TEF peaks are always seen at the expected focusing fields. For electrostatic edges, the peak amplitudes usually initially increase with increasing peak number, and the peak widths stay roughly constant (Beenakker *et al.*, 1988; van Houten *et al.*, 1988, 1989; Spector *et al.*, 1990a, 1990b, 1992; Heremens *et al.*, 1992; Gao *et al.*, 1994). For focused-ion-beam edges, the peak amplitudes usually decrease with increasing peak number and the peak widths increase.[2] In both cases, at temperatures well below 1 K, short-period oscillations usually appear in the TEF spectra. In one study, such oscillations were seen at 1.4 K with gate voltages negative enough to reduce the contact widths to ~20 nm (Gao *et al.*, 1994).

In this section, we focus on the following anomalous features of the data of Figs. 41–43 and 44(b): (1) the short-period oscillations; (2) the lack of peak broadening with increasing peak number; and (3) the increasing amplitudes of the first few TEF peaks in Figs. 41–43. In the next section we consider the inferred values of q for the 2D electron gas.

[2]See, for example, Hirayama and Saku, 1990; Nakamura *et al.*, 1990, 1991; Nihey *et al.*, 1990; Nakazato *et al.*, 1992; Takaoka *et al.*, 1992, 1994; Wakaya *et al.*, 1992; Hornsey, Thornton *et al.*, 1993; Tsukagoshi *et al.*, 1993; Wakayama *et al.*, 1994.

a. Short-period oscillations

Beenakker *et al.* (1988) attributed the short-period oscillations to interference arising from coherent electron focusing when $W\sim\lambda_{dB}$. They supported this attribution with a WKB calculation of the probability density of electrons at the collector, assuming $q=1$ and treating interference of coherently excited magnetic edge states (see also van Houten *et al.*, 1989). The model qualitatively reproduced some features of the data: (a) the main peak structure had the same periodicity as the usual TEF peaks; (b) the peaks exhibited short-period oscillations; and (c) the peak heights were nonmonotonic. However, the model predicted that the first few peak heights should be essentially constant and that the peak widths should increase with peak number. Neither prediction was borne out by the data. Also, to obtain qualitative agreement required assuming a very small value of W/L (see also Goldoni and Fasolino, 1991). The observed TEF linewidths suggest a larger effective contact width, averaging over which should smear out the oscillations. After publication of several increasingly sophisticated analyses of TEF quantum behavior (Okiji *et al.*, 1992; Ueta, 1993, 1994), the latest paper (Ueta, 1995) argues that the short-period oscillations are due mainly to diffraction of higher-order modes of the elec-

tron waves in the point contacts. However, introducing realistic parameters yields a structure an order of magnitude smaller than that seen, and the model predicts a monotonically increasing peak width with peak number. For comparison, short-period oscillations superimposed on TEF spectra were first seen in Bi, and initially attributed to quantized surface orbits (V. Tsoi, 1977). Komnik *et al.* (1996, 1997) and Andrievskii *et al.* (1996) later ascribed Bi fine structure to diffraction.

Note that focusing with quantum point contacts requires deviation from adiabatic injection (Landau number conservation; Glazman *et al.*, 1988). For example, if there is only a single-channel, adiabatic electron transmission between this channel and the zero-number Landau edge channel where electrons skip along the surface with trajectories enclosing half a quantum flux (or so) gives no singularity at B_0—no focusing occurs (Sec. II.B). But just such transmissions in and out of the current-carrying channels produce the collector voltage. So TEF fine-structure analysis may also require taking account of resonant electron transmission between the emitter and collector via edge states (Sec. VII).

We conclude that quantum interference and diffraction must be involved in the fine structure in the 2D electron gas, but the phenomenon is not yet completely understood.

b. Peak broadening

Most of the 2D electron-gas TEF analyses described in the previous section fail to explain the lack of peak broadening with increasing peak number seen in most studies of 2D electron-gas samples with electrostatic edges. The usual peak broadening seen in metals and Bi [Figs. 2 and 13(a)] is a geometrical effect due to constancy of the angle $\Delta\Omega$ within which electrons enter the collector at multiple fields (Sec. IV). The growth in peak width with increasing peak number is independent of the value of $\Delta\Omega$ or the divergence of the injected beam, but is set by the ratio B/B_0, where the first TEF peak is at B_0.

In the usual geometrical-model analysis, the width of the first TEF peak, ΔB, is set by the ratio W/L. Qualitatively the wide peaks in the spectra of Figs. 41–45 suggest that W/L is not small. Moreover, the data of Fig. 43 show that $\Delta B/B_0$ for the first peak is practically independent of W/L. Similar behavior is seen in Bi, where increasing L up to 1 mm does not lead to very narrow TEF peaks (V. Tsoi and N. Tsoi, 1977; V. Tsoi, 1978). Simply estimating a contact size W from the Sharvin (1965) formula modified for the 2D electron gas is not reliable. Apparently, increasing L increases the size of the effective emitter, retaining W/L. In Bi, a very narrow TEF line was obtained only by combining a short L (<100 μm), a nearly perfect contact installation (i.e., negligible disturbance of the contact area), and a very small current (0.5 μA; V. Tsoi, 1980). Increasing the current above ~ 10 μA converted this line into an ordinary broad one. Sometimes this procedure was not reversible—the peak stayed broad when the current was again reduced. The contact voltage for the larger current was still only $\sim 10^{-4}$ V (similar to values for the 2D electron gas so far), i.e., eV$\sim$1 K. Although the sample temperature was 4.2 K, this small voltage produced a drastic effect. A possible source of this behavior is that, even at such a small current (voltage), the electron drift velocity becomes equal to the sound velocity. Apparently, some characteristic of electron kinetics in microcontacts under high electron drift velocity ("high" accelerating voltage) increases the effective emitter size. If so, since the high dielectric constant of Bi ($[æ]\approx 100$, from Edel'man, 1976) greatly reduces electron-electron and electron-phonon interactions as compared to the 2D electron gas ($[æ]\sim 10$, from Bennakker and van Houten, 1991), any such effects should be even more important in the 2D electron gas.

The TEF peak width could also be affected by the angular distribution of emitted electrons (Beenakker and van Houten, 1989; Molenkamp *et al.*, 1990, Baranger *et al.*, 1991; Wakayama *et al.*, 1994). The distribution was found to depend upon the structure just at the outlet of the emitter wire, rather than the direction in which the wire points (Wakayama *et al.*, 1994). Collimation of an injected electron beam can reduce a TEF peak width. Refraction at a split-gate emitter should cause collimation, an effect similar to lens focusing (Spector *et al.*, 1990c, 1990d). The presence of collimation seems to be signalled by the absence of asymmetry in the TEF peaks in Figs. 41–43. This absence strongly suggests that refraction and collimation play important roles in determining 2D electron-gas TEF peak widths.

Lastly, we speculate about the possibility of reducing peak broadening. If a 2D electron-gas boundary is stepped, scattering should be diffuse for small angles of incidence, but specular for normal incidence. Such a $q(\theta)$ should cause the TEF peak wings to be suppressed at each reflection, reducing TEF peak broadening more the larger the number of reflections. This situation is opposite to that considered in Sec. VI.E.1, where diffuse scattering at normal incidence shifted and broadened the TEF peaks. Hornsey (1996) recently used Monte Carlo simulations in the classical regime (contact widths$\gg\lambda_F$) to study effects on the TEF spectrum of varying the injector and collector widths, the specularity coefficient, the injection divergence angle, and the electron mfp. While his calculations do not explain the lack of growth of peak width with increasing peak number, it should be straightforward to extend them to see if a $q(\theta)$ for a stepped boundary would properly suppress TEF peak broadening.

c. Increasing peak amplitude

In the usual TEF picture, the TEF amplitude can only increase from one peak to the next if defects reduce the amplitude of the lower field peak (Sato and Yonemitsu, 1986). Such a picture is not plausible for the systematic increase over several peaks seen in Figs. 41 and 43 for 2D electron-gas samples with electrostatic edges. The behavior is most pronounced for quantum contacts ($\lambda_{dB}\sim W\ll L$). As yet it has no satisfactory explanation.

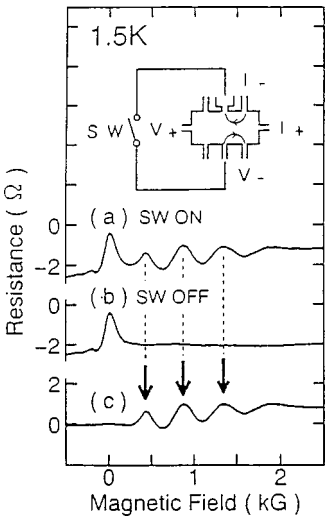

FIG. 46. Magnetoresistance due to TEF with two extra probes: (a) connected by an external circuit; (b) unconnected, (c) the magnetoresistance difference between (a) and (b). Peaks shown by arrows come from electrons emitted from the lower extra probes, as shown in the inset. The separation length between the emitter (collector) and the extra probe is 5 μm. The inset is a schematic view of the sample and the measuring configuration. From Takaoka *et al.*, 1994.

We suggest four possible contributions that warrant further study: (1) Magnetic-field-induced changes in the electron density in a given subband, both in the contacts and in the bulk electron gas. (2) Weak mfp effects, such as are seen in Monte Carlo simulations of TEF in the 2D electron gas (see Fig. 9 in Hornsey, 1996). (3) The phenomenon of ''pileup'' discussed in the following section. (4) Refraction (Spector *et al.*, 1990c, 1990d) at a split-gate collector—an effect similar to lens focusing (Spector *et al.*, 1990b, 1992)—which depends on R_c and thus on peak number.

2. Electron ''pileup''

Kolesnichenko *et al.* (1982) showed that the increase in local chemical potential at locations where electrons are focused could lead to ''trajectory reproduction,'' where these locations become additional emitters that can both enhance the usual TEF peaks and produce unusual peaks. The two-dimensional geometry of the 2D electron gas, combined with a relatively large emitter width W, will enhance this effect, giving a new phenomenon—electron ''pileup''—that can complicate TEF spectra analysis. Kolesnichenko *et al.* (1982) predict a peak amplitude due to ''pileup'' proportional to $\sim\exp\{(WR_c)^{1/2}/l_e\}$.

An apparent demonstration of this effect was the observation of a TEF spectrum with the setup of Fig. 46, with the emitter and collector on opposite sides of a wide 2D electron-gas channel so that regular TEF was excluded. Two extra probes were located at the same distance from the emitter and collector and either connected to make an external short circuit or not. Transverse electron focusing peaks were seen only when the circuit was shorted. Although the shorting wire was meters long, its resistance was low enough to adjust the electrochemical potentials of the extra probes to produce a pileup of nonequilibrium electrons at the probe nearest the collector C. Reemission of secondary nonequilibrium electrons then produced TEF peaks. An opening enhanced the apparent q due to pileup (Tsukagoshi *et al.*, 1993; Takaoka *et al.*, 1994), but an ohmic contact reduced q (Spector *et al.*, 1990b). The nature of the connection of the pileup region with the rest of the 2D electron-gas channel must be important, but details are not yet understood.

3. Inferred values of q

The large number of 2D electron-gas TEF peaks in Figs. 41–45 and similar studies listed above led their authors to infer that reflection from either an electrostatic or a wet chemically etched 2D electron-gas boundary is almost completely specular—$q\approx 1$, and that from a focused-ion-beam-produced boundary is substantially specular—$q\geqslant 0.5$. Two groups investigated the variation of q with n_s in focused-ion-beam samples and reported opposite results. As n_s decreased from 4 to $3\times 10^{15}\,\mathrm{m}^{-2}$, Wakaya *et al.* (1992) found q to decrease slightly (0.74–0.54), whereas Tsukagoshi *et al.* (1993) found it to increase slightly (0.5–0.65).

We agree that q is probably large in the 2D electron gas and generally smaller for focused-ion-beam boundaries than for electrostatic ones. But complications in determining q in the 2D electron gas suggest that deriving reliable values of q from q_M in the 2D electron gas is not straightforward.

First, for a cylindrical Fermi surface and a large enough ratio of W/L, q_M can be $\gg q$ (Sec. IV.D.2). The observed widths of the TEF peaks in the 2D electron gas (Figs. 41–46, 49, and 50) suggest that W/L is not small, and thus that q_M may be greater than q. Korzh (1975) and Tsoi and Kolesnichenko (1980) describe TEF calculations that include nonlocal effects by self-consistently solving the Boltzmann and charge neutrality equations subject to modified Fuchs boundary conditions (Lifshits *et al.*, 1973). The rather general classical model that they describe is easily solved numerically for a 2D electron gas, giving the results in Fig. 47. Remarkably, TEF peaks are present even when $q_{Fc}=0$, as first predicted by Tsoi and Kolesnichenko (1980).

Second, when $W/L\sim 1$ and l_b is short, the usual TEF peaks could be suppressed [Eq. (7)] more than the contributions from diffuse scattering and pileup (Sec. X.B.2).

Third, weak ''mfp effects'' leading to initially increasing peak heights were seen in Monte Carlo simulations of TEF (see Fig. 9 in Hornsey, 1996) even without taking account of pileup.

a. Mean-free-path studies

The TEF mean free path l_F has been derived for electrons (Spector *et al.*, 1990a, 1990b, 1992; Nakamura *et al.*, 1991; Takaoka *et al.*, 1992; Wakaya *et al.*, 1992;

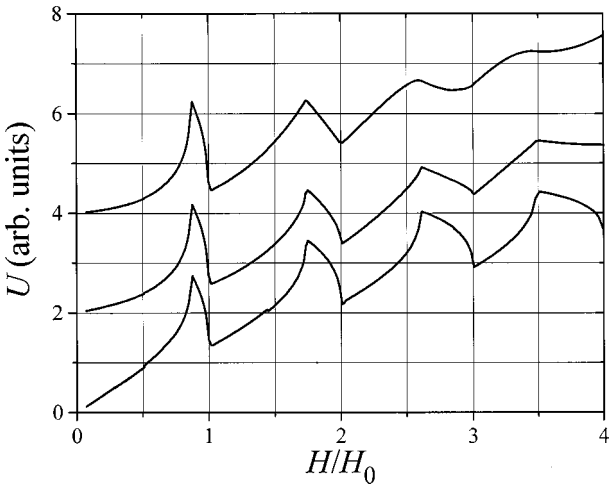

FIG. 47. Calculated TEF spectra in the 2D electron gas (see text) for an isotropic distribution of electrons injected and reflected from the surface. The Fuchs parameters q_{Fc} are 0 (top curve), 0.5 (middle curve), and 1 (bottom curve). The calculations assume $b/L=0.08$, where b is the emitter size and the collector is a point source (zero size). This zero size causes the sharp angles. A finite-size collector smears out the sharp angles. b was chosen to give a TEF peak width similar to that seen by van Houten *et al.* (1988, 1989).

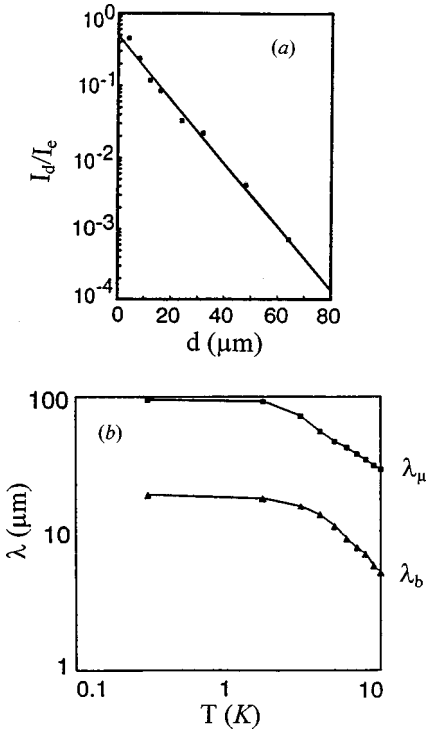

FIG. 48. Mean free paths. (a) Maximum peak amplitude of magneto-oscillations, normalized to the emitter voltage, vs emitter-collector distance L. (b) Mean free path vs temperature T. ■, l_μ; ▲, l_F. Sample mobility at $T=0.3$ K was 1.1×10^7 cm^2/(V s). From Spector *et al.*, 1992.

Tsukagoshi *et al.*, 1993) and holes (Heremans *et al.*, 1992) in the 2D electron gas by measuring how the amplitude of the first TEF peak decreases with increasing L [Eq. (7)]. Figure 48(a) illustrates the results. For comparison, some investigators deduced the mfp l_μ from mobility (μ) measurements, where $l_\mu=\tau v_F$, $\tau=m^*\mu/e$, and $v_F=\hbar k_F/(2\pi m^*)$, with τ the relaxation time and m^* the electron's effective mass. For $W/L \ll 1$, each scattering event is effective—it removes the electron from $\Delta\Omega$, thereby decreasing the TEF peak amplitude—and $l_F=l_b$ between two successive scatterings. More accurately (Tsoi and Gantmakher, 1969; Gantmakher, 1974; Gasparov and Huguenin, 1993), the efficiency of electron scattering depends on the electron's location on its orbit—the efficiency is less for an electron leaving the emitter or entering the collector.

In 2D electron-gas TEF studies of l_F, W/L is not small, so that under small-angle scattering $l_F \neq l_b$. Experiments also find $l_F<l_\mu$ (Spector *et al.*, 1990b, 1992; Nakamura *et al.*, 1991; Takaoka *et al.*, 1992; Wakaya *et al.*, 1992; Tsukagoshi *et al.*, 1993). Figure 48(b) shows typical behavior. At low temperatures, $l_F \sim 5-20$ μm, $l_\mu \sim (4-5)l_F$, and both l_μ and l_F decrease similarly with increasing temperature. This similarity in the temperature variations of l_F and l_μ has been attributed to the same scattering sources for both, with the smaller l_F ascribed to greater "effectiveness" of scattering events in removing electrons from the TEF signal—i.e., just a few small-angle scattering events can stop an electron from reaching the collector, but more are needed to reduce l_μ. Similar values of l_F and l_F/l_μ were found for holes (Heremens *et al.*, 1992).

Four groups have examined the effect upon l_F of changing n_s. Samples were prepared by e-beam lithography (Spector *et al.*, 1990a; Nihey *et al.*, 1990) or focused ion beams (Takaoka *et al.*, 1992; Tsukagoshi *et al.*, 1993), and n_s was varied electrostatically (Spector *et al.*, 1990a) or by illumination (Nihey *et al.*, 1990; Takaoka *et al.*, 1992; Tsukagoshi *et al.*, 1993). Figure 49 illustrates the results. All groups found that increasing n_s increased the size of the first peak, which they attributed to increasing l_F. The ratio l_F/l_μ was insensitive to n_s. Sources for increasing l_F include increased screening of remote impurities, decreased inhomogeneity in the 2D electron gas (Spector *et al.*, 1990a), and increasing v_F (since $l \propto v_F$).

b. Hot electrons

As noted in Sec. IX.E, reliable data on hot-electron focusing are difficult to achieve. Unless L is smaller than the electron mean free path $l(\varepsilon')$, which depends upon the excitation energy ε', "hot" electrons decay to near ε_F before reaching C, and the desired effects will be exponentially small [see Eq. (7)] and masked by other effects having nothing to do with highly nonequilibrium electrons. Also, the most fundamental quantity in hot-electron kinetics is the relaxation time τ [or scattering rate $1/\tau$; for needed modifications of Eq. (7), see M. Tsoi *et al.*, 1996] rather than l, since even when τ is constant, an increasing velocity with increasing ε' leads to increasing $l(\varepsilon')$, and thus increasing peak amplitude for electron excitations, whereas decreasing velocity with increasing e' leads to decreasing $l(e')$ and thus decreasing

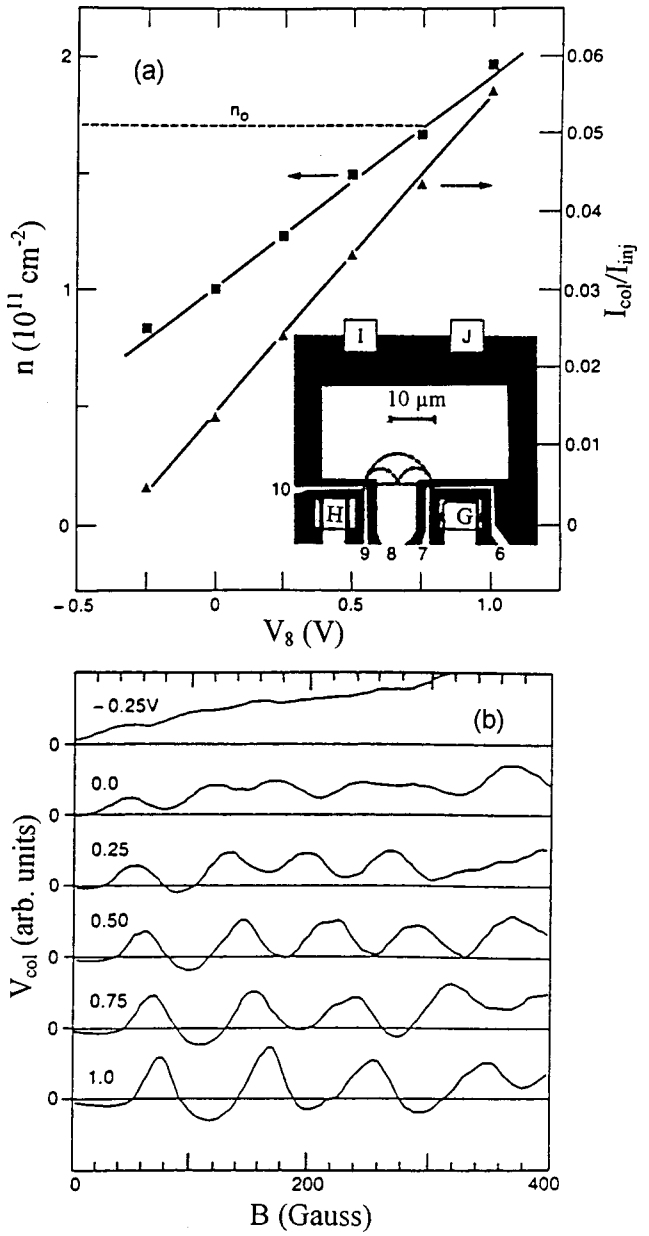

FIG. 49. Study of ballistic propagation vs density. (a) Inset—geometry used. Ohmic contacts are G–J and gates are 6–10. I and J are >100 μm apart. The dotted line shows the mesa edge; the dashed lines indicate electron paths for the first and second focusing peaks. The horizontal scale is the gate voltage (V_8). ■, electron density under gate 8 deduced from the oscillation period of the spectra in (b); n_0 density outside of gate 8; ▲, amplitude of the first peaks of (b), in units of collector current I_{coll} normalized to injector current I_{inj}. The lines are aids to the eye. (b) TEF spectra for the structure in the inset of (a). Electrons injected from G propagate ballistically under gate 8 and are collected at H. Each trace is taken at the indicated gate voltage V_8. After Spector *et al.*, 1990b.

peak amplitude. Lastly, increasing the emitter current can also cause local Joule heating, producing electrons and holes that might dominate the TEF spectra, since their energies are less (thus their l's longer) than those of the highly nonequilibrium excitations.

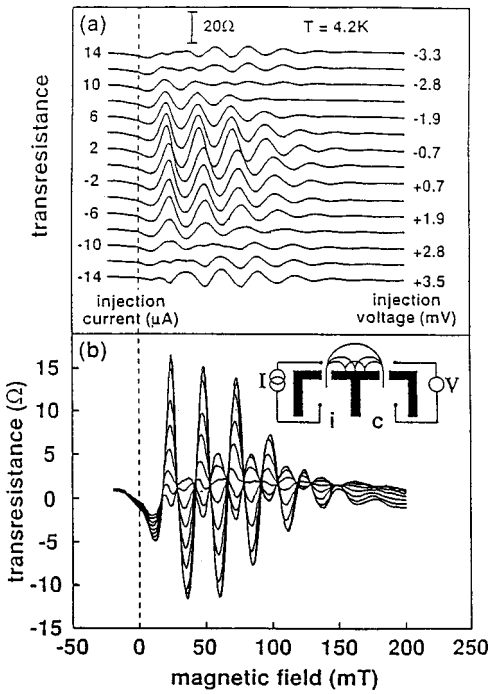

FIG. 50. Differential TEF magnetotransresistance for different negative (source) and positive (sink) injection currents: (a) For ±14 μA, with corresponding accelerating potentials; curves offset. (b) For positive values of injection current up to 14 μA; curves overlaid. The inset is a device schematic for transresistance measurement; i=emitter, c=collector. From Hornsey *et al.*, 1993b.

Several TEF studies have been made of highly nonequilibrium (hot) electrons in a 2D electron gas (Laikhtman *et al.*, 1990; Williamson *et al.*, 1990a, 1990b; Hornsey *et al.*, 1993b). For excitation energies up to about 5 mV, Fig. 50 shows that proper peak shifting in B and decreases of amplitude were observed, without any unusual behaviors, except that hot electrons with energy $\varepsilon' \sim 1.5\,\varepsilon_F$ give $l(\varepsilon')$ an order of magnitude larger than predicted (see das Sarma, 1992 and references therein). A similar result was also found with a quite different experimental technique (Sivan *et al.*, 1989). At higher excitation energies, however, singularities occur: new, small "TEF" peaks and *inverse* peaks similar to those without any bias voltage. Laikhtman *et al.* (1990) attributed such peaks to electron transport in the second subband. This attribution looks reasonable, since observing focusing means that adiabatic injection is disturbed (Sec. X.B.1). At high decelerating voltages, local heating might have dominated in the studies of Williamson *et al.* (1990b), Laikhtman *et al.* (1990), and Hornsey *et al.* (1993), leading to inverse TEF spectra because of strong suppression of contributions of highly excited holes having long traveling time from E to C and generation of electron excitations with low excitation energy. Superposition of all of these focusing peaks with different polarities could also produce observed small additional "TEF" peaks (V. Tsoi, 1978). In contrast, Hornsey *et al.* (1993b) argue, based in part on the data of Fig. 50, that the effects attributed by Laikhtman to second subband

transport are due instead to changes in the dc transverse electron focusing characteristics.

4. Miscellaneous

Goldman *et al.* (1994) and Smet *et al.* (1996) showed TEF evidence of composite fermions. Nakazato *et al.* (1992) found that a double grid structure gave complex focusing patterns that could be understood by combining transmission through and backscattering from the grids. Spector *et al.* (1991) found that beams of ballistic electrons in the 2D electron gas pass through each other without interacting. They ascribed this lack of interaction to the highly polarizable nature of the 2D electron gas, which strongly screens ballistically traveling electrons. A short interaction time can also explain the observations. Spector *et al.* (1990c, 1990d, 1992) studied ballistic electron optics.

Experiments (Heremans *et al.*, 1992) and theory (Goldoni and Fasolino, 1991) illustrate the use of TEF to measure Fermi-surface contours in the 2D electron gas and study anisotropy of the relaxation time $\tau(\mathbf{k})$. The principle of such studies is similar to that of the Gantmakher effect (Gantmakher, 1974; Gasparov and Huguenin, 1993). TEF is such a powerful tool for analyzing 2D electron-gas edge perfection and structure that it has been used to optimize parameters for focused ion beam implantation (Hornsey *et al.*, 1993).

5. Conclusion

TEF studies of the 2D electron gas have uncovered many interesting behaviors. Results at not too-low temperatures, and for contact widths $W > \lambda_{dB}$, can be understood using the same model as for TEF in metals and semimetals. Two items in this regime not yet understood for ''electrostatic'' samples are the growth in amplitude of the first few TEF peaks with increasing B and the nongrowth of the TEF peak widths. More theory is also still needed on the fine structure that occurs at low temperatures or with narrower (quantum) contacts. Because the Fermi surface is a circle, unless the ratio W/L is very small, a large q is not needed to obtain peak ratios near 1. As shown in Fig. 47, with the Fuchs boundary condition, large peaks can occur for $q_{Fc}=0$. Thus, while there is probably significant specular reflection from boundaries of the 2D, the precise size of q remains somewhat uncertain.

XI. SUMMARY, CONCLUSIONS, AND OPPORTUNITIES

We have described a variety of TEF studies, both of conduction-electrons scattering at surfaces and of interfaces in metals and semimetals. These studies have yielded important, often unique, information. However, relatively few of the possible applications of TEF have as yet been exploited. In this section we briefly summarize what has been learned and indicate some opportunities for future research. Most experiments can be analyzed with the geometrical model of ballistically propagating electrons.

We start with new vistas opened by recent experimental developments. The usual TEF needle contacts can be moved to different portions of a surface to survey its reflective properties, but once removed they cannot be returned to exactly the same place, and they limit studies to samples with mfp$\sim$100 μm. We described some measurements with needle-contact separations as small as $\sim$1 μm (see also V. Tsoi *et al.*, 1996), and even smaller separations should be possible with lithographic point contacts. Small separations allow the study of samples with short mean free paths, including excitation-energy dependence, since the mean free path (lifetime) decreases with increasing excitation energy off the Fermi surface. Lithographic point contacts allow leads to be attached at a series of fixed separations along chosen directions in the crystal lattice, thereby allowing studies of controlled processing of the reflecting interface and complementary STM studies of the exact same area. Focused light-generated excitations allow two-dimensional mapping of excitation motion. Combining such mapping with precisely positioned lithographic contacts should allow unique studies of interfaces.

The short de Broglie wavelength in metals, $\lambda_{dB} \sim 2-4$ Å, makes q sensitive to atomic-scale surface roughness. Thus TEF observations of $q>0.5$ for low-index planes of a wide range of metals indicate that these planes have atomically flat regions. But little more is known about the structures of the surfaces probed by TEF. In only two metals, Ag and W, have TEF studies been combined with STM studies of the microscopic surface structure. In neither case was the surface a simple Gaussian random distribution of heights. There is scope for combined TEF and STM studies of both low-angle index planes and miscut surfaces with well-defined steps. Only in W has the variation of q with λ_{dB} been studied, and the surfaces involved were not separately characterized. There has been only one TEF study of how q varies with coverage of adsorbed gases and only two on its variation with angle of incidence, $q(\theta)$.

Little as yet is known about the anisotropy of scattering from different crystallographic surfaces or about the energy dependence of scattering from metal surfaces. The new techniques described above should allow TEF studies of reflection and transmission of electrons from the interface between two metals, including magnetic metals, where conduction-electron/interface interactions should be spin dependent. There should now be enough precision to allow study of the structure and amplitude of metal corrugation surfaces, including the dependence of reflection upon the angle of incidence. Combining TEF and STM or atomic force microscopy measurements with ultrahigh-vacuum processing should permit the study of changes in reflection due to controlled addition of small amounts of surface adatoms up to adatom superlattices, chemical reactivity, surface phase transitions, and *in situ* surface modification by ion milling, ion implantation, and annealing. High electron excitation energy and higher temperatures should permit the study of inelastic electron-surface (interface) interactions, including the question of why surface phonons

are generally ineffective in electron kinetics (see, for example, Kim *et al.*, 1997). Transverse electron focusing could also be used to study the recently seen magnetic-field-induced intercrystalline boundary motion (Molodov and Shvindlerman, 1997).

In semimetals, large $\lambda_{dB} \sim 1000$ Å should lead to $q \sim 1$ for Gaussian atomic-scale roughness. While large q's are found for reflections from some atomic planes in Bi, much smaller q's are found for reflection from others. The smaller q's are ascribed to intervalley scattering, which can be very sensitive to surface roughness, but can also be screened by natural or artificially induced band bending. These phenomena warrant further study. Light-generated excitations have been used to study reflection and transmission from a particular angle grain boundary in Bi. Such studies can be extended to other angles and to interfaces between other materials. Elastic TEF peaks in Bi have also been induced by conduction-electron surface resonance due to an artificially imposed surface grating. Covering Bi with a material that induces upward band bending at the interface could give conduction-electron surface resonance without the need for a grating. In principle, this resonance may also be observed after inelastic trapping, as in molecular-beam scattering (Heinz *et al.*, 1982; Benedek and Valbusa, 1987). Transverse electron focusing plus conduction electron surface resonance may then be used to study surface-phonon dispersion.

TEF studies of normal metal/superconductor (N/S) interfaces have, so far, been limited to Bi/Sn and Ag/Pb. Such studies have shown qualitative evidence of all of the required properties of Andreev reflection and made possible introductory studies of its probability, its dependence on energy, and how it is affected by screening. In addition to more complete studies of these topics, studies are needed of the anisotropy of Andreev reflection, anisotropy of the energy gap, interface states near the N/S interface with energies less than the gap energy Δ, and Cooper coupling of electrons on different valleys. The new techniques described above should allow extension of some one- and two-point-contact TEF studies to high-T_c superconductors.

Transverse electron focusing studies should now be possible in mesoscopic (or ultradispersion) samples, where the conduction-electron/surface (or interface) interaction dominates. Lastly, diffraction patterns from gratings with period g can be observed with TEF both when $\lambda_{dB} \sim g$ and when $\lambda_{dB} \ll g$ (V. Tsoi, 1996). Transverse electron focusing thus has the potential to measure the conduction-electron coherence length, using an artificial surface grating of known structure and quality, or the vortex lattice parameter in a superconductor deposited onto a metal surface, using the known λ_{dB} and electron coherence length of the underlying metal.

Transverse electron focusing has already taught us much about scattering at surfaces and/or interfaces in metals, semimetals, and 2D electron gases. Nonetheless, experiments so far have barely scratched the surface of its potential. We hope that this review will stimulate further interest in the topic.

ACKNOWLEDGMENTS

V. T. and J. B. thank the Max-Planck-Institut für Festkörperforschung, Stuttgart for support, and V. T. thanks also the U.S. National Research Council CAST program. This review was also supported in part by U.S. NSF Grants No. DMR-94-23795 and DMR-98-20135, RU MST Grant No. 020/3, and Grant No. RFFR-98-02-16629.

REFERENCES

Andreev, A. F., 1964, Zh. Eksp. Teor. Fiz. **46**, 1823 [Sov. Phys. JETP **19**, 1228 (1964)].

Andreev, A. F., 1971, Usp. Fiz. Nauk **105**, 13 [Sov. Phys. Usp. **14**, 609 (1972)].

Andrievskii, V. V., and E. I. Ass, 1986, Fiz. Nizk. Temp. **12**, 543 [Sov. J. Low Temp. Phys. **12**, 307 (1986)].

Andrievskii, V. V., E. I. Ass, and Yu. F. Komnik, 1985, Fiz. Nizk. Temp. **11**, 1148 [Sov. J. Low Temp. Phys. **11**, 631 (1985)].

Andrievskii, V. V., Yu. F. Komnik, and S. V. Rozhok, 1996, Fiz. Nizk. Temp. **22**, 1418 [Sov. J. Low Temp. Phys. **22**, 1076 (1996)].

Ashcroft, N. W., and N. D. Mermin, 1976, *Solid State Physics* (Saunders, Philadelphia).

Azbel', M. Ya., and V. G. Peschanskii, 1965, Zh. Eksp. Teor. Fiz. **49**, 572 [Sov. Phys. JETP **22**, 399 (1966)].

Baranger, H. U., D. P. DiVincenzo, R. A. Jalabert, and A. D. Stone, 1991, Phys. Rev. B **44**, 10637.

Beenakker, C. W. J., 1995, in *Mesoscopic Quantum Physics: Proceedings of the Les Houches Summer School*, edited by E. Akkermans, G. Mautambaux, and U.-L. Pichard (North-Holland, Amsterdam), p. 279.

Beenakker, C. W. J., and H. van Houten, 1989, Phys. Rev. B **39**, 10445.

Beenakker, C. W. J., and H. van Houten, 1991, in *Solid State Physics*, Vol. 44, edited by H. Ehrenreich and D. Turnbull (Academic, New York), p. 1.

Beenakker, C. W. J., H. van Houten, and B. J. van Wees, 1988, Europhys. Lett. **7**, 359.

Benedek, G., and U. Valbusa, 1987, Eds., *Dynamics of Gas-Surface Interaction* (Springer, New York).

Benistant, P. A. M., 1984, Ph.D. thesis (University of Nijmegen, Netherlands).

Benistant, P. A. M., G. F. A. van de Walle, H. van Kempen, and P. Wyder, 1986, Phys. Rev. B **33**, 690.

Benistant, P. A. M., A. P. van Gelder, H. van Kempen, and P. Wyder, 1985, Phys. Rev. B **32**, 3351.

Benistant, P. A. M., H. van Kempen, and P. Wyder, 1983, Phys. Rev. Lett. **51**, 817.

Benistant, P. A. M., H. van Kempen, and P. Wyder, 1985, J. Phys. F **15**, 2445.

Binnig, G., and H. Rohrer, 1986, IBM J. Res. Dev. **30**, 355.

Birker, P. J. M. W. L., H. van Kempen, and P. Wyder, 1978, J. Phys. (Paris) C **6**, 1128.

Blonder, G. E., M. Tinkham, and T. M. Klapwijk, 1982, Phys. Rev. B **25**, 4515.

Boata, G., P. Cantini, and R. Tatarek, 1978, Phys. Rev. Lett. **40**, 887.

Bozhko, S. I., 1989, Kandidat Dissertation (Institute of Solid State Physics, Russian Academy of Sciences, Chernogolovka, Russia).

Bozhko, S. I., A. A. Mitryaev, O. A. Panchenko, I. I. Razgonov, and V. S. Tsoi, 1979, Fiz. Nizk. Temp. **5**, 739 [Sov. J. Low Temp. Phys. **5**, 351 (1979)].
Bozhko, S. I., I. F. Sveklo, and V. S. Tsoi, 1984, Pis'ma Zh. Eksp. Teor. Fiz. **40**, 480 [JETP Lett. **40**, 1316 (1984)].
Bozhko, S. I., I. F. Sveklo, and V. S. Tsoi, 1988, unpublished.
Bozhko, S. I., I. F. Sveklo, and V. S. Tsoi, 1989, Fiz. Nizk. Temp. **15**, 710 [Sov. J. Low Temp. Phys. **15**, 397 (1989)].
Bozhko, S. I., and V. S. Tsoi, 1987, Fiz. Nizk. Temp. **13**, 1139 [Sov. J. Low Temp. Phys. **13**, 644 (1987)].
Bozhko, S. I., V. S. Tsoi, and S. E. Yakovlev, 1982, Pis'ma Zh. Eksp. Teor. Fiz. **36**, 123 [JETP Lett. **36**, 152 (1982)].
Buckel, W., and R. Z. Hilsch, 1954, Physica (Amsterdam) **138**, 109.
Chester, P. F., and G. O. Jones, 1953, Philos. Mag. **44**, 1281.
Chien, C. L., 1990, J. Appl. Phys. **69**, 5267.
das Sarma, S., 1992, in *Hot Carriers in Semiconductor Nanostructures*, edited by J. Shah (Academic, New York), p. 53.
Datta, S., 1995, *Electronic Transport in Mesoscopic Systems* (Cambridge University, Cambridge, England).
Edel'man, V. S., 1976, Adv. Phys. **25**, 555.
Eisenmenger, W., and A. A. Kaplyanskii, 1986, Eds., *Nonequilibrium Phonons in Nonmetallic Crystals*, Modern Problems in Condensed Matter Sciences, No. 16 (North-Holland, Amsterdam).
Fal'kovskii, L. A., 1968, Usp. Fiz. Nauk **94**, 3 [Sov. Phys. Usp. **11**, 1 (1968)].
Fal'kovskii, L. A., 1983, Adv. Phys. **32**, 753.
Fomenko, V. S., 1970, *Emission Properties of Materials* (Naukova dumka, Kiev).
Fuchs, K., 1938, Proc. Cambridge Philos. Soc. **34**, 100.
Gaidukov, Yu. P., and E. M. Galyamina, 1976, Pis'ma Zh. Eksp. Teor. Fiz. **23**, 336 [JETP Lett. **23**, 301 (1976)].
Gaidukov, Yu. P., and E. M. Galyamina, 1978, Zh. Eksp. Teor. Fiz. **74**, 1936 [Sov. Phys. JETP **47**, 1008 (1978)].
Gantmakher, V. F., 1974, Rep. Prog. Phys. **37**, 317.
Gantmakher, V. F., and I. B. Levinson, 1987, in *Carrier Scattering in Metals and Semiconductors*, Modern Problems in Condensed Matter Sciences No. 19, edited by V. M. Agranovich and A. A. Maradudin (North-Holland, Amsterdam), p. 253.
Gao, J. R., B. J. van Wees, J. J. Kuipers, J. P. Heida, and T. M. Klapwijk, 1994, Appl. Phys. Lett. **64**, 2529.
Gasparov, V. A., and R. Huguenin, 1993, Adv. Phys. **42**, 393.
Glazman, L. I., G. B. Lesovik, D. E. Khmel'nitskii, and R. I. Shekhter, 1988, Pis'ma Zh. Eksp. Teor. Fiz. **48**, 218 [JETP Lett. **48**, 238 (1988)].
Goldman, V. J., B. Su, and J. K. Jain, 1994, Phys. Rev. Lett. **72**, 2065.
Goldoni, G., and A. Fasolino, 1991, Phys. Rev. B **44**, 8369.
Gray, K. E., 1988, Phys. Lett. B **2**, 1125.
Green, R. F., 1969, in *Solid State Surface Science*, Vol. 1, edited by M. Green (Marcel Dekker, New York), p. 87.
Grishin, A. M., 1983, Fiz. Tverd. Tela (Leningrad) **25**, 3407 [Sov. Phys. Solid State **25**, 1961 (1983)].
Hallmark, V. M., S. Chiang, J. F. Rabolt, J. D. Swalen, and R. J. Wilson, 1987, Phys. Rev. Lett. **59**, 2879.
Hasegava, H., L. He, H. Ohno, T. Sawada, T. Haga, Y. Abe, and H. Takahashi, 1987, J. Vac. Sci. Technol. B **5**, 1097.
Heil, J., A. Böhm, M. Primke, and P. Wyder, 1996, Rev. Sci. Instrum. **67**(1), 307.
Heil, J., M. Primke, K. U. Wurz, and P. Wyder, 1995, Phys. Rev. Lett. **74**, 146.
Heinz, K., K. Müller, T. Engel, and K.-H. Rieder, 1982, *Structural Studies of Surfaces*, Springer Tracts in Modern Physics No. 91 (Springer, Berlin/New York).
Heremens, J. J., M. B. Santos, and M. Shayegan, 1992, Appl. Phys. Lett. **61**, 1652.
Hirayama, Y., and T. Saku, 1990, Phys. Rev. B **42**, 11408.
Hoevers, H., 1992, Ph.D. thesis (University of Nijmegen, Netherlands).
Hoevers, H. F. C., J. G. H. Hermsen, and H. van Kempen, 1989, Rev. Sci. Instrum. **60**, 1316.
Hoevers, H. F. C., P. J. M. van Bentum, L. E. C. van de Leemput, H. van Kempen, A. J. G. Schellingerhout, and D. van der Marel, 1988, Physica C **152**, 105.
Hoevers, H. F. C., P. J. M. van Bentum, and H. van Kempen, 1992, Phys. Rev. B **45**, 3845.
Hoevers, H. F. C., P. J. M. van Bentum, H. van Kempen, A. J. G. Schellingerhout, and D. van der Marel, 1989, IBM J. Res. Dev. **33**, 389.
Hoevers, H. F. C., and H. van Kempen, 1991, Physica B **175**, 253.
Holzl, J., F. K. Schulte, and H. Wagner, 1979, *Solid Surface Physics*, Springer Tracts in Modern Physics No. 85 (Springer, Berlin/New York).
Hornsey, R. I., 1996, J. Appl. Phys. **79**, 832.
Hornsey, R. I., J. R. A. Cleaver, and H. Ahmed, 1993a, J. Vac. Sci. Technol. B **11**, 2579.
Hornsey, R. I., J. R. A. Cleaver, and H. Ahmed, 1993b, Phys. Rev. B **48**, 14 679.
Hornsey, R. I., T. J. Thornton, J. R. A. Cleaver, and H. Ahmed, 1993, J. Appl. Phys. **73**, 3203.
Jaeger, M. D., V. Tsoi, and B. Golding, 1996, Appl. Phys. Lett. **68**, 1282.
Jing, T. W., Z. Z. Wang, and N. P. Ong, 1989, Physica C **162–64**, 1061.
Kaganov, M. I., and V. S. Edelman, 1985, Eds., *Conduction Electrons* (Nauka, Moscow).
Kapeliovich, A. I., 1988, Zh. Eksp. Teor. Fiz. **78**, 987 [Sov. Phys. JETP **51**, 498 (1988)].
Khaikin, M. S., 1960, Zh. Eksp. Teor. Fiz. **39**, 212 [Sov. Phys. JETP **12**, 152 (1961)].
Khaikin, M. S., 1969, Adv. Phys. **18**, 1.
Khaikin, M. S., and V. S. Edel'man, 1964, Zh. Eksp. Teor. Fiz. **47**, 878 [Sov. Phys. JETP **20**, 587 (1965)].
Kikuchi, S., and S. Nakagawa, 1933, Sci. Pap. Inst. Phys. Chem. Res. (Jpn.) **21**, 256.
Kim, S., H. Suhl, and I. K. Schuller, 1997, Phys. Rev. Lett. **78**, 322.
Kirichenko, O. V., V. G. Peschanskii, and S. N. Savel'eva, 1974, Zh. Eksp. Teor. Fiz. **67**, 1451 [Sov. Phys. JETP **40**, 722 (1975)].
Kolesnichenko, Yu. A., 1992, Fiz. Nizk. Temp. **18**, 1059 [Sov. J. Low Temp. Phys. **18**, 741 (1992)].
Kolesnichenko, Yu. A., V. G. Peschansky, and V. S. Tsoi, 1982, Zh. Eksp. Teor. Fiz. **83**, 1464 [Sov. Phys. JETP **56**, 843 (1982)].
Komnik, Yu. F., V. V. Andrievskii, and S. V. Rozhok, 1996, Fiz. Nizk. Temp. **22**, 1406 [Sov. J. Low Temp. Phys. **22**, 1066 (1996)].
Komnik, Yu. F., V. V. Andrievskii, and S. V. Rozhok, 1997, Phys. Rev. B **56**, 4023.
Korzh, S. A., 1975, Zh. Eksp. Teor. Fiz. **68**, 144 [Sov. Phys. JETP **41**, 70 (1975)].

Korzh, S. A., 1981, Fiz. Nizk. Temp. **7**, 314 [Sov. J. Low Temp. Phys. **7**, 153 (1981)].
Kosevich, A. M., 1985, Fiz. Nizk. Temp. **11**, 1106 [Sov. J. Low Temp. Phys. **11**, 611 (1985)].
Kosevich, A. M., and I. M. Lifshitz, 1955, Zh. Eksp. Teor. Fiz. **29**, 743 [Sov. Phys. JETP **2**, 646 (1956)].
Kravchenko, V. Ya., and E. I. Rashba, 1969, Zh. Eksp. Teor. Fiz. **56**, 1713 [Sov. Phys. JETP **29**, 918 (1969)].
Krylov, I. P., 1980, in *Soviet Scientific Review, Section A: Physics Reviews*, Vol. 2, edited by I. M. Khalatnikov (Harwood Academic, London), p. 85.
Krylov, I. P., and Yu. V. Sharvin, 1970, Pis'ma Zh. Eksp. Teor. Fis. **12**, 102 [JETP Lett. **12**, 71 (1970)].
Laikhtman, B., U. Sivan, A. Yacoby, C. P. Umbach, M. Heiblum, J. A. Kash, and H. Shtrikman, 1990, Phys. Rev. Lett. **65**, 2181.
Landau L. D., and E. M. Lifshitz, 1965, *Quantum Mechanics* (Pergamon, Oxford).
Lessie, D., 1979, Phys. Rev. B **20**, 2491.
Levy, P. M., 1994, in *Solid State Physics: Advances in Research and Applications*, Vol. 47, edited by H. Ehrenreich and D. Turnbull (Academic, New York), p. 367.
Lifshits, I. M., M. Ya. Azbel', and M. I. Kaganov, 1973, *Electron Theory of Metals* (Consultants Bureau, New York).
Lutsishin, P. P., O. A. Panchenko, Yu. G. Ptushinskii, and N. P. Katrich, 1975, Surf. Sci. **47**, 681.
Mamin, H. J., E. Ganz, D. W. Abraham, R. E. Thomson, and J. Clarke, 1986, Phys. Rev. B **34**, 9015.
Martin, T. P., 1996, Ed., *Large Clusters of Atoms and Molecules, Proceedings of the NATO Advanced Study Institute*, Vol. 313 (Kluwer Academic, Dordrecht, Netherlands).
Mattera, L., R. Musenich, C. Salvo, and S. Terreni, 1985, Faraday Discuss. Chem. Soc. **80**, 1.
McKelvey, J. P., 1966, *Solid-State and Semiconductor Physics* (Harper and Row, New York).
McRae, E. G., 1979, Rev. Mod. Phys. **51**, 541.
McRae, E. G., and C. W. Galdwell, 1964, Surf. Sci. **2**, 509.
Mitryaev, A. A., O. A. Panchenko, I. I. Razgonov, and V. S. Tsoi, 1978, Surf. Sci. **75**, 376.
Molenkamp, L. W., A. A. M. Staring, C. W. J. Beenakker, R. Eppenga, C. E. Timmering, G. G. Williamson, C. J. P. M. Harmans, and C. T. Foxon, 1990, Phys. Rev. B **41**, 1274.
Molodov, D. A., and L. S. Shvindlerman, 1997, private communication.
Mönch, W., 1993, *Semiconductor Surfaces and Interfaces*, Springer Series in Surface Sciences No. 26 (Springer, New York).
Murzin, S. S., 1982, Zh. Eksp. Teor. Fiz. **82**, 515 [Sov. Phys. JETP **55**, 298 (1982)].
Nakamura, K., F. Nihey, H. Toyoshima, T. Itoh, and D. C. Tsui, 1991, Superlattices Microstruct. **9**, 235.
Nakamura, K., D. C. Tsui, F. Nihey, H. Toyoshima, and T. Itoh, 1990, Appl. Phys. Lett. **56**, 385.
Nakazato, K., R. I. Hornsey, R. J. Blaikie, J. R. A. Cleaver, H. Ahmed, and T. J. Thornton, 1992, Appl. Phys. Lett. **60**, 1093.
Nee, T. W., and R. E. Prange, 1967, Phys. Lett. **25A**, 582.
Nihey, F., K. Nakamura, M. Kuzuhara, N. Samoto, and T. Itoh, 1990, Appl. Phys. Lett. **57**, 1218.
Obretenov, W., M. Hopfner, W. J. Lorenz, E. Budevski, G. Staikov, and H. Siegenthaler, 1992, Surf. Sci. **271**, 191.
Okiji, A., N. Negishi, and A. Nakamura, 1992, J. Phys. Soc. Jpn. **61**, 1145.
Okulov, V. I., and V. V. Ustinov, 1979, Fiz. Nizk. Temp. **5**, 213 [Sov. J. Low Temp. Phys. **5**, 101 (1979)].
Panchenko, O. A., A. A. Kharlamov, and Yu. G. Ptushinskii, 1974, Zh. Eksp. Teor. Fiz. **67**, 780 [Sov. Phys. JETP **40**, 386 (1974)].
Panchenko, O. A., P. P. Lutsishin, and Yu. G. Ptushinskii, 1974, Zh. Eksp. Teor. Fiz. **66**, 2191 [Sov. Phys. JETP **39**, 1079 (1974)].
Panchenko, O. A., P. P. Lutsishin, Yu. G. Ptushinskii, and V. V. Shishkov, 1973, Surf. Sci. **34**, 187.
Parrott, I. E., 1965, Proc. Phys. Soc. London **85**, 1143.
Pippard, A. B., 1965, *The Dynamics of Conduction Electrons* (Gordon and Breach, New York).
Primke, M., 1997, *Electron Focusing: Imaging of Anisotropic Carrier Propagation in Metallic Single Crystals* (Hartung-Gorre, Konstanz).
Pryadkin, S. L., and V. S. Tsoi, 1988, Zh. Eksp. Teor. Fiz. **94**, 336 [Sov. Phys. JETP **67**, 621 (1988)].
Rashba, E. I., E. S. Gribnikov, and V. Ya. Kravchenko, 1976, Usp. Fiz. Nauk. **119**, 3 [Sov. Phys. Usp. **19**, 1 (1976)].
Sato, H., and F. J. Kimura, 1984, J. Phys. F **14**, 1905.
Sato, H., and K. Yonemitsu, 1986, J. Phys. F **16**, 2053.
Schumacher, D., 1993, *Surface Scattering Experiments with Conduction Electrons*, Springer Tracts in Modern Physics No. 128 (Springer, New York).
Sharvin, Yu. V., 1965, Zh. Eksp. Teor. Fiz. **48**, 984 [Sov. Phys. JETP **21**, 655 (1965)].
Sharvin, Yu. V., and N. I. Bogatina, 1969, Zh. Eksp. Teor. Fiz. **56**, 772 [Sov. Phys. JETP **29**, 419 (1969)].
Sharvin, Yu. V., and L. M. Fisher, 1965, Pis'ma Zh. Eksp. Teor. Fiz. **1**, 54 [JETP Lett. **1**, 152 (1965)].
Sharvin, Yu. V., and V. F. Gantmakher, 1963, Prib. Tekh. Eksp. **15**, 101.
Sharvin, Yu. V., and D. Yu. Sharvin, 1979, Zh. Eksp. Teor. Fiz. **77**, 2153 [Sov. Phys. JETP **50**, 1033 (1979)].
Sivan, U., M. Heiblum, and C. P. Umbach, 1989, Phys. Rev. Lett. **63**, 992.
Smet, J. H., D. Weiss, R. N. Blick, G. Lutjering, K. von Klitzing, R. Fleishmann, R. Ketmerick, T. Geisel, and G. Weimann, 1996, Phys. Rev. Lett. **77**, 2272.
Smoluchowski, R., 1941, Phys. Rev. **60**, 661.
Soler, J. H., A. M. Baro, N. Garcia, and H. Rohrer, 1986, Phys. Rev. Lett. **57**, 444.
Spector, J., H. L. Stormer, K. W. Baldwin, L. N. Pfeifer, and K. W. West, 1990a, Surf. Sci. **228**, 283.
Spector, J., H. L. Stormer, K. W. Baldwin, L. N. Pfeifer, and K. W. West, 1990b, Appl. Phys. Lett. **56**, 967.
Spector, J., H. L. Stormer, K. W. Baldwin, L. N. Pfeifer, and K. W. West, 1990c, Appl. Phys. Lett. **56**, 1290.
Spector, J., H. L. Stormer, K. W. Baldwin, L. N. Pfeifer, and K. W. West, 1990d, Appl. Phys. Lett. **56**, 2433.
Spector, J., H. L. Stormer, K. W. Baldwin, L. N. Pfeifer, and K. W. West, 1991, Appl. Phys. Lett. **58**, 263.
Spector, J., J. S. Weiner, H. L. Stormer, K. W. Baldwin, L. N. Pfeiffer, and K. W. West, 1992, Surf. Sci. **263**, 240.
Stampfl, A. P. J., J. A. Con Foo, R. C. G. Leckey, J. D. Riley, R. Denecke, and L. Ley, 1995, Surf. Sci. **331–333**, 1272.
Sutton, A. P., and R. W. Balluffi, 1995, *Interfaces in Crystalline Materials* (Clarendon, Oxford).
Sveklo, I. F., and V. S. Tsoi, 1989a, Pis'ma Zh. Eksp. Teor. Fiz. **49**, 290 [JETP Lett. **49**, 331 (1989a)].
Sveklo, I. F., and V. S. Tsoi, 1989b, Zh. Eksp. Teor. Fiz. **95**, 2259 [Sov. Phys. JETP **68**, 1305 (1989)].

Sveklo, I. F., and V. S. Tsoi, 1992, Pis'ma Zh. Eksp. Teor. Fiz. **56**, 536 [JETP Lett. **56**, 523 (1992)].
Sveklo, I. F., and V. S. Tsoi, 1993, Zh. Eksp. Teor. Fiz. **103**, 1705 [Sov. Phys. JETP **76**, 839 (1993)].
Takaoka, S., K. Tsukagoshi, S. Wakayama, K. Murase, K. Gamo, and S. Namba, 1992, Solid State Commun. **83**, 775.
Takaoka, S., S. Wakayama, S. G. Inoue, K. Tsukagoshi, K. Oto, K. Murase, and K. Gamo, 1994, Phys. Rev. B **50**, 11661.
Thornton, T. J., M. Pepper, H. Ahmed, D. Andrews, and G. J. Davies, 1986, Phys. Rev. Lett. **56**, 1198.
Troyanovskii, A. M., and V. S. Edel'man, 1993, Pis'ma Zh. Eksp. Teor. Fiz. **57**, 429 [JETP Lett. **57**, 445 (1993)].
Troyanovskii, A. M., and V. S. Edel'man, 1994, Pis'ma Zh. Eksp. Teor. Fiz. **60**, 285 [JETP Lett. **60**, 300 (1994)].
Trzcinski, R., E. Gmelin, and J. Queisser, 1987, Phys. Rev. B **35**, 6373.
Tsoi, M. V., 1997, unpublished.
Tsoi, M. V., A. Böhm, M. Primke, V. S. Tsoi, and P. Wyder, 1997, Phys. Rev. B **56**, R15581.
Tsoi, M. V., and V. S. Tsoi, 1995, Pis'ma Zh. Eksp. Teor. Fiz. **62**, 223 [JETP Lett. **62**, 237 (1995)].
Tsoi, M. V., and V. S. Tsoi, 1996a, Prib. Tekh. Eksp. **4**, 147 [Instrum. Exp. Tech. **39**, 608 (1996)].
Tsoi, M. V., and V. S. Tsoi, 1996b, Physica B **218**, 14.
Tsoi, M. V., V. S. Tsoi, and P. Wyder, 1996, Pis'ma Zh. Eksp. Teor. Fiz. **64**, 835 [JETP Lett. **64**, 894 (1996)].
Tsoi, V. S., 1974, Pis'ma Zh. Eksp. Teor. Fiz. **19**, 114 [JETP Lett. **19**, 70 (1974)].
Tsoi, V. S., 1975, Zh. Eksp. Teor. Fiz. **68**, 1849 [Sov. Phys. JETP **41**, 927 (1975)].
Tsoi, V. S., 1977, Pis'ma Zh. Eksp. Teor. Fiz. **25**, 289 [JETP Lett. **25**, 264 (1977)].
Tsoi, V. S., 1978, Doctoral dissertation (Institute of Solid State Physics, Russian Academy of Sciences, Chernogolovka, Russia).
Tsoi, V. S., 1980, in *Soviet Scientific Review, Section A: Physics Reviews*, Vol. 2, edited by I. M. Khalatnikov (Harwood Academic, London), p. 395.
Tsoi, V. S., 1985, in *Conduction Electrons*, edited by M. I. Kaganov and V. S. Edel'man (Nauka, Moscow).
Tsoi, V. S., 1996, Physica B **218**, 1.
Tsoi, V. S., J. Bass, P. A. M. Benistant, H. van Kempen, E. L. M. Payens, and P. Wyder, 1979, J. Phys. F **9**, L221.
Tsoi, V. S., J. Bass, and P. Wyder, 1992, Adv. Phys. **41**, 365.
Tsoi, V. S., Y. de Wilde, T. Noller, A. G. M. Jansen, P. Wyder, D. Heitmann, and M. Riek, 1996, Europhys. Lett. **35**, 43.
Tsoi, V. S., and V. F. Gantmakher, 1969, Zh. Eksp. Teor. Fiz. **56**, 1232 [Sov. Phys. JETP **29**, 663 (1969)].
Tsoi, V. S., M. D. Jaeger, B. Golding, M. V. Tsoi, and J. Bass, 1996, Physica B **218**, 22.
Tsoi, V. S., and Yu. A. Kolesnichenko, 1980, Zh. Eksp. Teor. Fiz. **78**, 2041 [Sov. Phys. JETP **51**, 1027 (1980)].
Tsoi, V. S., and I. I. Razgonov, 1976, Pis'ma Zh. Eksp. Teor. Fiz. **23**, 107 [JETP Lett. **23**, 92 (1976)].
Tsoi, V. S., and I. I. Razgonov, 1977, Pis'ma Zh. Eksp. Teor. Fiz. **25**, 30 [JETP Lett. **25**, 26 (1977)].
Tsoi, V. S., and I. I. Razgonov, 1978, Zh. Eksp. Teor. Fiz. **74**, 1137 [Sov. Phys. JETP **47**, 597 (1978)].
Tsoi, V. S., and N. P. Tsoi, 1977, Zh. Eksp. Teor. Fiz. **73**, 289 [Sov. Phys. JETP **46**, 150 (1977)].
Tsoi, V. S., and N. P. Tsoi, 1992, unpublished.
Tsoi, V. S., N. P. Tsoi, and S. E. Yakovlev, 1989, Zh. Eksp. Teor. Fiz. **95**, 921 [Sov. Phys. JETP **68**, 530 (1989)].
Tsoi, V. S., and S. E. Yakovlev, 1987, Pis'ma Zh. Eksp. Teor. Fiz. **46**, 370 [JETP Lett. **46**, 467 (1987)].
Tsukagoshi, K., S. Takaoka, K. Murase, K. Gamo, and S. Namba, 1993, Appl. Phys. Lett. **62**, 1609.
Ueta, T., 1993, J. Phys. Soc. Jpn. **62**, 3633.
Ueta, T., 1994, J. Phys. Soc. Jpn. **63**, 4506.
Ueta, T., 1995, J. Phys. Soc. Jpn. **64**, 4813.
van Duzer, T., and C. W. Turner, 1981, *Principles of Superconductive Devices and Circuits* (Elsevier, Amsterdam).
van Houten, H., C. W. J. Beenakker, J. G. Williamson, M. E. I. Broekaart, P. H. M. van Loosdrecht, B. J. van Wees, J. E. Mooij, C. T. Foxon, and J. J. Harris, 1989, Phys. Rev. B **39**, 8556.
van Houten, H., B. J. van Wees, J. E. Mooij, C. W. W. Beenakker, J. G. Williamson, and C. T. Foxon, 1988, Europhys. Lett. **5**, 721.
van Hove, M. A., and S. Y. Tong, 1985, *Structure of Surfaces* (Springer, New York).
Wakaya, F., Y. Takagaki, S. Takaoka, K. Murase, Y. Yuba, K. Gamo, and S. Nambu, 1992, Superlattices Microstruct. **11**, 273.
Wakayama, S., K. Tsukagoshi, K. Oto, S. Takaoka, K. Murase, and K. Gamo, 1994, Solid State Commun. **92**, 413.
Williamson, J. G., H. van Houten, C. W. J. Beenakker, M. E. I. Broekaart, L. I. A. Spendeler, B. J. van Wees, and C. T. Foxon, 1990a, Surf. Sci. **229**, 303.
Williamson, J. G., H. van Houten, C. W. J. Beenakker, M. E. I. Broekaart, L. I. A. Spendeler, B. J. van Wees, and C. T. Foxon, 1990b, Phys. Rev. B **41**, 1207.
Windmiller, L. R., 1966, Phys. Rev. B **149**, 472.
Wintterlin, J., J. Wiechers, H. Brune, T. Gritsch, H. Hofer, and R. J. Behm, 1989, Phys. Rev. Lett. **62**, 59.
Zangwill, A., 1988, *Physics at Surfaces* (Cambridge University, Cambridge).
Zavaritsky, N. V., 1960, Zh. Eksp. Teor. Fiz. **38**, 1673 [Sov. Phys. JETP **11**, 1207 (1960)].
Ziman, J. M., 1960, *Electrons and Phonons* (Clarendon, Oxford).
Zuger, O., and U. Durig, 1992, Phys. Rev. Lett. **46**, 7319.